DESIGN AND ANALYSIS OF TUBULAR PHOTOBIOREACTORS FOR BIOHYDROGEN PRODUCTION

A THESIS SUBMITTED TO
THE GRADUATE SCHOOL OF NATURAL AND APPLIED SCIENCES
OF
MIDDLE EAST TECHNICAL UNIVERSITY

BY

EMINE KAYAHAN

IN THE PARTIAL FULFILLMENT OF THE REQUIREMENTS
FOR
THE DEGREE OF MASTER OF SCIENCE
IN
DEPARTMENT OF CHEMICAL ENGINEERING

SEPTEMBER 2015

Approval of the thesis:

DESIGN AND ANALYSIS OF TUBULAR PHOTOBIOREACTORS FOR BIOHYDROGEN PRODUCTION

submitted by **EMİNE KAYAHAN** in the partial fulfillment of the requirements for the degree of **Master of Science in Chemical Engineering Department, Middle East Technical University** by,

Prof. Dr. Gülbin Dural Ünver
Dean, Graduate School of **Natural and Applied Sciences** _____

Prof. Dr. Halil Kalıpçılar
Head of Department, **Chemical Engineering** _____

Prof. Dr. İnci Eroğlu
Supervisor, **Chemical Engineering Dept, METU** _____

Asst. Prof. Dr. Harun Koku
Co-supervisor, **Chemical Engineering Dept, METU** _____

Examining Committee Members:

Prof. Dr. Ufuk Gündüz
Department of Biological, METU _____

Prof. Dr. İnci Eroğlu
Chemical Engineering Dept, METU _____

Asst. Prof. Dr. Harun Koku
Chemical Engineering Dept, METU _____

Assoc. Prof. Dr. Serkan Kıncal
Chemical Engineering Dept, METU _____

Assoc. Prof. Dr. Başar Uyar
Chemical Engineering Dept., Kocaeli University _____

Date: 01.09.2014

I hereby declare that all information in this document has been obtained and presented in accordance with academic rules and ethical conduct. I also declare that as required by these rules and conduct, I have fully cited and referenced all material and results that are not original to this work.

Name, Last Name: Emine Kayahan

Signature :

ABSTRACT

DESIGN AND ANALYSIS OF TUBULAR PHOTOBIOREACTORS FOR BIOHYDROGEN PRODUCTION

Kayahan, Emine

M.S., Department of Chemical Engineering

Supervisor : Prof. Dr. İnci Eroğlu

Co-supervisor : Asst. Prof. Dr. Harun Koku

September 2015, 195 pages

Hydrogen can be produced sustainably by utilizing organic wastes through photofermentation. In order to obtain an economically feasible operation, the photobioreactor design is of crucial importance. An optimal photobioreactor design should provide uniform velocity and light distribution, low pressure drop, low gas permeability and efficient gas-liquid separation. The aim of this study was to design a pilot-scale photobioreactor satisfying these criteria and to test the reactor under outdoor conditions with purple non sulphur bacteria. A glass, stacked tubular bioreactor aimed at satisfying these criteria has been designed for outdoor photofermentative hydrogen production. The design consists of 4 stacked U-tubes and 2 vertical manifolds. The hydrodynamics of the 3-dimensional model of this reactor was solved via COMSOL Multiphysics 4.1. Two reactors, whose volumes were 9 and 11 L, were constructed based on the dimensions obtained by the model. A reactor was constructed based on the dimensions obtained by the model. The reactor was operated with recirculation of culture containing *Rhodobacter capsulatus YO*$_3$ (hup$^-$). Every morning 10% of the culture was replaced by fresh feed. Experiments were lasted 10-

20 days. When molasses was used as the carbon source under outdoor conditions, the highest hydrogen productivity was found as 0.311 mol $H_2/(m^3.h)$. Another parallel reactor working with acetic acid which was also run in July 2015, the highest productivity was found as 0.114 mol $H_2/(m^3.h)$. Compared to nearly horizontal tubular reactors, the glass stacked tubular reactor design results in less ground area and longer life time.

Keywords: Photofermentation, manifold model, photobioreactor design, biohydrogen, *Rhodobacter capsulatus*

ÖZ

BİYOLOJİK HİDROJEN ÜRETİMİ İÇİN BORUSAL FOTOBİYOREAKTÖRLERİN DİZAYNI VE ANALİZİ

Kayahan, Emine

Yüksek Lisans, Kimya Mühendisliği Bölümü

Tez Yöneticisi : Prof. Dr. İnci Eroğlu

Ortak Tez Yöneticisi : Yrd. Doç. Dr. Harun Koku

Eylül 2015, 195 sayfa

Hidrojen, fotofermentaston ile organik atıkları kullanarak sürdürülebilir bir şekilde üretilebilir. Ekonomik bir üretim elde edebilmek için fotobiyoreaktör dizaynı son derece önemlidir. Optimum fotobiyoreaktör tasarımında, homojen bir akış ve ışık dağılımı, düşük basınç farkı, düşük gaz geçirgenliği ve verimli çalışan bir gaz-sıvı ayırma ünitesi olmalıdır. Bu çalışmanın amacı, bu kriterleri sağlayacak pilot-ölçekli bir fotobiyoreaktör tasarımı yapmak ve reaktörü mor sülfürsüz bakteri kullanarak açık havada test etmektir. Açık havada fotofermentaston ile hidrojen üretimi amacını taşıyan ve bu kriterleri sağlayacak, bir cam, borusal biyoreaktör tasarlanmıştır. Dizayn 4 adet U-tüpü, ve 2 adet dikey manifolddan oluşmaktadır. Bu reaktörün hidrodinamiği 3 boyutlu olarak COMSOL Multiphysics 4.4 kullanılarak çözülmüştür. Boyutları model sonuçlarına dayandırılan 9 ve 11 L hacme sahip iki reaktör kurulmuştur. Reaktör *Rhodobacter capsulatus YO₃* (hup^-) suş kültürü devirdaim ettirilerek çalıştırılmıştır. Her sabah reaktörlerden %10 kültür alınmış ve yerine besiyeri verilmiştir. Deneyler 10-20 gün sürmüştür. Açık havada yapılan deneyde, karbon kaynağı olarak melas kullanıldığı zaman en yüksek hidrojen üretim hızı 0.311 mol $H_2/(m^3.sa)$ olarak

bulunmuştur. Temmuz 2015'te gerçekleştirilen paralel bir deneyde asetik asit ile içeren besiyeriyle elde edilen en yüksek üretim hızı 0.114 mol $H_2/(m^3.sa)$ dir. Dikey borusal cam reaktör, hafif eğimli yatay plastik borusal reaktörlere göre daha az alan kaplar ve daha uzun ömre sahiptir.

Anahtar Kelimeler: Fotofermentasyon, manifold modeli, fotobioyoreaktör tasarımı, biyohidrojen, *Rhodobacter capulatus*

To my family,

ACKNOWLEDGEMENTS

I would like to express my sincere gratitude to my supervisor, Prof. Dr. İnci Eroğlu. Her guidance, advice, support and kindness gave me motivation during my thesis. I would like to thank to my co-supervisor Asst. Prof. Dr. Harun Koku for his suggestions and valuable contributions on my thesis. I also thank to Prof. Dr. Ufuk Gündüz and Prof. Dr. Meral Yücel for their recommendations on biological systems.

I am indebted to Dominic Deo Androga for valuable comments, discussions, and help. With the light of the information I gained while working with Dominic, I was able to carry out my experiments. I also would like to acknowledge Emrah Sağır with his help especially on working with bacteria. I would like to thank Dr. Siamak Alipour about his contributions during the construction of the reactors. I am very happy having worked with such friends.

I am thankful to chemical engineering student, Yağmur Özdemir, with whom I worked on the light intensity distribution and absorption of molasses. I special thanks go to Nihal Bayaki, Onurcan Arslan and Efe Seyyal. Their help in the pump selection, and the development of a method for HPLC analysis was very valuable for me.

I would like to thank to the technical assistant Gülten Orakçı for her help in HPLC analysis. I also would like to thank İsa Çağlar, Süleyman N. Kuşhan and Adil Demir, who work in the Chemical Engineering Workshop.

I would like to express my gratitude to Gökçe Avcıoğlu. Her friendship and advices on the large scale operations gave me motivation during my studies. I am grateful to Ezgi Yavuzyılmaz, Necip Berker Üner and C. Güvenç Oğulgönen for their support, friendship and priceless brainstorming on chemical engineering topics. I also would like to thank Barış Erdoğan who gave motivation and encouragement to me during my thesis with his invaluable comments and guidance. I also would like to thank Esen Özcan, Barış Özcan and Bilgi Alver for their friendship and support.

I would like to thank to my family for their invaluable support, love and faith in me. I especially thank to my sister, Nagehan Kayahan for her precious friendship and support not just only in this thesis but also in my whole life. I also thank to my mother, father and grandfather. Their endless love and support gave me encouragement in throughout my thesis.

I thank to Kazım Yılmaz and Ayhan İldam who work in İldam Cam for their help and suggestions on the glass reactor.

This study was a part of the ongoing project funded by TÜBİTAK (114M436) and by the METU BAP project (BAP-07-02-2014-007-538).

TABLE OF CONTENTS

ABSTRACT v
ÖZ vii
TABLE OF CONTENTS xii
LIST OF TABLES xv
LIST OF FIGURES xvii
LIST OF SYMBOLS xxiii
LIST OF ABBREVIATIONS xxv
CHAPTERS
1. INTRODUCTION 1
2. LITERATURE SURVEY 7
2.1 Hydrogen as an Energy Carrier 7
2.2 Commercial Hydrogen Production Techniques 8
2.2.1 Natural Gas Steam Reforming 8
2.2.2 Partial Oxidation of Hydrocarbons 9
2.2.3 Coal Gasification 9
2.2.4 Biomass Gasification 10
2.2.5 Electrolysis 10
2.3 Review of Biohydrogen Production Technologies 10
2.3.1 Photolysis 12
2.3.2 Dark Fermentation 13
2.3.3 Photofermentation 21
2.3.4 Integrated Systems 33
2.3.5 Mixed Cultures for Simultaneous Dark and Photofermentation 35
2.4 Photobioreactors for Hydrogen Production 39
2.4.1 Panel Photobioreactors 39
2.4.2 Tubular Photobioreactors 41
2.5 Flow Distribution in Manifolds 44
3. STACKED U-TUBE PHOTOBIOREACTOR DESIGN 53

3.1 Design Strategy 53
3.1.1 Reactor Selection 53
3.1.2 Method of Attack 57
3.2 Methods 58
3.3. Mesh Convergence Study 63
3.3 Effect of Design Parameters on Velocity and Pressure Distribution 69
3.4 Evaluation and Final Selection 74
4. CONSTRUCTION AND OPERATION 77
4.1 Materials and Methods 77
4.1.1 The Bacterial Strain 77
4.1.2 Culture Media 77
4.1.3. Analyses 79
4.2 Construction 82
4.2.1 Inlet and Outlet Manifolds 83
4.2.2 Tubing 84
4.2.3 Stand 86
4.3 Pump Selection 86
4.4 Process Flow Diagram 89
4.5 Operation 90
4.5.1 Sterilization and Leakage Test 90
4.5.2 Inoculation 90
4.5.3 Continuous Feeding 91
4.5.4 Sampling 94
5. RESULTS AND DISCUSSION 95
5.1 September 2014 Outdoor Experiment with *Rhodobacter capsulatus YO$_3$* (hup$^-$) on Molasses (Run 092014) 95
5.2 July 2015 Outdoor Experiments with *Rhodobacter capsulatus YO$_3$* (hup$^-$) (Run 072015) 101
5.2.1 Run 072015-R1: Outdoor Experiment with *Rhodobacter capsulatus YO$_3$* (hup$^-$) on Artificial Medium 102
5.2.2 Run 072015-R2: Outdoor Experiment with *Rhodobacter capsulatus YO$_3$* (hup$^-$) on Molasses in July 107

5.3 Overall Evaluation of the Stacked U-tube Reactor and the Comparison of Productivities with Other Outdoor Studies 115
6.CONCLUSIONS AND RECOMMENDATIONS 121
REFERENCES 125
APPENDICES
A. COMPOSITION OF THE GROWTH MEDIA 137
B. MOLASSES ANALYSES 139
C. DIAMETER SELECTION 143
C.1. Light Intensity Measurements 143
C.2. Photon Count Measurements 145
C.3. Absorbance Experiments 147
D. PUMP SELECTION 149
D.1. Experimental Procedure for Pump Selection 149
D.2. pH variation 150
D.3. Experimental Data of the Pump Selection 151
E. CALIBRATION CURVE OF THE DRY CELL WEIGHT 153
F. LIGHT ABSORPTION SPECTRA OF *Rhodobacter capsulatus YO3* (hup$^-$) 155
G. SAMPLE GAS CHROMATOGRAM FOR GAS ANALYSIS 157
H. SAMPLE HPLC CHROMATOGRAM AND CALIBRATION CURVES OF ORGANIC ACIDS AND SUCROSE 159
I. MODEL OUTPUTS 163
J. OUTDOOR EXPERIMENTAL DATA 165
K. SAMPLE CALCULATION 193
K.1 Sample Calculation for Productivity 193
K.2 Sample Calculation for Substrate Conversion Efficiency 194
K.3 Sample Calculation for Light Conversion Efficiency 194

LIST OF TABLES

TABLES

Table 2.1: The comparison of dark fermentation studies in terms of their productivities and substrate conversion efficiencies 18
Table 2.2: The comparison of indoor photofermentation studies in terms of their productivities and substrate conversion efficiencies 27
Table 2.3: Comparison of productivities and yields for mixed cultures for simultaneous dark and photofermentation 37
Table 3.1: The default values of Newton's method 62
Table 3.2: Details of runs done for the mesh convergence study. The volumetric flow rate was 25 L/h (Ret=92), the tube pitch was 10.5 cm and the tube length was 1.4 m. 66
Table 3.3: Results of mesh convergence study 68
Table 3.4: The summary of the parameters studied and corresponding non-uniformity parameter. 74
Table 5.1: The feeding strategy 99
Table 5.2: The experimental results of hydrogen in outdoors with *R. capsulatus* YO_3 on artificial medium under non-sterile conditions (RUN072015-R1). 106
Table 5.3: The experimental results of hydrogen production outdoors with *R. capsulatus* YO_3 on molasses (RUN072015-R2) 113
Table 5.4: Summary of the results of experimental results 116
Table 5.5: The comparison of outdoor studies in terms of productivities and substate conversion efficiencies 117
Table D.1: The daily temperature and light intensity change 151

Table D.2: OD, and pH values for peristaltic and centrifugal pump 152
Table J.1: Daily variation in pH and cell concentration of RUN 092014. The experiment started on September 10, 2014..... 165
Table J.2: Daily variation in organic acid and sucrose concentration of RUN 092014. The experiment started on July 10, 2014. 166
Table J.3: Daily variation in cell concentration of RUN 072015-R1. The experiment started on July 12, 2015..... 167
Table J. 4: Daily variation in pH of RUN 072015-R1. The experiment started on July 12, 2015. 168
Table J.5: Daily variation in organic acid concentrations of RUN 072015-R1. The experiment started on July 12, 2015..... 169
Table J. 6: Biogas production of RUN 072015-R1. The experiment started on July 12, 2015. 170
Table J.7: Daily variation in cell concentration of RUN 072015-R2. The experiment started on July 12, 2015..... 171
Table J.8: Daily variation in pH of RUN 072015-R2. The experiment started on July 12, 2015. 172
Table J. 9: Daily variation in organic acid and sucrose concentrations of RUN 072015-R2. The experiment started on July 12, 2015. 173
Table J.10: Biogas production of RUN 072015-R2. The experiment started on July 12, 2015. 174
Table J.11: Data taken from the weather station on July 21, 2015. 174
Table J.12: Temperature data taken on July 21, 2015..... 185

LIST OF FIGURES

FIGURES

Figure 2.1: Share of different energy supplies in global primary energy demand. ("Other renewables" includes wind, solar (photovoltaic and concentrating solar power), geothermal, and marine.) (Mtoe means million tons of oil equivalent) (International Energy Agency, 2015). 8
Figure 2.2: Microbial bioenergy: Pathways for hydrogen production in dark fermentation. 15
Figure 2.3: Chronological summary of hydrogen productivities in dark fermentation studies. 17
Figure 2.4: Hydrogen production pathway by photofermentation in PNSB (Androga, Özgür, Eroglu, et al., 2012). 23
Figure 2.5: Chronological summary of hydrogen productivities in photofermentation studies. 24
Figure 2.6: Comparison of productivities of photofermentation 24
Figure 2.7: Cost items for two-stage biological H_2 production 34
Figure 2.8: Breakdown of capital costs for two-stage biological H_2 production 34
Figure 2.9: Operating costs for photofermentation 34
Figure 2.10: Chronological summary of hydrogen productivities in mixed cultures for simultaneous dark and photofermentation 36
Figure 2.11: Panel type PBRs (4 L) operated in outdoor conditions with internal cooling 40
Figure 2.12: Various types of tubular PBRs (Dasgupta et al., 2010) 42
Figure 2.13: Nearly horizontal tubular PBR (90 L) operated with *Rhodobacter* capsulatus (Boran et al., 2012b). 43

Figure 2.14: Velocity distribution of a manifold type PBR. The yellow streamlines indicate the distribution of particle trajectory (Androga, 2014)..... 43
Figure 2.15: Flow distribution among the tubes of a manifold a type PBR (Androga, 2014)..... 44
Figure 2.16: (a) U type manifolds (b) Z type manifolds 45
Figure 2.17:Domain discretization (a) higher level discretization in T-junctions (b) lower level discretization in the tubes (Ablanque et al., 2010) 47
Figure 3.1: The stacked U-tube PBR geometry solved via COMSOL Multiphysics 4.4. The tube pitch is 10.5 and the tube length is 4.0 m……63
Figure 3.2: Twenty meshes distributed around the manifolds (Distribution 1). 64
Figure 3.3: Twenty meshes distributed around the inlet and outlet pipes (Distribution 2)..... 64
Figure 3.4: Twenty meshes were distributed along the inlet pipe (Distribution 3).... 65
Figure 3.5: Twenty meshes were distributed around the tubes (Distribution 4). 65
Figure 3.6: Effect of tube length on the fractional volumetric flow rate for a volumetric flow rate of 25.0 L/h (Re_t=92) and tube pitch 10.5 cm 71
Figure 3.7: Effect of tube pitch for a volumetric flow rate of 25.0 L/h and a tube length of 1.4 m 72
Figure 3.8: Effect of fractional volumetric flow rates for tube pitch and tube lengths of 10.5 and 1.4 m, respectively..... 73
Figure 3.9: Pressure drop with respect to volumetric flow rate. The tube pitch and lengths are 10.5 cm and 1.4 m..... 73
Figure 4.1: Inlet and Outlet manifolds (a) front view (b) side view……..84
Figure 4.2: a) U – tubes b) Tees for sampling and thermocouples 85
Figure 4.3: U-tube PBRs operated with an aquarium pump (left) and a peristaltic pump (right). The experiment started on December 28, 2014 and lasted 3 days. 87
Figure 4.4: Variation in cell concentration for different pump types for the first day. The experiment started on December 28, 2014..... 88
Figure 4.5: Variation in cell concentration for different pump types for 3 days. The experiment started on December 28, 2014. 88

Figure 4.6: Process flow diagram of the stacked U-tube PBR. T1 – T12 are the temperature probes. V1 and V2 are check valves (1/3 psi), V4, V5, V6 and V7 are ball valves. CW-in and CW-out are cooling water inlet and outlet, respectively. 90
Figure 4.7: A photograph of the experimental set up (RUN 091025). The experiment performed with *R. capsulatus* YO_3 on molasses. 91
Figure 4.8: Side views of the Reactor 1. Experiment performed with *R. capsulatus* YO_3 on acetic acid (RUN 072015 – R1) 92
Figure 4.9: Side views of the Reactor 2. Experiment performed with *R. capsulatus* YO_3 on molasses (RUN 072015 – R2). 93
Figure 4.10: The parallel reactors run in July 2015. (RUN 072015-R1 and RUN 072015-R2). 94
Figure 5.1: (a) Comparison of temperature variation with time for different tubes on the 6th day of the experiment (T1, T5 and T9 were measured from the entrance, midpoint and exit ports in tube 4, respectively) (b) Comparison of temperatures along the length of the PBR on the 6th day of the experiment. The experiment started on September 9, 2014. (T9, T10, T11 and T12 were measured from the exit ports of tube 4, tube 3, tube 2 and tube 1, respectively.)……...96
Figure 5.2: (a) Comparison of temperature change along the length of the PBR on the 10th day of the experiment. (T1, T5 and T9 were measured from the entrance, midpoint and exit ports in tube 4, respectively.) (b) Comparison of temperature change for different tubes on the 10th day of the experiment. Experiment started on September 9, 2014. (T9, T10, T11, T12 were measured from the exit ports of tube 4, tube 3, tube 2 and tube 1, respectively.) 97
Figure 5.3: Relation between the temperature change and the daily solar radiation for RUN072015-R1. T9 is measured from the exit port of the tube 4. Experiment started on September 9, 2014. 98
Figure 5.4: Organic acid and pH variation in the reactor. Experiment started on September 9, 2014. 100
Figure 5.5: Daily sucrose concentration change. Daily sucrose concentration change. Experiment started on September 9, 2014. 100

Figure 5.6: Daily cell concentration change. Experiment started on September 9, 2014. 101
Figure 5.7: (a) Comparison of temperature variation with time for different tubes on the 9th day of the experiment (T1, T5 and T9 were measured from the entrance, midpoint and exit ports in tube 4, respectively) (b) Comparison of temperatures along the length of the PBR (RUN072015-R1) on the 9th day of the experiment. Experiment started on July 12, 2015. (T9, T10, T11, T12 were measured from the exit ports of tube 4, tube 3, tube 2 and tube 1, respectively.) 103
Figure 5.8: Relation between the temperature change and the daily solar radiation for RUN072015-R1. T9 is measured from the exit port of the tube 4. The experiment was started on July 12, 2015. 104
Figure 5.9: (a) Variation in cell concentration (b) Daily hydrogen production in outdoors with *R. capsulatus YO3* on artificial medium under non-sterile conditions (RUN072015-R1). 105
Figure 5.10: Variation in pH and organic acid concentration in outdoors with *R. Capsulatus YO3* on artificial medium under non-sterile conditions (RUN072015-R1). The starting date of the experiment was 12.07.2015. Feeding started on the 4th day. 107
Figure 5.11: Relation between the temperature change and the daily solar radiation for RUN072015-R2. T4 and T12 were measured from after the distribution manifold and before the combination manifold, respectively. Both of them were on the Tube 1. Experiment started on July 12, 2015. 109
Figure 5.12: The comparison of the temperatures for RUN072015-R1 and RUN072015-R2. R1-T12 and R2-T12 were measured on the Tube 1 just before the combination manifold. Experiments started on July 12, 2015. 109
Figure 5.13: Daily variation in sucrose concentration for RUN 072915-R2. The initial sucrose concentration was 5 mM (data not shown). The starting date of the experiment was July 12, 2015. 110
Figure 5.14: Variation in pH and organic acid concentration in outdoors with *R. capsulatus YO3* on molasses (RUN072015-R2). The starting date of the experiment was 12.07.2015. Feeding started on the 5th day. 110

Figure 5.15: Cell concentration and hydrogen production in outdoors with *R. Capsulatus YO3* on molasses (RUN072015-R2). The starting date of the experiment was 12.07.2015. 112
Figure 5.16: Daily hydrogen productivity. The starting date of the experiment was 12.07.2015. 112
Figure 5.17: Mol fractions of carbon dioxide, carbonate and bicarbonate with respect to pH. 114
Figure C.1: Light intensity variations at different depths according to different sucrose concentrations. Compartments were filled with pure sucrose at different concentrations 144
Figure C.2: Light intensity variations at different depths according to different sucrose concentrations. The compartments were filled with diluted molasses containing different amounts of sucrose. 144
Figure C.3: Light intensity variation for 3 cm depth according to different sucrose concentrations. The compartments were filled with diluted molasses containing different amounts of sucrose. 145
Figure C.4: Schematic representation of the spectroradiometer 145
Figure C.5: Photon counts with respect to wavelength for 19 mM sucrose containing molasses at different thicknesses 146
Figure C.6: Photon counts with respect to wavelength for different concentrations of sucrose in molasses. 147
Figure C.7: Comparison of absorbance values for different molasses dilutions 148
Figure D.1: pH variation for different pump types for the first day. The starting date of the experiment was Decemeber 12, 2014 150
Figure D.2: pH variation for different pump types for the first day. The starting date of the experiment was Decemeber 12, 2014. 150
Figure E.1: Calibration curve for the dry cell weight versus OD_{660} of the *Rhodobacter capsulatus YO3* (hup-) (Öztürk, 2005). Optical density of 1.0 at 660 nm corresponds to 0.4656 gdcw/L_c 153

Figure F.1: Light absroption spectra of *Rhodobacter capsulatus YO3* (hup$^-$). Optical density at 660 nm was 1.4……..155

Figure G.1: A sample gas chromotogram (Androga, 2009)…….....157

Figure H.1: A sample HPLC chromotogram. (Androga, 2009). Retention times of lactic, formic, acetic, propionic and butyric acid are 22.0, 24.5, 26.5, 31.3 and 38.6 min, respectively……...159

Figure H.2: HPLC calibration for lactic acid 160
Figure H.3: HPLC calibration for formic acid 160
Figure H.4: HPLC calibration for acetic acid 160
Figure H.5: HPLC calibration for propionic acid 161
Figure H.6: HPLC calibration for butyric acid 161
Figure I.1: Velocity profile for 3.8 m tube length, 10.5 cm tube spacing and 25 L/h volumetric flow rate……..163

Figure I.2: Pressure profile for 3.8 m tube length, 10.5 cm tube spacing and 25 L/h volumetric flow rate. 163

LIST OF SYMBOLS

a_d	Ratio of the diameter to length in the distribution manifolds	___
a_c	Ratio of the diameter to length in the combination manifolds	___
C_p	Specific heat capacity at constant pressure	J/(kg.K)
F	Volume force vector	N/m^3
F_0	Friction in the straight tube section	___
I	Light intensity	W/m^2
I	Identity tensor	___
M	Ratio of all the port areas to the manifold area of the manifold	___
M_0	Momentum flow at the entrance	___
n	Boundary normal unit vector pointing out of the domain	___
N	Number of channels	___
p	Pressure	Pa
p_{out}	Outlet pressure	Pa
q	Heat flux vector	W/m^2
$\dot{Q}$	Heat sources	W/m^3

Q_0	Total volumetric flow rate	m^3/s
Q_i	Flow rate of the *i*th channel	m^3/s
Re_p	Reynolds in the pipes of the manifold	__
s	Spacing between the tubes	m
S	Strain – rate tensor	__
t_{H2}	Duration of the hydrogen production process	h
T	Absolute temperature	K
u	Velocity vector	m/s
u_{wall}	Velocity at the solid boundary	m/s
V_{H2}	Volume of the produced hydrogen	L

Greek Letters

β	Dimensionless volumetric flow rate	___
ζ	Average total head loss coefficient for port flow	___
η	Percent light conversion efficiency	___
μ	Dynamic viscosity	Pa
ρ	Density	kg/m^3
ρ_{H2}	Density of hydrogen gas	g/L
τ	Viscous stress tensor	Pa

Note: Vectors are shown in bold.

LIST OF ABBREVIATIONS

BP	Biebl and Phening
CFD	Computational fluid dynamics
CO_2	Carbon dioxide
DFE	Dark fermenter effluent
GC	Gas chromatography
gdcw	gram dry cell weight
H_2	Hydrogen
HPLC	High performance liquid chromatography
L_c	Liter culture
LDPE	Low-density polyethylene
OD	Optical density
PBR	Photobioreactor
PMMA	Poly(methyl methacrylate)
PNSB	Purple non-sulfur bacteria
PU	Polyurethane
PVC	Polyvinyl chloride
R1	Reactor 1
R2	Reactor 2

CHAPTER 1

INTRODUCTION

The global energy demand is escalating due to the increase in the world population and industrialization. Today, oil and gas constitute 80% of the global primary energy supply (Ball & Wietschel, 2009). However, it is obvious that this energy demand cannot be supplied from fossil fuels forever, due to the depletion of fossil fuels and climate change which is caused by the excessive usage of carbon based energy carriers. Furthermore, there is an urgent need to replace fossil fuels with alternative energy supplies in order to prevent irreversible changes in climate. Being aware of the risks, international organizations are working with governments in order to avoid 'dangerous anthropogenic interference with the climate change'. In 2015, COP21 (Conference of Parties 21), aimed to keep global warming below 2ºC via a legal universal agreement after 20 year of United Nations' negotiations ("UNFCCC COP 21 Paris France - Climate Conference," 2015). International Energy Agency (IEA) assessed the effects of the Intended Nationally Determined Contributions (INDCs), which is submitted by the countries in advance of COP21, on the energy sector. According to the INDC Scenario, global energy related emissions' growth have been reduced with the help of national pledges. IEA predicted that the share of fossil fuels in the world energy supply will decline to 75 % by 2030 (International Energy Agency, 2015).

With its carbon-free combustion products and its high energy content, hydrogen is a promising alternative to fossil fuels. On a mass basis, hydrogen has 2.4, 2.8 and 4 times higher energy content compared to methane, gasoline and coal, respectively (Marbán & Valdés-Solís, 2007). Actually, the use of hydrogen as an energy carrier is not a new

concept. Hydrogen was utilized for street lightning and home energy supply in many countries until the 1960s. With the advances in fuel cell technology in the late 1990s, hydrogen is now attracting more attention. Today, 700 billion Nm^3 hydrogen is being produced. This amount of hydrogen is enough for 600 million fuel cell cars. Most of the produced hydrogen is utilized as a reactant in chemical and petrochemical industries. 50% of the produced hydrogen is used in the ammonia production. Crude oil processing utilizes 40% of the produced hydrogen (Ball & Wietschel, 2009).

Natural gas reforming, coal gasification and water electrolysis are the main hydrogen production routes used in industrial scale. (Ball & Wietschel, 2009). Current hydrogen production technologies depend heavily on fossil fuels. 40 % of the hydrogen is produced from natural gas, 30% from crude oil and 18% from coal, and 4% of hydrogen is obtained from water electrolysis (Brentner, Peccia, & Zimmerman, 2010). Natural gas reforming is the most commonly used hydrogen production method. It is the cheapest hydrogen production method with low CO_2 emissions compared to other fossil fuel dependent methods. However, in order to be sustainable, hydrogen has to be produced from renewable energy sources (Ball & Wietschel, 2009). Electrolysis of water (by utilizing energy coming from wind power, hydropower or photovoltaics), biomass conversion by gasification or pyrolysis could be counted as renewable routes for hydrogen production. Each route has its own challenges mostly related with high cost requirements. Biological hydrogen production methods have the potential to produce hydrogen with an economically feasible operation from renewable energy sources (Androga, 2014; Brentner et al., 2010)

There are different ways of producing biological hydrogen. Direct and indirect biophotolysis, dark fermentation, and photofermentation are the main biological hydrogen production methods. In direct and indirect biophotolysis, hydrogen can be produce directly from water utilizing sunlight. In dark fermentation, a variety of carbon sources including organic wastes could be utilized to produce hydrogen. In photofermentation, carbon sources including organic acids and wastes can be

converted into hydrogen with the help of light under anoxygenic conditions (Nath & Das, 2004). Das and Veziroglu (2001) reported that photofermentation is the most promising microbial system for biohydrogen production. The advantages of photofermentation can be listed as follows (Das & Veziroglu, 2001; Fernandez-Sevilla, Acien-Fernandez, & Molina-Grima, 2014):

- Theoretically, high substrate conversion efficiencies (high yields),
- Lack of O_2 evolution, which inhibits enzymes responsible for H_2 production,
- Ability to utilize various organic substrates including wastewaters,
- Ability to capture a wide range of solar spectrum (from 300 to 1000 nm).

Purple non sulfur bacteria (PNSB), which are the members of the *Rhodobacter* species, are the most commonly used microorganisms in photofermentation. (I. Eroglu, Özgür, Eroglu, Yücel, & Gündüz, 2014). There is an optimum biomass concentration (0.5 – 0.7 gdcw/L_c) for hydrogen production. The optimum temperature ranges from 30ºC to 35ºC. Phosphate buffer is generally utilized to keep pH in the range between 6.5 and 9. (Sasikala, Ramama, & Raghuveer Rao, 1991). There have been different approaches on the modification of the microorganism so that higher hydrogen productivities could be obtained. Öztürk improved the hydrogen production by deleting the gene coding for the uptake hydrogenases, which is responsible for hydrogen consumption, of *Rhodobacter capsulatus* YO_3 (hup^-) modified by Öztürk was used in this study (Öztürk et al., 2006).

Purple non-sulfur bacteria can produce hydrogen from a wide variety of organic substrates such as short chain organic acids (acetate, butyrate, propionate and lactate), and sugars (glucose and sucrose). The initial organic acid and sugar concentration affects the hydrogen production, biomass growth rate and the time. When artificial media is utilized, supplementary nutrients such as iron, molybdenum, trace elements and vitamins are added. Vitamins and trace elements are already available in many of

the reel feedstock. Therefore, real feedstocks that are used in the photofermentation are generally dark fermenter effluents (DFE) of different wastes obtained from pulp and paper industry, sugar processing industry, cheese manufacturing and olive mill factories (I. Eroglu et al., 2014). Single stage photofermentation of sugar industry wastes have also been studied. Productivity was found as 0.41 mol $H_2/(m^3.h)$ utilizing *Rhodobacter capsulatus* YO_3 on molasses (Sağır, 2012). In another study, hydrogen production improved with single stage photofermentation of molasses compared with the DFE of molasses. The highest productivity from black strap and beet molasses was found as 1.59 and 1.44 mol $H_2/(m^3.h)$ (Keskin & Hallenbeck, 2012).

For photofermentation to be economically feasible, the process should be carried out in large scale, under natural sunlight and using cheap feedstock. Large scale photobioreactors (PBR) should be assessed and compared in terms of their biological hydrogen production capacities (productivities). Some of the important criteria for an optimum PBR configuration are listed below.

- The PBR should have large illuminated area to ground area ratio.
- PBR material should be impermeable to hydrogen and air.
- The material should be transparent, allowing maximum light penetration.
- The reactor material should be inert and easy to clean.
- The reactor should be easy to cool.

So far, two common types of PBRs have been used: panel and tubular. Panel type PBRs are advantageous in terms of illuminated area to ground area compared to tubular reactors (Jakub Gebicki, Modigell, Schumacher, Van Der Burg, & Roebroeck, 2010). However, it is hard to mix panel type PBRs. In tubular reactors, mixing is achieved by circulating the reactor contents by means of a pump. The mixing rate is known to have an effect on the hydrogen production (Li et al., 2011). Gebicki studied with a manifold type PBR and observed the highest hydrogen production when

Reynolds number was 240 (Jakub Gebicki et al., 2010). However, when flow is distributed with manifolds, the flow rate varies significantly from the tube to tube according to Reynolds number, and manifold diameter to length ratio (Ahn, Lee, & Shin, 1998). A proper flow model can provide insight on the uniformity of flow rate.

The aim of this work was to design a tubular PBR which has good light and velocity distribution, efficient cooling system and high illuminated area to ground area ratio and an efficient gas collection unit. Moreover, the reactor material should have low hydrogen and air permeability, and should be durable in outdoor conditions. Another aim was to test the designed PBR in outdoor conditions. While designing the reactor, a hydrodynamic model was developed. Two reactors were constructed whose dimensions were based on the model results. The volume of the reactors was about 10 L. 3 experiments were performed in outdoor conditions to test the new reactor configuration. In two experiments, *Rhodobacter capsulatus* YO_3 on molasses was utilized. In another experiment, *Rhodobacter capsulatus* YO_3 was on artificial medium containing acetate was studied.

In the following chapter (Chapter 2), commercial hydrogen production techniques and biological hydrogen production processes are reviewed. PBR types are explained. The effect of different parameters on the flow distribution in manifolds, which are commonly used to distribute the flow to the tubes in PBRs are mentioned.

Chapter 3 describes the stacked U-tube PBR design. The parameters that needs to be considered while designing PBRs are given. The design strategy, method of attack was described. Hydrodynamics of a manifold type PBR (stacked U-tubes PBR) was modelled with COMSOL 4.4. The methods and the results were told in detail. The dimensions of the stacked U-tube PBR was determined by investigating the flow uniformity.

The details about construction and operation of stacked U-tube PBR was told in Chapter 4. The experimental procedure was also given in this chapter. The experimental results about the pump selection was discussed.

Chapter 5 covers the results of the outdoor pilot scale experiments that are performed in September 2014 and July 2015 by utilizing *Rhodobacter capsulatus* YO_3.

In the final chapter (Chapter 6), conclusions and further recommendations are stated. The thesis is concluded with the references and appendices parts.

CHAPTER 2

LITERATURE SURVEY

2.1 Hydrogen as an Energy Carrier

Today, world's energy demand is met mainly by fossil fuels. The consumption of the fossil fuels are increasing due to the industrialization of the developing nations and the increase in the world population. Currently, renewable energy sources constitute 14 % of the total world energy demand. The renewable energy sources are expected to play a major role in the worlds energy supply in the future, increasing the standard of living (Panwar, Kaushik, & Kothari, 2011). The share of various energy supplies in global primary energy demand from 2000 to 2030 is shown in Figure 2.1. From Figure 2.1, it can be concluded that the share of low carbon-sources in the worlds' fuel supply starts to increase especially after 2020 (International Energy Agency, 2015).

Hydrogen with its high energy content and carbon free combustion products is a dream fuel for the future. However, being the most abundant element in planet, hydrogen is not found in its elemental form in nature. 99 % of the hydrogen is produced from fossil fuels. Steam reforming of natural gas or naphtha, partial oxidation of hydrocarbons, coal gasification, biomass gasification and electrolysis of water are the commercial hydrogen production methods that are currently used. These processes are highly energy intensive and not environmentally friendly. On the other hand, microorganisms could be utilized to catalyze thermodynamically unfavored reactions. The interest in biohydrogen is started to increase in the early 90s when the effects of fossil fuel based pollution on the climate change became evident. Such biological systems can solve the

energy problem locally where biomass and wastes are available. By this way, costs for energy transport could be decreased. Additionally, with the new job areas in rural areas associated with the energy production, the mitigation to cities from towns could be reduced (Nath & Das, 2004; Panwar et al., 2011).

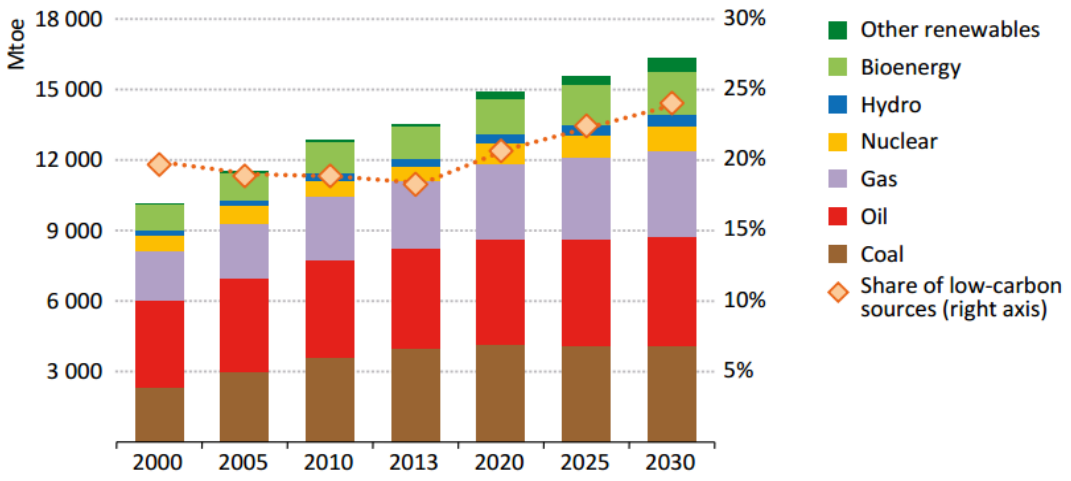

Figure 2.1: Share of different energy supplies in global primary energy demand. ("Other renewables" includes wind, solar (photovoltaic and concentrating solar power), geothermal, and marine.) (Mtoe means million tons of oil equivalent) (International Energy Agency, 2015).

In this chapter, commercial hydrogen production techniques were summarized and biological hydrogen production methods were reviewed. Then, PBR types were investigated. Manifold type PBR was selected for this study. Lastly, some of the manifold models in the literature were mentioned.

2.2 Commercial Hydrogen Production Techniques

2.2.1 Natural Gas Steam Reforming

Currently, most of the hydrogen is produced by the steam reforming process. Steam reforming is an endothermic process operating in the temperature range of 970 – 1100 K and at a pressure up to 3.5 MPa. Generally, nickel catalysts are preferred. The basic

reactions are shown below. Generally, natural gas is used as feedstock; however, heavier hydrocarbons up to naphtha can also be used. Large amounts of CO_2 are released during natural gas steam reforming process since fossil fuels are used both as a raw material and as a heat source. (Kothari, Buddhi, & Sawhney, 2008).

$$C_nH_m + nH_2O \longrightarrow nCO + (n + m/2)H_2 \quad (2.1)$$

$$CO + H_2O \longrightarrow CO_2 + H_2 \quad (2.2)$$

2.2.2 Partial Oxidation of Hydrocarbons

Partial oxidation of hydrocarbons utilizes oxygen and steam. The reaction is exothermic and it is carried out at moderately high pressures.

$$2C_nH_m + H_2O + 23/2\ O_2 \longrightarrow nCO + nCO_2 + (m+1)\ H_2 \quad (2.3)$$

The use of catalyst depends upon the feedstock type and process. All kinds of gaseous and liquid fuels including heavy oil or petroleum residual oils could be utilized in partial oxidation processes. The major drawback of this process is carbon monoxide emission along with carbon dioxide. (Kothari et al., 2008).

2.2.3 Coal Gasification

Pulverized coal is reacted with pure oxygen at high temperatures. Syngas (mixture of CO_2 and H_2) is obtained after the desulfurization process. Hydrogen is obtained from syngas with pressure swing adsorption. The basic coal gasification reaction is shown below (Kothari et al., 2008).

$$CH_{0.8} + 0.6\ O_2 + 0.7\ H_2O \longrightarrow CO_2 + H_2 \quad (2.4)$$

2.2.4 Biomass Gasification

Biomass gasification is similar to coal gasification. The gasification process, gas cleaning section, the water gas shift reaction and the pressure swing adsorption are the main sections of biomass gasification. Since biomass does not contain sulfur, gas cleaning is relatively easier. The biomass gasification process has not been fully commercialized and needs further research (Pilavachi, Chatzipanagi, & Spyropoulou, 2009).

2.2.5 Electrolysis

In electrolysis, water is broken down into hydrogen and oxygen when electricity is passed through an aqueous electrolyte.

$$2H_2O \longrightarrow 2H_2 + O_2 \qquad (2.5)$$

Electricity used in electrolysis could be taken from any source such as off-peak power, solar and wind sources. Different kinds of electrolyzers could be utilized. (Ogden, 1999).

2.3 Review of Biohydrogen Production Technologies

Biological hydrogen production has the potential to complement the global hydrogen supply and help reduce the dependence on fossil fuels. During the past two decades, many improvements have been made in biological hydrogen production such as identifying the producer microorganisms, modifying microorganisms genetically to improve hydrogen production, and improve reactor designs (Brentner et al., 2010).

Biophotolysis, dark fermentation and photofermentation are the main biological routes for hydrogen production. Light energy could be utilized directly as in biophotolysis

and photofermentation. As in the case of dark fermentation, light could be utilized indirectly by consuming carbon compounds that are themselves the products of photosynthesis (Hallenbeck & Ghosh, 2009). In order to quantify and compare hydrogen production efficiencies in biological systems, definitions such as yield, productivity and light conversion efficiency are utilized.

Substrate conversion efficiency (Y_{H2}) is an important measure for the substrate utilization in such systems. In most of the biological systems, substrate conversion efficiency is defined as shown in Equation 2.6.

$$Substrate\ conversion\ efficiency\ (\%) = \frac{moles\ of\ H_2\ produced}{\begin{array}{c}Theoretical\ moles\ of\ H_2\ that\ could\ be\ produced \\ if\ all\ the\ substate\ was\ used\ for\ H_2\ production\end{array}}\ x\ 100 \quad (2.6)$$

Productivity, which is shown in Equation 2.7, is another important definition quantifying the hydrogen production in biological systems. Productivity is defined as the amount of hydrogen produced per reactor volume per time. Productivity is also defined as the hydrogen produced per ground area per time. Throughout this thesis, productivity is attributed to the former definition.

$$Productivity = \frac{Amount\ \ of\ H_2\ produced}{Volume\ of\ the\ reactor\ x\ Time} \quad (2.7)$$

Light conversion efficiency is another measure for hydrogen production via photolysis and photofermentation. Light conversion efficiency (Equation 2.8) is termed as the ratio of the heat of combustion of hydrogen to the total energy input come with the light radiation.

$$\eta = \frac{V_{H2} \cdot \rho_{H2} \cdot 33.61}{I \cdot A \cdot t_{H2}} \cdot 100 \quad (2.8)$$

where η is the percent light conversion efficiency, 33.61 is the energy density of hydrogen gas (W.h/g), V_{H2} is the volume of the produced hydrogen (L), ρ_{H2} is the density of hydrogen gas (g/L), I is the light intensity (W/m^2) $t_{H2}$is the duration of the hydrogen production process (h).

The main routes for biological hydrogen production are photolysis, dark fermentation and photofermentation. These modes of production are summarized next.

2.3.1 Photolysis

Direct and indirect biophotolysis could be utilized with the purpose of biohydrogen production. In direct biophotolysis, solar energy is used to convert water to oxygen and hydrogen by photosynthetic reaction.

$$2\ H_2O + \text{`light energy'} \longrightarrow 2\ H_2 + O_2 \qquad (2.9)$$

The existence of such a reaction in green algae was suggested in 1958 (Spruit, 1958). In 1973, Reaction 2.9 was demonstrated for a cell free chloroplast-ferredoxin-hydrogenase system (Benemann, Berenson, Kaplan, & Kamen, 1973).

Some green algae which have Fe-hydrogenase enzyme have the ability to carry out direct photolysis. The Fe – hydrogenase enzyme is highly O_2 sensitive, which is the main problem of direct photolysis. A partial pressure of O_2 less than 0.1 %, which corresponds to 1 micromolar O_2 in liquid phase, is essential for the simultaneous production of O_2 and H_2. Therefore, a large amount of diluent gas is required which requires a large power input (Hallenbeck & Benemann, 2002).

In indirect biophotolysis, the oxygen sensitivity of the photolysis is overcome by separating the O_2 and H_2 evolution reactions (Reactions 2.10 & 2.11). Cyanobacteria have the ability to use CO_2 in the air as the carbon source, and are able to produce hydrogen under sunlight (Manish & Banerjee, 2008).

$$6\ H_2O + 6\ CO_2 + \text{‘light energy’} \longrightarrow C_6H_{12}O_6 + 6\ O_2 \quad (2.10)$$

$$C_6H_{12}O_6 + 6\ H_2O + \text{‘light energy’} \longrightarrow 12\ H_2 + 6\ CO_2 \quad (2.11)$$

For indirect biophotolysis to be economically feasible, new PBR designs are needed. Photochemical efficiencies of such systems are still low. Therefore, metabolic engineering is also required to improve the efficiency (Brentner et al., 2010).

2.3.2 Dark Fermentation

A wide variety of bacteria could produce hydrogen, organic acids and CO_2 from carbohydrates under anaerobic conditions through dark fermentation. In general, a mixture of unknown microorganisms (sludge) is fed to the bioreactor. Hydrogen production is mainly dominated by *Clostridium* species (Brentner et al., 2010). *Clostridium butyricum* (Kataoka, Miya, & Kiriyama, 1997), *Clostridium pasteurianum* (Chun Yen Chen, Yang, Yeh, Liu, & Chang, 2008), *Clostridium beijerinkii* (Jeong, Cha, Yoo, & Kim, 2007), activated sludge (W. Q. Guo et al., 2008), *Escherichia coli* (Redwood & Macaskie, 2006), *Enterobacter cloacae* (Nath, Muthukumar, Kumar, & Das, 2008) microflora (Tao, Chen, Wu, He, & Zhou, 2007), *Ruminococcus albus* (Ntaikou, Gavala, Kornaros, & Lyberatos, 2008), and Caldicellulosiruptor owensensis (Zeidan & van Niel, 2010) are the preferred species in dark fermentation. As a consortium of microorganisms is generally preferred, dark fermentation systems are more stable, and can adapt to environmental changes easily. (Brentner et al., 2010). Usually, monosaccharides are the main carbon source. The metabolic pathway differs among the microbes.

The hydrogen production pathways of dark fermentation are shown in Figure 2.2 (Hallebeck, 2014). In dark fermentation as in other fermentation types, sugars, typically glucose, are broken down to pyruvate, and NADH and ATP are generated. Then, pyruvate is converted to acetyl-CoA. During this process, two different pathways could be followed. One is the formate production through pyruvate formate lyase (PFL) pathway, while the other is the reduced ferredoxin and CO_2 production through the pyruvate ferredoxin oxidoreductase (PFO) pathway. Hydrogen and CO_2 could be produced from formate by hydrogen lyase pathway containing [NiFe] hydrogenase (the Ech hydrogenase), or by a formate dependent [FeFe] hydrogenase pathway depending on the microorganism. NADH produced during pyruvate formation is oxidized by the production of other carbon compounds such as ethanol. Different types of [FeFe] hydrogenases are utilized to produce hydrogen by reoxidizing ferredoxin. NADH could also be used in hydrogen production. Other fermentation products are also produced if NADH is in excess (Hallebeck, 2014).

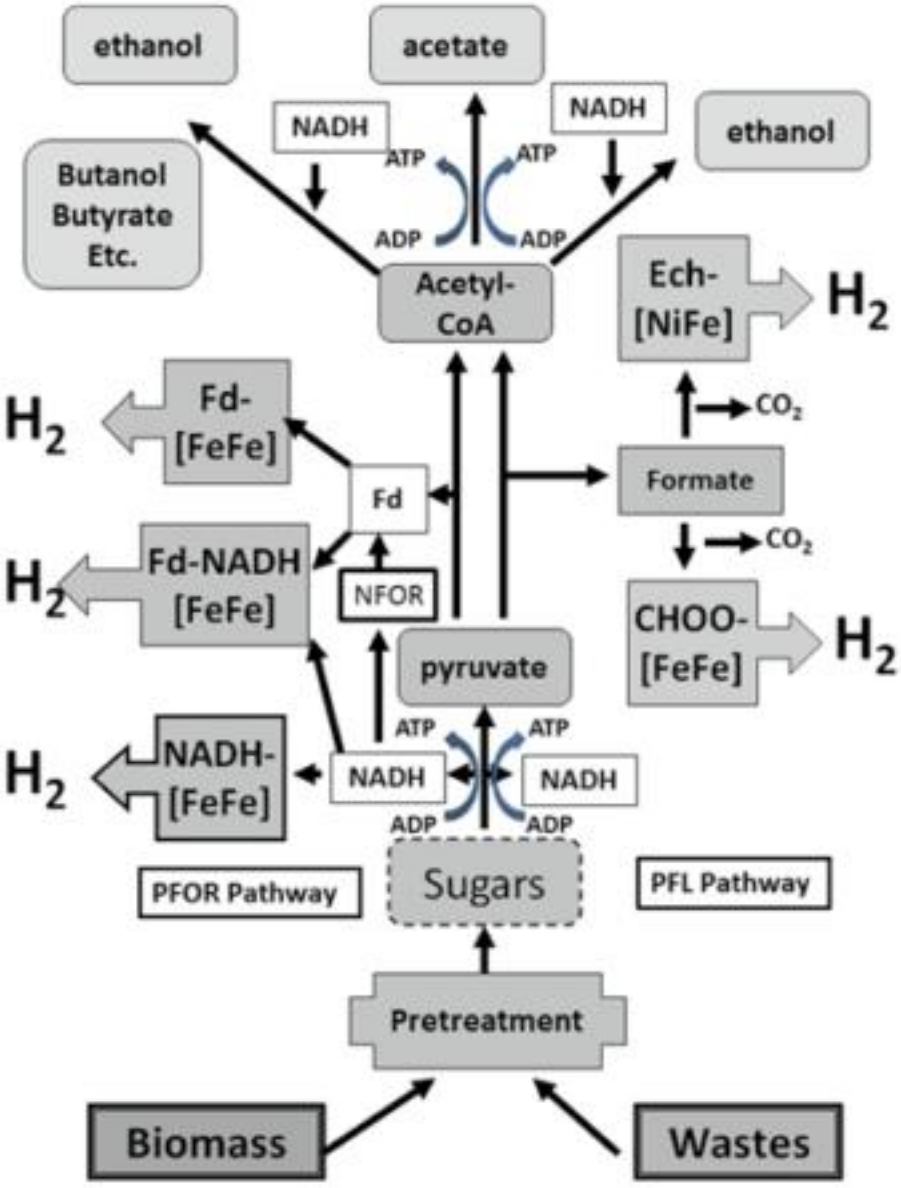

Figure 2.2: Microbial bioenergy: Pathways for hydrogen production in dark fermentation.

Glucose and sucrose are the two common substrates for dark fermentation. Depending on the metabolism, organic acids such as acetic acid, butyric acid, propionic acid and formic acid are produced from these substrates. The dark fermentation of glucose is shown in Equation 2.12 when acetic acid is the only end product of the fermentation

process. The theoretical hydrogen yield through dark fermentation is 4 mole of H_2 per mole of glucose if the acetic acid pathway is used. (Argun & Kargi, 2011; Hawkes, Dinsdale, Hawkes, & Hussy, 2002) Hydrogen production from glucose when butyrate is the fermentation end product is shown in Equation 2.13. The theoretical yield is 2 mole of hydrogen per mole of glucose when the butyrate pathway is used during fermentation (Hawkes et al., 2002).

$$C_6H_{12}O_6 + 2\ H_2O \longrightarrow 2\ CH_3COOH + 4\ H_2 + 2\ CO_2 \quad (2.12)$$

$$C_6H_{12}O_6 \longrightarrow 2\ CH_3CH_2CH_2COOH + 2\ H_2 + 2\ CO_2 \quad (2.13)$$

Propionic acid production from glucose is shown in Equation 2.14 [52].

$$C_6H_{12}O_6 + 2\ H_2 \longrightarrow 2\ CH_3CH_2COOH + 2\ H_2O \quad (2.14)$$

Theoretical hydrogen yield from sucrose is 8 mole of hydrogen as shown in Equation 2.15 by sequential dark and photofermentation if acetic acid is the only VFA.

$$C_{12}H_{22}O_{11} + 5\ H_2O \longrightarrow 4\ CH_3COOH + 8\ H_2 + 4CO_2 \quad (2.15)$$

CSTRs (continuous stirred tank reactor) are generally used in dark fermentation for continuous operation (Chun Yen Chen et al., 2008; Yokoi et al., 2001; Yokoi, Tokushige, Hirose, Hayashi, & Takasaki, 1998a). However, the optimum reactor configuration was found as one combining the moving bed and trickling bed operation in the Hyvolution project carried under EU 6th Framework Programme between 2006 – 2010 (Urbaniec & Grabarczyk, 2014).

The productivities of different studies are shown in

Figure 2.3. Typically dark fermentation values in literature are in between 10 and 50 mol $H_2/(m^3.h)$ (Androga, Özgür, & Eroglu, 2012; Datar et al., 2007; Zeidan & van Niel, 2010). These productivities are higher compared to photofermentation.

However, the major drawback of dark fermentation is its low yield and low hydrogen purity. The biogas obtained by dark fermentation has to be purified to recover the hydrogen (Brentner et al., 2010). When glucose is consumed without any side products; 12 moles of hydrogen should be produced. However, the yields obtained are about a third of this theoretical maximum. Due to such low yields, large amounts of side products are produced, which causes a huge waste disposal problem (Hallebeck, 2014).

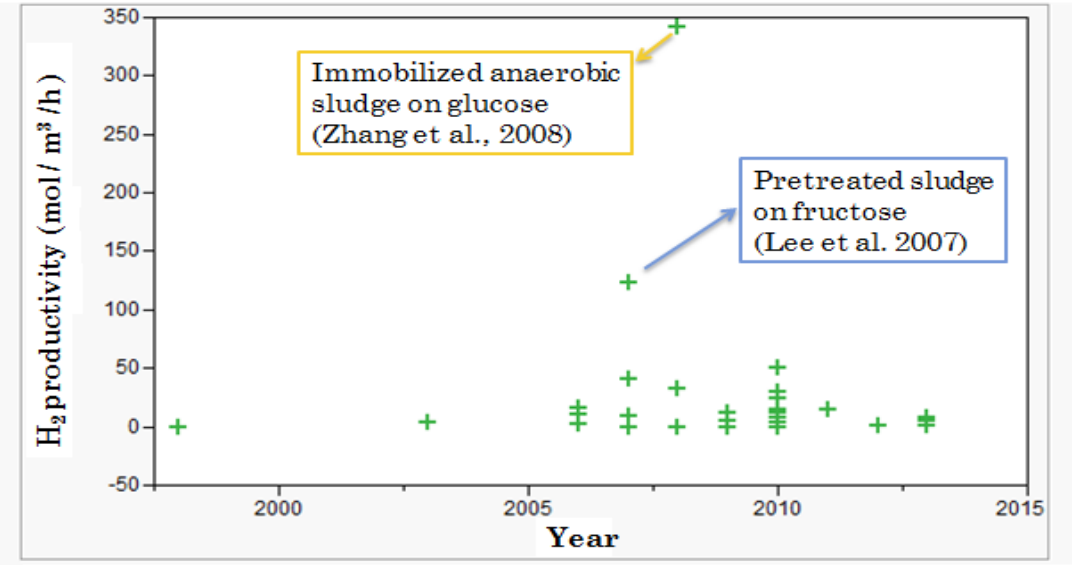

Figure 2.3: Chronological summary of hydrogen productivities in dark fermentation studies.

The studies with the highest productivities are highlighted in Figure 2.3. All the studies shown in Figure 2.3 are given in Table 2.2.

Table 2.1: The comparison of dark fermentation studies in terms of their productivities and substrate conversion efficiencies

Mode of operation	**Type of the bacteria**	**Suspended /Immobilized**	**Carbon source**	**H_2 productivity (mol H_2/(m^3.h)**	**H_2 yield (mol H_2/mol glucose)**	**Reference**
Continuous	seed sludge rich in Clostridium sp.	Suspended	Condensed molasses fermentation solubles	0.02	2.1	(Lay et al., 2010)
Continuous	Sludge	Immobilized	Molasses from a local beet sugar refinery	31.91	1.7	(W. Q. Guo et al., 2008)
Continuous	Clostridium butyricum and Enterobacter aerogenes	Immobilized	Starch (without any reducing agent)	58.42	2.6	(Yokoi et al., 1998a)
Batch	Enterobacter cloacae DM11	Immobilized	Glucose	29.42	3.3	(Nath et al., 2008)
Batch	Caldicellulosiruptor saccharolyticus DSM 8903	Suspended	Molasses	7.1	2.1	(Özgür, Mars, et al., 2010)

Table 2.1.continued

Mode of operation	Type of the bacteria	Suspended /Immobilized	Carbon source	H2 productivity (mol H2/(m3.h)	H2 yield (mol H2/mol glucose)	Reference
Batch	*Clostridium butyricum KBH1*	Suspended	Oil palm empty fruit branch molasses	0.92	—	(Abdul et al., 2013)
Batch	Pre-heated activated sludge	Suspended	Hydrolyzed cassava strach	11.79	2.0	(Su, Cheng, Zhou, Song, & Cen, 2009b)
Batch	Anaerobic sludge	Suspended	Ground wheat solution	3.11	1.9	(Argun & Kargi, 2010b)
Batch	Anaerobic mixed bacteria (mainly Clostridium species)	Suspended	Cassava stach	15.05	2.5	(Cheng, Su, Zhou, Song, & Cen, 2011)
Batch	Clostridium pasteurianum CH4	Suspended	Sucrose	—	1.9	(Chun Yen Chen, Yeh, Lo, Wang, & Chang, 2010)

Table 2.1.continued

Mode of operation	Type of the bacteria	Suspended /Immobilized	Carbon source	H2 productivity (mol H2/(m3.h)	H2 yield (mol H2/mol glucose)	Reference
Batch	Clostridium butyricum CGS5	Suspended	Sucrose	11.95	0.5	(Perera, Ketheesan, Gadhamshetty, & Nirmalakhandan, 2010)
Batch	Ruminococcus albus	Suspended	Sweet sorghum	4.73	3.1	(Ntaikou et al., 2008)
Batch	Pre-treated anaerobic sludge	Suspended	Corn stover acid hydrolyzate (20%, v/v)	0.12	3.0	(Datar et al., 2007)
Batch	Caldicellulosiruptor owensensis OLT (DSM 13100)	Suspended	Glucose suplemented with a rich vitamin soln.	15	3.8	(Zeidan & van Niel, 2010)
Continous	Caldicellulosiruptor owensensis OLT (DSM 13100)	Suspended	Glucose	10.43	4.6	(N. Ren, Li, Li, Wang, & Liu, 2006)
Continous	Heat shocked agricultural soil	Suspended	Glucose	3.64	2.8	(Van Ginkel & Logan, 2005)

2.3.3 Photofermentation

Purple non sulfur bacteria (PNSB) are able to convert organic acids into H_2 and CO_2 under anaerobic and nitrogen limited conditions by utilizing sunlight. Some PNSB commonly used in photofermentation are *Rhodopseudomonas palustris* (Chun Yen Chen et al., 2008), *Rhodobacter sphaeroides* (Redwood & Macaskie, 2006), and *Rhodobacter capsulatus* (Androga, Özgür, & Eroglu, 2012; Özgür, Uyar, et al., 2010). Pure cultures used in photofermentation enables the engineering of the metabolisms according to the needs (Brentner et al., 2010).

Nitrogenase is the enzyme responsible from hydrogen production in photofermentation. The following reaction shows the nitrogen fixation by nitrogenase to produce hydrogen (Androga, Özgür, Eroglu, Gündüz, & Yücel, 2012).

$$N_2 + 8H^+ + 8e^- + 16\ ATP \longrightarrow NH_3 + H_2 + 16\ ADP + 16\ P_i \quad (2.16)$$

Under nitrogen limited conditions, nitrogenase works similar to hydrogenase and catalyzes protons to produce molecular hydrogen. Therefore, under nitrogen limited conditions, with the same energy consumption, 4 times more hydrogen can be produced (Androga, Özgür, Eroglu, et al., 2012).

$$2H^+ + 2e^- + 4\ ATP \longrightarrow H_2 + 4\ ADP + 4\ P_i \quad (2.17)$$

Hydrogen can also be produced via the membrane-bound H_2-uptake hydrogenase through the reversible reaction (Androga, Özgür, Eroglu, et al., 2012):

$$2H^+ + 2e^- \longleftrightarrow H_2 \quad (2.18)$$

The metabolic pathway of the hydrogen production is affected by three external factors: carbon source, light and oxygen availability. PNSB can utilize many carbon

sources such as sugars, short chain organic acids, amino acids, alcohol and polyphenols. The hydrogen production pathway by photofermentation in PNSB is shown in Figure 2.4. By the oxidation of organic acids, electrons are generated. Electrons are then transferred to cytochrome c (Cyt c). Then, by passing through a number of electron transport proteins electrons are transferred to ferredoxin (Fd). At the same time, protons are pumped through the membranes and a proton gradient is formed. This gradient triggers the ATP synthase and ATP is produced. Electrons are transferred to nitrogenase enzyme with the help of ferredoxin and molecular hydrogen is produced (Androga, Özgür, Eroglu, et al., 2012).

Three different nitrogenase enzymes are known: Nif, Vnf and Anf whose active metals are Mo, V and Fe, respectively. Besides nitrogenase, hydrogenase is also an important enzyme in photofermentative hydrogen production, which is responsible for the oxidation of molecular hydrogen to form protons and the reduction of protons to form H_2. The hydrogenase types are [FeFe]-hydrogenase, [NiFe]-hydrogenase and [Fe]-hydrogenase. Hydrogen is consumed by [NiFe]-hydrogenase; whereas hydrogen is produced by the activities of [FeFe]-hydrogenase enzyme (Androga, Özgür, Eroglu, et al., 2012).

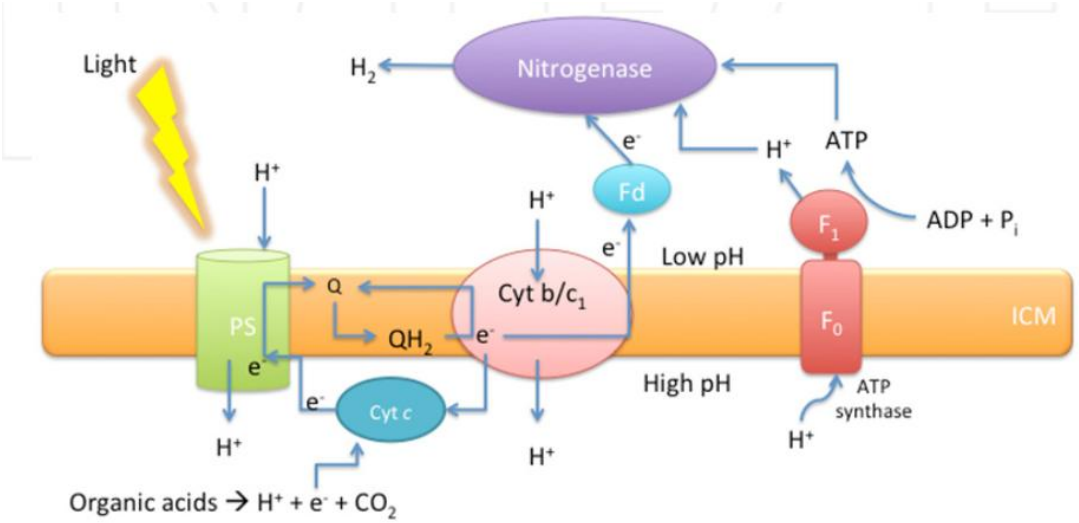

Figure 2.4: Hydrogen production pathway by photofermentation in PNSB (Androga, Özgür, Eroglu, et al., 2012).

PNSB has the ability to utilize sunlight as mentioned above and drive thermodynamically unfavorable reactions (Brentner et al., 2010). Acetate, which is the most common carbon source used for photofermentation can be consumed by photosynthetic bacteria through the following reaction. The theoretical hydrogen yield is 4 mole of H_2 per mole of acetic acid when acetic acid is the only carbon source (Manish & Banerjee, 2008).

$$CH_3COOH + 2\ H_2O \longrightarrow 4\ H_2 + 2\ CO_2 \qquad (2.16)$$

Photosynthetic microorganisms can divert all of the electrons from an organic substrate. Therefore, high yields are obtained from photofermentation. This is a noteworthy advantage over dark fermentation (Brentner et al., 2010).

The hydrogen productivities according to years are shown in Figure 2.5. In order to see the improvement in productivities in years, a comparison of productivities with the most promising data found from literature is shown in Figure 2.6. In general, hydrogen productivities in photofermentation are in the order of 1 mol $H_2/(m^3.h)$.

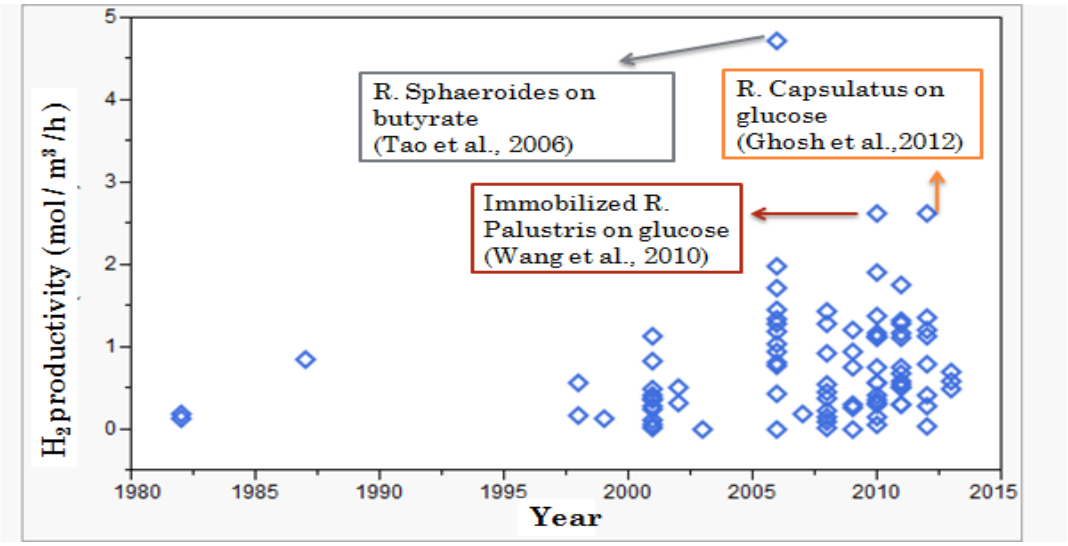

Figure 2.5: Chronological summary of hydrogen productivities in photofermentation studies

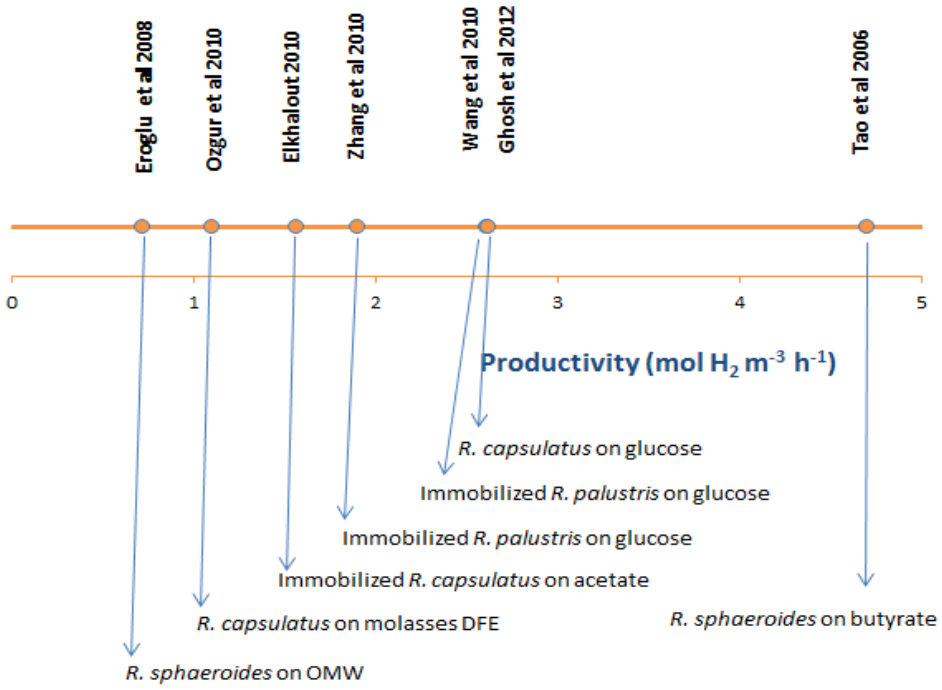

Figure 2.6: Comparison of productivities of photofermentation

The major advantages of photofermentation are listed below (Fernandez-Sevilla et al., 2014):

- Oxygen, which inhibits the enzymes responsible for hydrogen production, is not produced.
- A wide variety of organic substrates and waste waters can be utilized.
- PNSB can utilize a wide range of the solar spectrum, between 300 to 1000 nm.

Since PNSB are able to utilize all the energy coming from the sunlight to produce hydrogen, among the biological hydrogen production methods, this mechanism seems to be the most promising one (Das & Veziroglu, 2001).

Tao et al (2006) reported a productivity of 105 mL H_2/L/h (4.72 mol H_2/(m^3.h). To the best of our knowledge, this is the highest hydrogen productivity found in literature among photofermentation studies. In this study, butyrate was the sole carbon source. *Rhodobacter sphaeroides* SH2C was used in batch cultures under 4000 lux illumination, at 30°C and at a pH of 7. The hydrogen yield is found as 6.91 mol H_2/mol butyrate (Tao, et al. 2006)

In another study, hydrogen productivity was found as 1.4 L H_2/(L.day) (2.62 mol H_2/(m^3.h)) using glucose as the carbon source. The experiment was carried out in batch cultures for 6 days with *Rhodobacter capsulatus* JP91 (Ghosh, Sobro, & Hallenbeck, 2012).

Wang et al (2010) used a panel PBR with entrapped gel granules packed within. Productivity was found as 2.61 mol H_2/(m^3.h). Immobilized *Rhodopseudomonas palustris* CQK 01 on glucose was utilized during the experiment (Wang, Liao, Zhu, Tian, & Zhang, 2010).

Though not directly proportional, the productivity increases as the number of carbon atoms increases in the substrate, as suggested by Figure 2.4 and Figure 2.5, Therefore, single stage photofermentation of high carbon substrates could be advantageous. However, for an economically feasible operation, waste water such as molasses should be utilized. There are very limited studies in literature about the single stage photofermentation of molasses. Keskin and Hallenbeck studied the single stage photofermentation using beet molasses, black strap molasses and sucrose. (Keskin & Hallenbeck, 2012). Sağır also studied photofermentation by utilizing different *Rhodobacter* species (*Rhodobacter capsulatus* DSM 1710, *Rhodobacter capsulatus* YO3 (Hup^-), *Rhodopseudomonas palustris* DSM 127, *Rhodobacter sphaeroides* O.U.001 (DSM 5864)) on 5, 7.5 and 10 mM sucrose containing molasses. The highest productivity was found as 0.55 mol $H_2/(m^3.h)$ from *Rp. Palustris* on 5 mM sucrose containing molasses, whereas a comparable productivity was found with *R. capsulatus* YO3 (0.41 mol $H_2/(m^3.h)$) on 5 mM sucrose containing molasses (Sağır, 2012).

The details of the studies shown in Figure 2.5 are given in Table 2.2. Outdoor studies are also shown in Figure 2.5. The details of outdoor studies are given in Table 5.5.

Table 2.2: The comparison of indoor photofermentation studies in terms of their productivities and substrate conversion efficiencies

Mode of operation	**Type of the bacteria**	**Reactor volume (L)**	**Carbon source**	**H2 productivity (mol H2/(m^3.h))**	**Substrate conversion efficiency, %**	**Reference**
Batch	*Rp. palustris WP 3-5*	1	DFE	0.921 – 1.429	–	(Chun Yen Chen et al., 2008)
Continuous	*Rp. palustris WP 3-5*			1.164	–	
Fed-batch	*Rp. palustris WP3-5*	0.8	Acetate	0.593 – 0.697	41 - 43	(C. Chen, Lee, & Chang, 2006)
Batch				0.391	27	
CSTR				0.607	33	
Column PBR	*R. sphaeroides U.O.001*	0.6	DFE of glucose	1.209	37 - 43	(Nath et al., 2008)
Batch	*R. sphaeroides SH2C*	0.036	DFE of sucrose	1.449	7 -17	(Tao et al., 2007)
			Butyrate	4.719	–	
Batch	*Rp. palustris*	0.8	Acetate	1.281 - 1.968	74 - 91	(Chun Y. Chen & Chang, 2006)
Continous	*Rp. palustris WP3-7*		Acetate	1.977	89	
Continous	*Rp. palustris CQK 01*	9	Glucose	1.12	6	(Liao et al., 2010)

Table 2.1.continued

Mode of operation	Type of the bacteria	Reactor volume (L)	Carbon source	H2 productivity (mol H2/(m^3.h))	Substrate conversion efficiency, %	Reference
Batch	*R. capsulatus Hup-(YO3)*	0.055	DFE of molasses	1.11 – 1.16	79 - 90	(Androga, Özgür, & Eroglu, 2012)
Batch	*R. capsulatus JP91*	0.1	Glucose	2.621	46	(Ghosh et al., 2012)
Batch	*R. capsulatus JP92*	0.1	Glucose	0.468	25	(Abo-Hashesh, Ghosh, Tourigny, Taous, & Hallenbeck, 2011)
Fed - batch	*R. capsulatus Hup-(YO3)*	4	Acetate from DFE	1.36	77	(Özkan et al., 2012)
Batch	*R. capsulatus DSM 1710*	0.055	Acetate from	0.4	34	(Özgür, Afsar, et al., 2010)
Batch	*R. capsulatus DSM 1710*		DFE of molasses	1.1	39	
Batch	*R. capsulatus DSM 1710*		DFE of PSP hydrolysate	0.55	24	

Table 2.1.continued

Mode of operation	Type of the bacteria	Reactor volume (L)	Carbon source	H2 productivity (mol H2/(m^3.h))	Substrate conversion efficiency, %	Reference
Batch	*R. capsulatus DSM 1710*	0.055	DFE of molasses	1.1	39	(Özgür, Mars, et al., 2010)
Batch	*R. capsulatus hup-*		DFE of molasses	1.37	58	
Batch	*Rp. palustris DSM127*		DFE of molasses	1.16	46	
Batch	*R. capsulatus hup - (YO3)*	0.055	DFE of barley straw hyrolysate	0.49 – 0.58	36 - 37	(Özgür & Peksel, 2013)
Batch	*R. sphaeroides O.U.001 (DSM 5864)*	0.36	olive mill wastewater (OMW)	0.288	17	(E. Eroglu, Gunduz, Yucel, & Eroglu, 2011)
Batch	*R. sphaeroides O.U.001 (DSM 5864)*	1	DL malic acid	0.292	75	(Basak & Das, 2009)
Batch	*Rp. palustris WP3-5*	0.5	Formate	_	_	(Lo, Chen, Lee, & Chang, 2011)
			Acetate	0.571	67	
			Lactate	0.508	73	
			Butyrate	0.548	68	
			Ethanol	_	_	

Table 2.1.continued

Mode of operation	Type of the bacteria	Reactor volume (L)	Carbon source	H2 productivity (mol H2/(m^3.h))	Substrate conversion efficiency, %	Reference
Batch	*Rp. palustris CQK 01*	0.1	Glucose based synthetic wastewater	1.908	6	(Zhang et al., 2010)
Batch	*Rp. palustris CQK 01*	0.8	Glucose	2.61	30	(Y. Z. Wang et al., 2010)
Continuous	*Rp. palustris CQK 01*	0.125	Glucose	0.74 - 1.75	–	(C. L. Guo et al., 2011)
Batch	*Rp. palustris*	0.25	DFE	0.737	7	(Su et al., 2009b)
Batch	*R. Spheroides RV*	0.31	DFE	0.392	22	(Argun & Kargi, 2010b)
Batch	*R. sphaeroides*	0.055	DFE	1.317	40	(Afsar et al., 2011)
Batch	*R. palustris WP3-5*		DFE	0.567	18	(Perera et al., 2010)
Continous	*R. palustris WP3-6*		DFE	0.292	21	
Repeated batch	*R. sphaeroides M-19*	0.05	DFE	—	37 -38	(Yokoi et al., 2001)

Table 2.1.continued

Mode of operation	Type of the bacteria	Reactor volume (L)	Carbon source	H2 productivity (mol H2/(m^3.h))	Substrate conversion efficiency, %	Reference
Batch	*R. sphaeroides DSM 158*	0.2	DFE	0.764	7	(Fang, Zhu, & Zhang, 2006)
Batch	*R. palustris*	_	Acetate and butyrate containing DFE	1.209	35	(Su, Cheng, Zhou, Song, & Cen, 2009a)
Batch	*R. sphaeroides*	0.15	Lactate	0.481	10	(Barbosa, Rocha, Tramper, & Wijffels, 2001)
		0.15	Malate	0.049	7	
		0.15	Butyrate	0.342	8	
		0.15	Acetate	1.132	73	
	R. palustris	0.15	Lactate	0.409	13	
		0.15	Malate	0.261	36	
		0.15	Butyrate	0	0	
		0.15	Acetate	0.099	15	
	Microbiology strain	0.15	Lactate	0.355	14	
		0.15	Malate	0.27	37	
		0.15	Butyrate	0.009	0.3	
		0.15	Acetate	0.238	35	

Table 2.1.continued

Mode of operation	**Type of the bacteria**	**Reactor volume (L)**	**Carbon source**	**H2 productivity (mol H2/(m^3.h))**	**Substrate conversion efficiency, %**	**Reference**
Batch	*Rp. palustris WP3-5*	–	Acetate	0.767	—	(Chun Y. Chen, Lee, & Chang, 2006)
Continous	*R. sphaeroides NRRL-B1727*	7	DFE	0.051	11	(Ozmihci & Kargi, 2010)
Fed - batch	*Rhodopseudomonas faecalis RLD - 53*	0.25	Acetate	0	80	(N. Q. Ren et al., 2009)
Batch	*R. capsulatus YO3 (hup-)*	0.1	Beet molasses	1.44	7.5	(Keskin & Hallenbeck, 2012)
		0.1	Black Strap Molasses	1.59	29	
		0.1	Sucrose	1.35	25	

2.3.4 Integrated Systems

The organic acids produced in dark fermentation could be utilized in photofermentation to increase hydrogen yield. Since this is a two stage process, it is not practical to report productivity for sequential dark and photofermentation. 12 moles of hydrogen can be produced from one mole of glucose by sequential dark and photofermentation as shown in the following equation (Argun & Kargi, 2011; Manish & Banerjee, 2008).

$$CH_3COOH + 2\ H_2O \longrightarrow 4\ H_2 + 2\ CO_2 \quad (2.16)$$

When only acetic acid is produced, 24 mole of hydrogen could be produced from one mole of sucrose. The overall reaction is obtained by summing up the Reactions 2.15 and 2.16 (Urbaniec & Grabarczyk, 2014).

$$C_{12}H_{22}O_{11} + 13\ H_2O \longrightarrow 24\ H_2 + 12\ CO_2 \quad (2.17)$$

Urbaniec and Grabarczyk (2013) studied the economics of a hydrogen production plant utilizing dark fermentation followed by photofermentation. The economic analysis was done for a hypothetical plant with 60 kg/h H_2 production capacity which corresponds to 2000 kW. In this hypothetical plant, hydrogen was produced at a rate of 10 h/day. As it can be seen from Figure 2.7, hydrogen production cost was mainly due to capital cost. This capital cost included land price and equipment cost. The large land area occupied by the PBR was the main reason of this high capital cost. 93 % of the capital cost was due to photofermentation Figure 2.8). Urbaniec and Grabarczyk (2013) investigated a manifold type tubular PBR with LDPE channels that is used in the work of Boran (Boran, Özgür, Yücel, Gündüz, & Eroglu, 2012a, 2012b) They found that LDPE tubes are the main operating cost item as shown in Figure 2.9. Therefore, in the light of this work, it could be concluded that the reactor used in photofermentation needs to be improved for an economically feasible operation (Urbaniec & Grabarczyk, 2014).

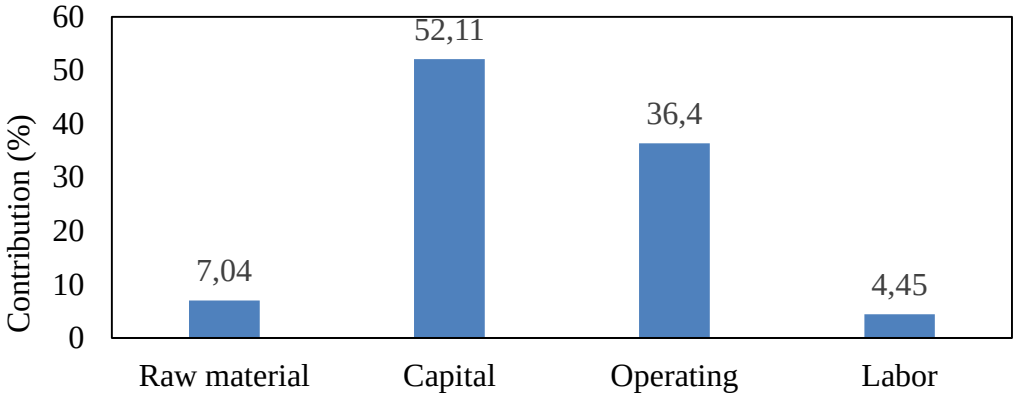

Figure 2.7: Cost items for two-stage biological H_2 production

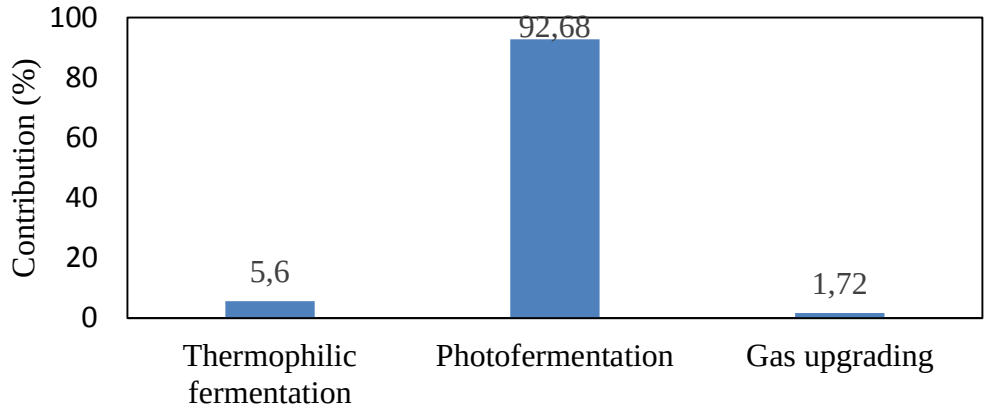

Figure 2.8: Breakdown of capital costs for two-stage biological H_2 production

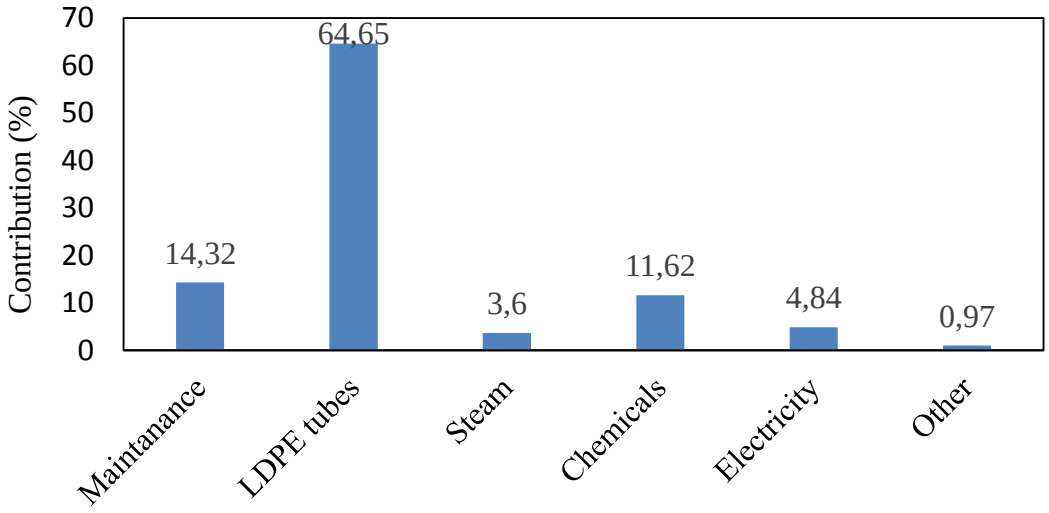

Figure 2.9: Operating costs for photofermentation

2.3.5 Mixed Cultures for Simultaneous Dark and Photofermentation

Instead of using two different reactors for dark and photofermentation, researchers have also tried to use co-cultures of dark and photo fermentation bacteria. Asada et al (2006) co-immobilized *Lactobacillus delbrueckii* NBRC13953 and *Rhodobacter sphaeroides*-RV and found a productivity of 1.89 mol $H_2/m^3/h$. Glucose was used as the carbon source. The maximum yield was reported as 7.1 mol H_2/mol glucose [73].

Ding et al (2009) reported a maximum productivity of 33.85 ml H_2/(L.h) (1.52 mol $H_2(m^3.h)$ obtained by using 6 g/L glucose. Co – culture of *Clostridium butyricum* and immobilized *Rhodopseudomonas faecalis RLD – 53* was utilized under 8000 lux illumination. The ratio of dark to photo bacteria was 1:10. The hydrogen yield was reported as 4.13 mol H_2/mol glucose (Ding et al., 2009).

Productivity reported in literature for combined dark and photofermentation is up to 2 mol $H_2/m^3/h$ (Figure 2.10).

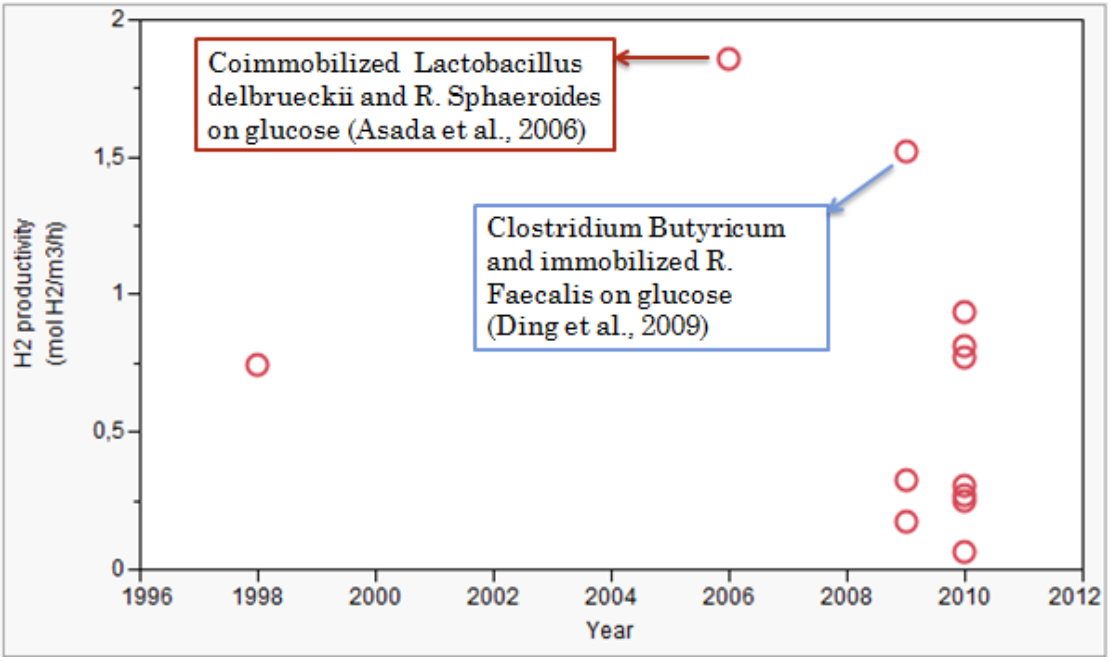

Figure 2.10: Chronological summary of hydrogen productivities in mixed cultures for simultaneous dark and photofermentation

The studies with the highest productivity are highlighted in Figure 2.10. The details of all the studies depicted in Figure 2.10 are given in Table 2.3.

Table 2.3: Comparison of productivities and yields for mixed cultures for simultaneous dark and photofermentation

Mode of operation	**Type of the bacteria**	**Suspended /Immobilized**	**H2 productivity (mol H_2/(m^3.h)**	**Feed**	**H_2 yield (mol H_2/mol glucose)**	**Reference**
Batch	*Clostridium butyricum DSM 10702* and *Rhodobacter sphaeroides DSM 158*	Suspended	0.34	Glucose (5 g/ L)	0.86	(Fang et al., 2006)
Batch	*Clostridium butyricum andRhodopseudomonas faecalis RLD-53*	Suspended	0.936	Glucose (9 g/ L)	1.98	(Liu et al., 2010)
Batch	*Clostridium acidisoli* and *Rhodobacter sphaeroides*	Suspended	3.12	Sucrose (11.43 g / L)	5.08	(Sun et al., 2010)
Batch	Anaerobic sludge and *Rhodobacter sp. RV*	Suspended	0.301	Ground wheat starch (4.3 g/ L)	1.45	(Argun & Kargi, 2010a)
Batch	Anaerobic sludge and mixture of *Rhodobacter sp (NRRL B-1727) Rhodobacter sp (DSMZ-158) Rhodopseudomonas palustris (DSMZ-127) Rhodobacter sp. RV*	Suspended	0.173	Ground wheat starch (4.1 g /L)	1.16	(Argun, Kargi, & Kapdan, 2009)

Table 2.3.continued

Mode of operation	**Type of the bacteria**	**Suspended /Immobilized**	**H2 productivity (mol H_2/(m^3.h)**	**Feed**	**H_2 yield (mol H_2/mol glucose)**	**Reference**
Batch	Anaerobic sludge and mixture of *Rhodobacter sp (NRRL B-1727) Rhodobacter sp (DSMZ-158) Rhodopseudomonas palustris (DSMZ-127) Rhodobacter sp. RV*	Suspended	0.32	Ground wheat starch (3.9 g/L)	1.03	(Argun et al., 2009)
Batch	*Lactobacillus delbrueckii NBRC13953 and Rhodobacter sphaeroides-RV*	Immobilized	1.855	Glucose (4.5 g/ L)	7.1	(Asada et al., 2006)
Batch	*Clostridium butyricum and Rhodopseudomonas faecalis RLD-53*	Immobilized	1.521	Glucose (6 g / L)	4.13	(Ding et al., 2009)74
Batch	*Ethanoligenens harbinense B49 and Rhodopseudomonas faecalis RLD-53*	Immobilized	0.773	Glucose (6 g / L)	3.1	(Xie et al., 2010)
Repeated fed-batch	*Clostridium butyricum* and *Rhodobacter sp. M-19*	Suspended	0.742	Starch (50 g / L)	6.6	(Yokoi, Tokushige, Hirose, Hayashi, & Takasaki, 1998b)

2.4 Photobioreactors for Hydrogen Production

Photobioreactors (PBRs) are reactors in which photosynthetic microorganisms are cultivated, utilizing a light source. PBRs can be open systems such as raceway ponds, lagoons and lakes, or closed systems such as flat plate and tubular. Since anaerobic conditions are necessary, open systems are not suitable for photofermentative hydrogen production. The key parameters in the design of PBRs can be listed as follows (Androga, Özgür, Eroglu, et al., 2012).

- The reactor material should be impermeable to hydrogen and air.
- The reactor material should transmit light easily.
- The reactor material should be inert and durable under outdoor conditions.
- The surface to volume ratio should be as high as possible.

Panel and tubular PBRs are the two commonly used reactor types for photofermentative hydrogen production (Androga, Özgür, Eroglu, et al., 2012).

2.4.1 Panel Photobioreactors

Panel PBRs consists of two transparent plates (e.g. PMMA or glass) that are attached to each other by a frame (Androga, Özgür, Eroglu, et al., 2012). Illuminated surfaces are typically oriented in the east – west direction for the efficient use of sunlight, since purple non sulfur bacteria mainly utilize long wave radiation which is more dominant in the morning and in the evening. The spacing between the panels is adjusted according to the targeted light and temperature distribution. The hydrostatic pressure at the bottom limits the panel height (I. Eroglu et al., 2014). A typical panel PBR is shown in Figure 2.11.

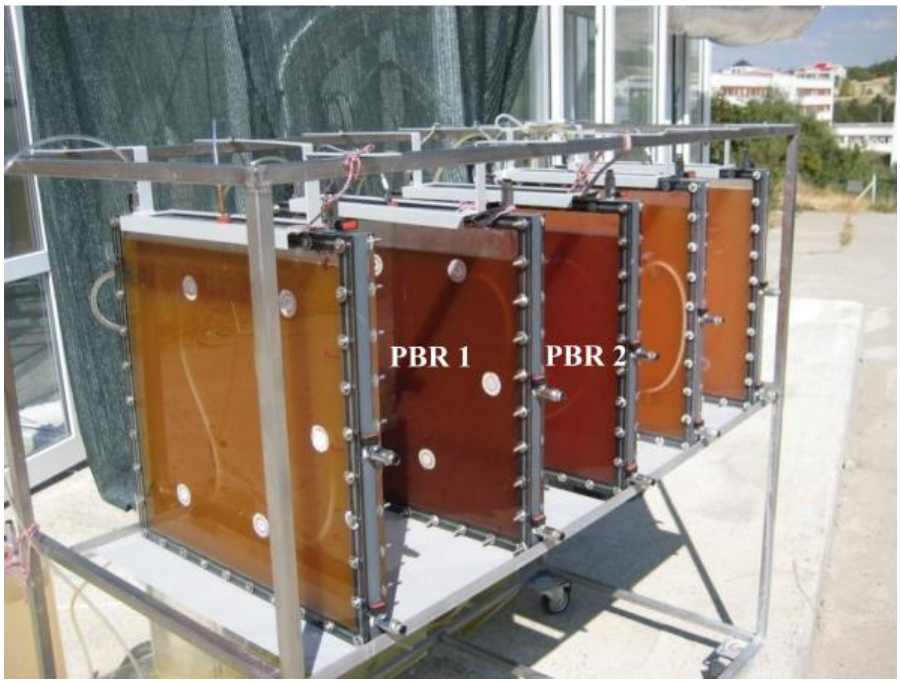

Figure 2.11: Panel type PBRs (4 L) operated in outdoor conditions with internal cooling

For panel PBRs, the ratio of illuminated reactor surface to the occupied ground area for panel reactors is about 8:1. This ratio is quite high when compared to tubular PBRs whose illuminated surface area to ground area ratio is typically 1:1 (Jakub Gebicki et al., 2010). Despite this significant advantage in terms of required ground area, panel PBRs have several drawbacks. Due to mechanical restrictions arising from the design, mixing becomes a problem in panel type PBRs whereas it could easily be achieved in tubular PBRs by a recirculation pump. There is also an upper limit for the volume of panel type PBRs; the mechanical integrity of the design begins to suffer beyond a certain size. Avcioglu observed severe swelling and deformation due to pressure in a PVC-panel PBR with 1m x 1m dimensions (Avcioglu, 2010).

2.4.2 Tubular Photobioreactors

Tubular PBRs have long transparent tubes whose diameters are in the range of 3 to 6 cm with the length of the tubes ranging from 10 to 100 m (Akkerman, Janssen, Rocha, & H, 2002). Different types of tubular PBRs are shown in

Figure 2.12. Tubular PBRs could be vertical, horizontal, nearly horizontal, helical or α-shaped. Bubble column and airlift reactors are examples of vertical PBRs. In vertical type PBRs, a gas is generally supplied to the system for mixing purposes. However, these systems are not suited well to photofermentative hydrogen production, since any inert gas supplied to the system will dilute the product gas and require additional costs for separation. Horizontal tubular PBRs are preferred since they can utilize sunlight with high light conversion efficiency. Helical PBRs are made up of flexible materials. Cooling is achieved by an external heat exchanger. In α-shaped helical reactors, the liquid is raised to a reservoir and flows down using an inclined tube. The liquid is collected in another air riser. Then the process is repeated (Dasgupta et al., 2010).

Some tubular PBRs are nearly horizontal, and have several parallel tubes connected to each other by manifolds. Mixing is achieved by recirculation of the liquid culture medium. An example of such a tubular PBR operated in outdoors on thick juice dark fermenter effluent is shown in Figure 2.13 (Boran et al., 2012b). Androga modelled flow in this manifold type PBR for a 255 mL/min volumetric recirculation rate. The results (Figure 2.14 and Figure 2.15) showed that the flow distribution among the tubes differs considerably. (Androga, 2014).

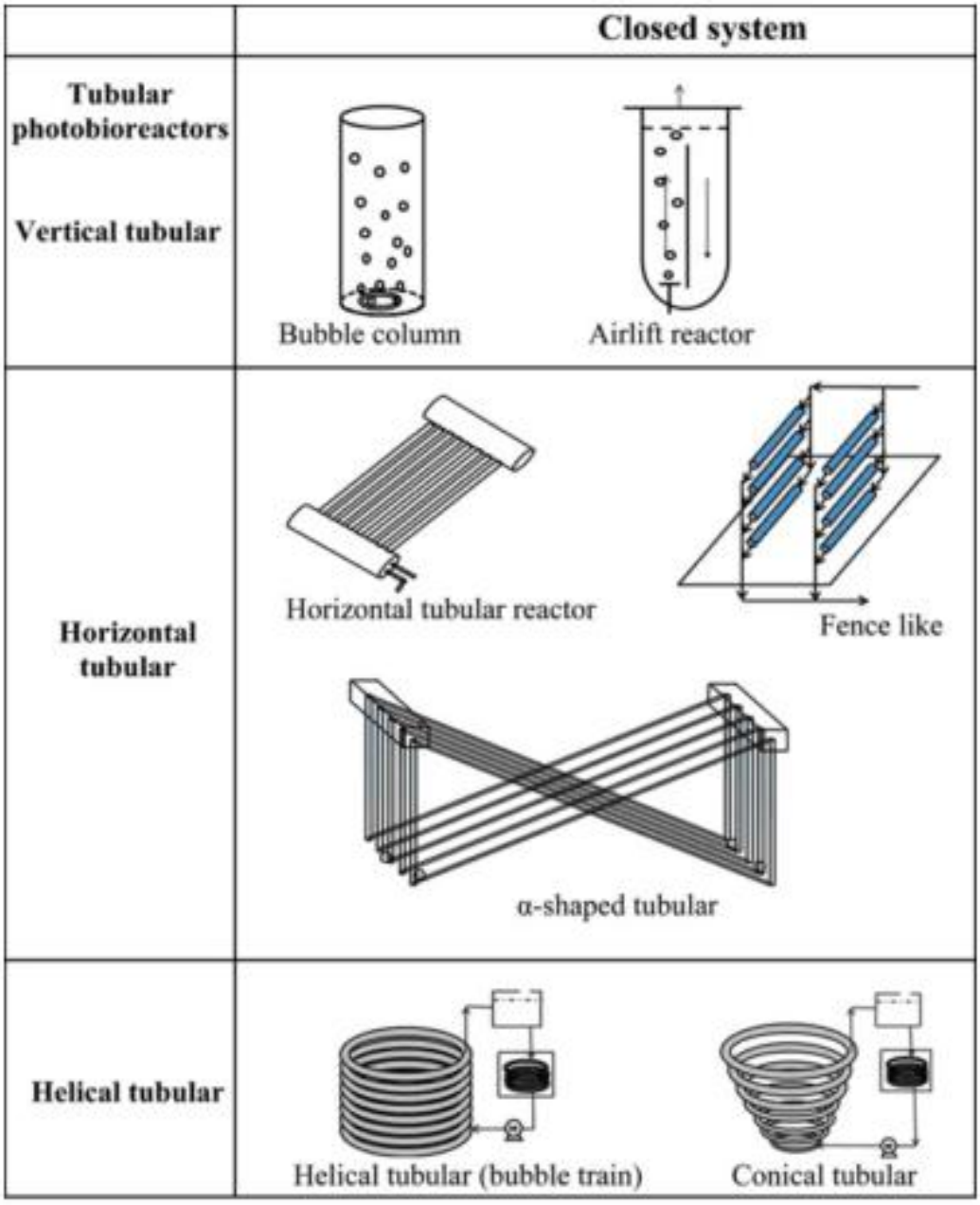

Figure 2.12: Various types of tubular PBRs (Dasgupta et al., 2010)

Figure 2.13: Nearly horizontal tubular PBR (90 L) operated with *Rhodobacter* capsulatus (Boran et al., 2012b).

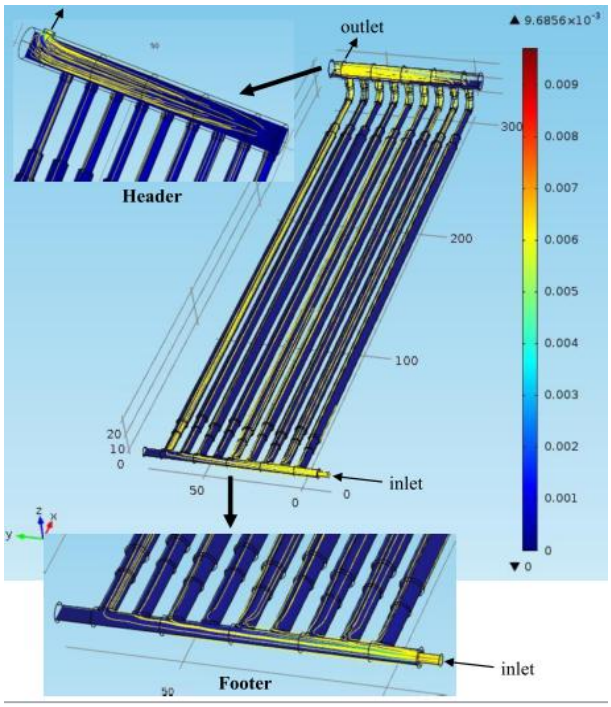

Figure 2.14: Velocity distribution of a manifold type PBR. The yellow streamlines indicate the distribution of particle trajectory (Androga, 2014).

Actually, distributing the feedstock with a manifold has many advantages. Internal cooling is easier with this reactor configuration. However, the flow distribution is a problem. As it can be seen from the Figure 2.15, the flow rate varies significantly with respect to each tube. In other words, the residence times of the individual tubes differ, which probably influences the productivity in every tube. Therefore, a flow model is needed for a manifold type PBR to obtain the optimal reactor dimensions.

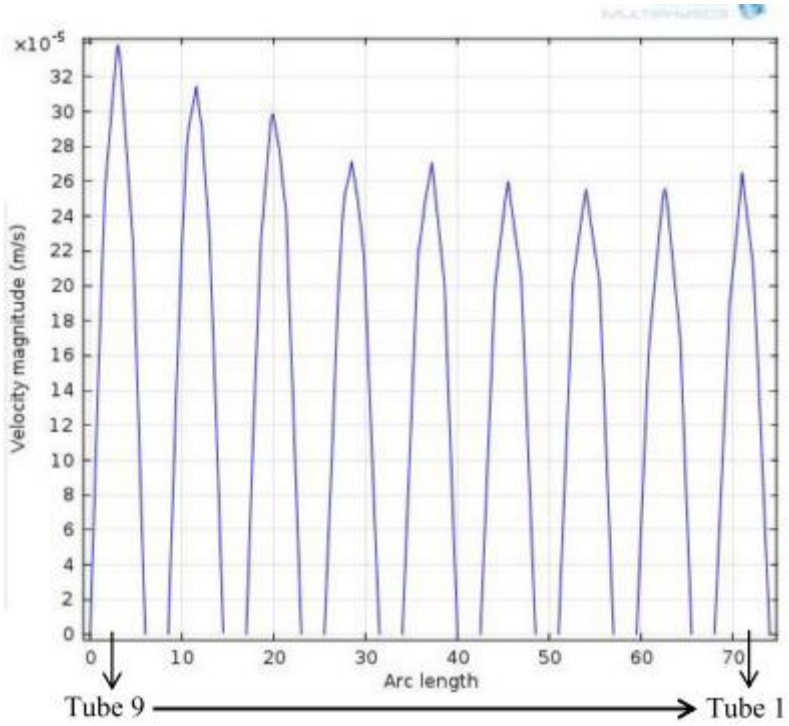

Figure 2.15: Flow distribution among the tubes of a manifold a type PBR (Androga, 2014)

2.5 Flow Distribution in Manifolds

Flow is distributed to multiple parallel channels by means of manifolds in many devices such as solar collectors (Ángel, Manuel, Omar, Antonio, & Armando, 2013; Fan, Shah, & Furbo, 2007), fuel cells (C.-H. Chen, Jung, & Yen, 2007), heat exchangers (Ablanque, Oliet, Rigola, Pérez-Segarra, & Oliva, 2010) and reactors (Boran et al., 2012a). The flow and pressure maldistribution in the manifolds

significantly affect the performance of such systems. With an optimal manifold design, an increase in efficiency and a reduction in the operation cost could be accomplished.

The geometric configuration of the manifold affects the flow distribution. Manifolds can be divided into two general groups in terms of their configuration: U-type (reverse) (J. Wang, 2008) and Z-types (parallel) (J. Wang, 2010) as shown in **Error! Reference ource not found.**. Manifolds could be placed vertically or horizontally.

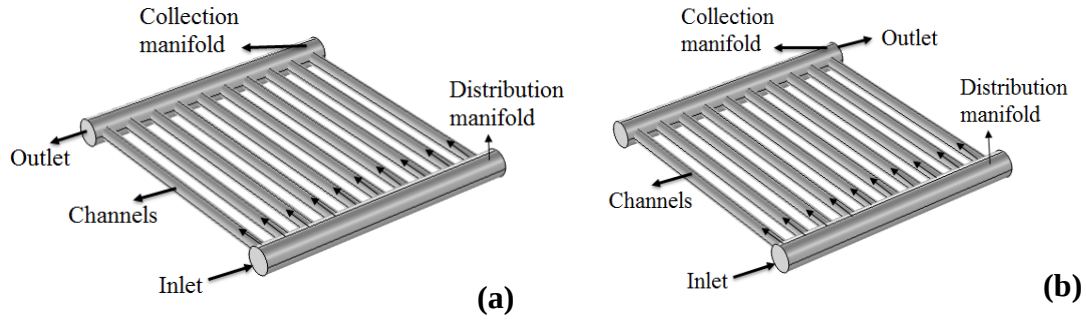

Figure 2.16: (a) U type manifolds (b) Z type manifolds

The flow distribution in the manifold for a single phase flow is determined by the wall friction and momentum changes. In the distribution manifold, as the fluid moves along the manifold, friction increases, whereas the fluid loses momentum with the loss of fluid to the channels. In the collection manifold, both the momentum and friction effects work in the same direction, as the fluid moves towards the outlet. The pressure also changes along the manifold due to friction and momentum effects. Pressure decreases in the direction of the fluid due to friction whereas momentum effects tend to rise the pressure along the distribution manifold. In the collection manifold, both friction and momentum effects cause pressure drop towards the outlet (Acrivos, Babcock, & Pigford, 1959). In the manifold design, the dimensions of the distribution manifold are the main design criterion, since it is important to balance the momentum and friction effects. However, it is important to understand the combined frictional and momentum effects in the collection manifold. The findings of Ahn et al (1997) also

confirms that the diameter to length ratio of the distribution manifold affects the flow distribution more than the dimensions of combination manifold does (Ahn et al., 1998). Acrivos and his coworkers observed a pressure rise near the channel outlet in the collection manifold experimentally (Acrivos et al., 1959).

The pressure and flow characteristics in a manifold can be modeled by means of discrete models (network models), analytical models and computational fluid dynamics (CFD). In discrete models, the manifold consists of multiple junctions. Momentum, mass and energy conservation equations are solved at each junction (Ablanque et al., 2010). Analytical models, also called continuous models, represent the domain in a continuous manner. In analytical models, the mass, momentum and energy conservation equations are written for a control volume, and differential equations are obtained from these equations. Analytical models are the fundamentals of most of the discrete models. As the number of junctions approaches infinity in discrete models, analytical models are obtained (J. Wang, 2011). In CFD, the geometry is discretized and conservation of mass, momentum and energy equations are solved at each mesh point. Then, a global solution is obtained by combining the information of each mesh point (Ahn et al., 1998; Comsol, 2012b; Fan et al., 2007) In the following paragraphs, different manifold models found in literature are mentioned. The effects of different parameters on the flow distribution are given.

Acrivos, Babcock, and Pigford (1959) modelled the flow distribution in a manifold using both a discrete and an analytical model. 3 parameters were investigated in this study: momentum flow (ratio of fluid pressure to specific kinetic energy) at the entrance (M_0), the friction in the straight tube section (F_0) and the spacing between the channels (s). (For notational consistency, Δy in the work of Acrivos et al. is changed with s). M_0 could be changed by changing the entrance velocity. From the results of Acrivos and his coworkers, it was found that there was no pair of F_0 and M_0 that would make a perfect uniform distribution. Therefore, the aim should be obtaining the most uniform flow distribution as possible. Acrivos et al (1959) changed the spacing

between the channels by decreasing the channel number. They found that increasing the spacing provides a more uniform distribution until the distance became so great that the friction effects becomes significant (Acrivos et al., 1959).

Ablanque et al (2010) studied the flow distribution in manifolds using a discrete model. The domain discretization is shown in Figure 2.17. Two types of discretization were used: higher level and lower level discretization. In higher level discretization, T-junction models were solved, whereas in lower level discretization, the tube is branched and 2-phase flow models are solved. With the global model, three different numerical models were coupled. First, at the T-junctions, the pressure change (distribution and collection manifolds) and phase split (in two-phase flow distribution junctions) were predicted. Secondly, the continuity, momentum conservation and energy conservation equations were solved through the tubes. Finally, the equations solved for the tubes and the junctions were coupled with the global momentum conservation and continuity equations (Ablanque et al., 2010).

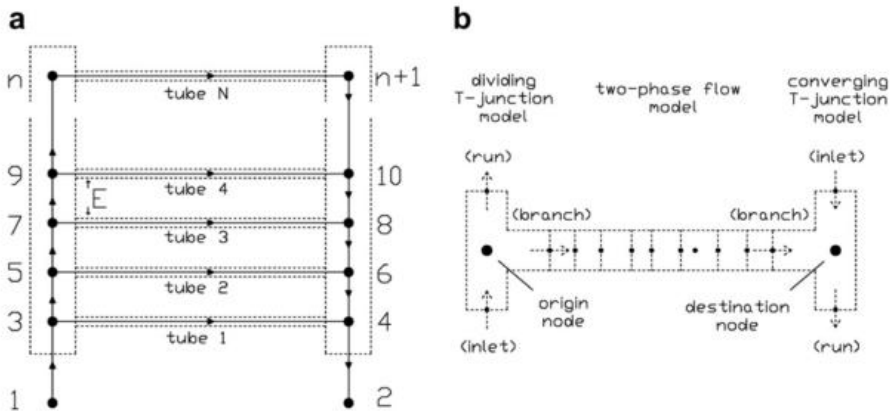

Figure 2.17:Domain discretization (a) higher level discretization in T-junctions (b) lower level discretization in the tubes (Ablanque et al., 2010)

Ablanque et al. (2010) studied single phase flow for two different tube pitches (0.1 m and 1 m) for reverse (U type) and parallel (Z type) manifold configurations and compared their results with the model developed by Wang and Yu (1989). Wang and Yu (1989) also performed some experiments to validate the model. The working fluid

was water. Both the manifold and the tubes were held horizontal. 10 parallel tubes with 12.5 mm diameter and 3 m length were used. The distribution manifold diameter was 25 mm. The inlet flow rate was 0.227 kg/s. The error between the experimental data of Wang and Yu (1989) and the corresponding predictions made by Ablanque et al. (2010) were lower than 8%. Ablanque et al. compared their model results with the model results of Wang and Yu. The most uniform flow distribution is obtained with reverse configuration (U-type) and smaller pitch (E=0.1). It is concluded from the results that the flow distribution is remarkably affected by the distribution manifold pressure profile (Ablanque et al., 2010; X. A. Wang & Yu, 1989).

Ablanque et al. also modelled the two phase flow and compared the model results with the experiments performed by Sivert (2003). The working fluid was water and carbon dioxide. Horizontal manifold with vertical tubes was used. The manifold configuration was reverse. 10 parallel tubes with 4 mm in diameter and 0.9 m in length were utilized. The distribution manifold diameter was 16 mm. The inlet mass flow rate was 0.033 kg/s. Different inlet gas fractions such as 0.14, 0.28, 0.43 and 0.54 were used. The mean prediction error in two phase flow was 32 %. Although this value was significantly high, Ablanque et al. managed to predict the general trends (Ablanque et al., 2010; Sievert, 2003).

Wang (2011) studied the flow distribution in a manifold using an analytical model. Wang tried to obtain the most generalized equations defining the flow inside the distribution and collection manifolds by reviewing the literature in the past fifty years. Wang (2011) developed a model by unifying the models developed by Acrivos (1959), Wang (2008) and Wang (2010). Wang (2011) claimed that they developed the most generalized equations for distribution and collection manifolds (Equations 19 and 20 in Wang (2011)). Varying friction and pressure recovery factors can be adopted to their model. Wang (2011) studied effect of 3 characteristic parameters (E, M and ζ) and Reynolds number on flow distribution and pressure drop. E is defined as the ratio of the manifold length to diameter. M is the ratio of all the port areas to the area of the

manifold. ζ is average total head loss coefficient for port flow. Their results show that momentum and friction effects work in opposite directions and these parameters needs to be adjusted in order to obtain a uniform flow distribution. 3 different E values (3, 5 and 100) were studied when Re, M and ζ were 2000, 2 and 2 respectively. Wang (2011) found that as E increases the friction term becomes dominant and the flow distribution tends to distribute unequally. By studying 3 different M values (0.5, 2 and 3), Wang (2011) concluded that as M was increased, the flow was distributed to the ports unequally. As M increases, the momentum effects became significant and they could not balance the friction effects. In order to obtain a uniform a flow distribution, ζ needs to be high also. As ζ approaches infinity, the most uniform flow distribution is expected in the distribution manifold, since there will be no flow branching. Wang (2011) also studied the effect of Reynolds number. He found that the effect of Reynolds number increases as M decreases. An increase in Reynolds number causes a decrease in the friction term and an increase in the pressure recovery factor (J. Wang, 2011). Therefore, it can be concluded that momentum and friction affects the flow distribution in the manifold. Their effects are in opposite direction. As the length of the manifold increases, the effect of the friction becomes significant in the distribution manifold. The fluid loses momentum as it branches to the pipes. When the length of the distribution manifold is smaller, the flow distribution is mainly affected by the momentum.

Ahn et al (1997) studied the flow distribution in manifolds for low Reynolds numbers by using a CFD approach. They modelled a manifold which has 8 parallel pipes by utilizing Fluent 4.3. Water was the working fluid. They studied the effect of 2 structural parameters a_c and a_d which were defined as the ratio of the diameter to length in the distribution and collection manifolds, respectively. Ahn and his coworkers (1997) found a correlation for uniform flow distribution. They studied 3 different values of a_c and a_d which are 1/16, 1/8 and 1/4 while keeping Reynolds number in the pipes as constant at 100. As a_d decreases the flow tends to go through the channels that are closest to the entrance. Ahn and his coworkers found that the effect of the pipe length in the flow distribution was insignificant since the resistance caused by the

length of the pipes was smaller than the resistance of the manifolds. a_d was found as the main parameter affecting the flow distribution in this model. Ahn et al (1998) also conducted an experiment and compared their model results with the experimental results. The measured flow rates in the parallel pipes showed a great agreement with the model (Ahn et al., 1998).

Fan, Shah and Furbo (2007) investigated the flow and temperature distribution in a solar collector panel by using CFD, and compare their model results with their experimental results. They used different operating parameters such as flow rate, properties of solar collector fluid (water to glycol ratio), inlet fluid temperature and collector tilt angle. The distribution manifold and collection manifold diameter were both 0.0256 m. 16 quadrangular absorber tubes with a hydraulic diameter of 0.0067 m were used. U tube configuration was used. They used Equation 2.1 while calculating the flow maldistribution. The definition of flow non-uniformity parameter, Φ, was similar to the standard deviation with the only difference that non-uniformity parameter is divided by the mean value (1/N) (Fan et al., 2007).

$$\Phi = \sqrt{\frac{\sum_{i=1}^{N}(\beta_i - 1/N)^2}{N}} \text{ x N x 100 \%} \qquad (2.1)$$

In a previous study, the flow non-uniformity parameter (ϕ), shown in Equation 2.1 was defined to quantify the flow distribution. This parameter is analogous to standard deviation and could be defined as the fractional volumetric flow rate when the flow is distributed equally to all channels (Fan et al., 2007).

In Equation 2.1, N is the number of channels and β is the dimensionless volumetric flow rate defined by Equation 2.2.

$$\beta_i = \frac{Q_i}{Q_0} \qquad (2.2)$$

where Q_0 is the total volumetric flow rate, and Q_i is the flow rate of the *i*th channel.

In order to understand the effect of the buoyancy forces better, Fan and his coworkers introduced the ratio of Grashof number (Gr) to square root of Reynolds number (Re^2). When this ratio is larger than unity, it could be concluded that buoyancy forces affects the flow distribution (Fan et al., 2007).

Fan and his coworkers studied 5 different inlet flow rates: 2.5, 4.0, 10.0 and 25.0 L/min with constant temperature of 60ºC. They observed that the relative flow non-uniformity parameter increases from 2.8 % to 6.4 % when the flow rate increases from 2.5 L/min to 25.0 L/min. In order to investigate the effects of collector tilt angle, 40º inclination was given to the collector panel. The collector panel was heated with a solar radiation of 800 W/m^2 and the ambient temperature was 20ºC. It was concluded that for lower flow rates, the effect of buoyancy forces are high. The most uniform flow distribution was observed when the inlet flow rates were 10.0 L/min and 25.0 L/min.

CHAPTER 3

STACKED U-TUBE PHOTOBIOREACTOR DESIGN

3.1 Design Strategy

3.1.1 Reactor Selection

In order to gain acceptance as a viable route for hydrogen production, photofermentative hydrogen production has to be implemented in large-scale PBRs under natural sunlight. Up to now, many of the problems encountered in large scale outdoor operations have been identified (Adessi, Torzillo, Baccetti, & De Philippis, 2012; Avcıoglu, Özgur, Eroglu, Yücel, & Gündüz, 2011; Boran et al., 2012a).

Running PBRs in outdoor conditions introduces complications such as fluctuating temperature and light intensity values, which limits productivity. Moreover, large scale applications differ from the small scale ones in terms of light distribution, reactor material, gas collection and mixing.

In this part the thesis, issues related to the scale up of PBRs are reviewed and accordingly, a new reactor design is proposed. Some of these issues are discussed below.

The effect of temperature on photofermentative hydrogen production has previously been investigated via small-scale experiments under fluctuating temperatures in the

range of 15ºC and 40ºC, using wild type *Rhodobacter capsulatus* and its hup$^-$ mutant. Furthermore, the bacteria were subjected to 16 h light and 8 h dark cycles in order to mimic the diurnal cycle. As control, bacteria were grown under continuous illumination and a constant temperature of 30ºC. The variation in temperature decreased the hydrogen productivity from 0.7 mol H_2 /(m^3.h) to 0.25 mol H_2/(m^3.h). The light/dark cycles further decreased the productivity to 0.2 mol H_2/(m^3.h). The authors hypothesized that the bacteria spent some of its energy for adaptation to the temperature changes and light/dark cycles (Özgür, Uyar, et al., 2010).

Light/dark cycles are inevitable in outdoor operation, but their effects are relatively minor compared to the impact of temperature extremes, especially during summer months, which are usually preferred for outdoor campaigns due to the abundance of sunlight. With efficient cooling systems, however, the decrease in productivity due to temperature fluctuations could be mitigated. A study has been implemented where the reactor temperature was kept under 30, 33, 35 and 40 ºC by shading or water spraying. The highest productivity (0.32 mol H_2/(m^3.h)) was obtained when the reactor temperature was kept at 33ºC or lower; on the other hand, the lowest productivity was observed to be 0.22 mol H_2/(m^3.h), when the reactor temperature was allowed to reach as high as 40ºC (Özgür, Uyar, et al., 2010).

Light distribution within the PBR is critical for scale-up. For large culture depths, light penetration to the inner regions of the PBR becomes the limiting factor for productivity. Furthermore, when the available light is below a certain threshold, the bacteria could shift to completely unfavorable metabolic modes such as dark-fermentation. This could be prevented by increasing the surface to volume (or length to thickness) aspect ratio of the PBRs (Androga, Özgür, Eroglu, et al., 2012). In one study, hydrogen production rates were measured using Roux bottles of varying depths. Hydrogen production was observed mainly at bottles with depths smaller than 1.5 cm (Nakada, Asada, Arai, & Miyake, 1995). It should be kept in mind, however, that high surface-to-volume ratios will increase the required land area, and may complicate the

reactor construction and operation. Therefore a total thickness of 3 cm would be a proper compromise between good light distribution and limited surface area.

Another factor to consider is gas and more specifically hydrogen, permeability. Especially in large-scale systems, hydrogen loss through the reactor walls should be reduced as much as possible due to safety and economic considerations. Since a large surface area is inevitable due to light penetration requirements, it is necessary to decrease the permeability of the material as much as possible. The hydrogen permeability of the candidate PBR materials was assessed and experimentally verified in a previous study (Avcioglu, 2010). The permeability of poly (methyl methacrylate) (PMMA), glass, polyurethane (PU), polyvinyl chloride-plasticized (PVC-plasticized) and low-density polyethylene (LDPE) are $1.88x10^{-14}$, $4.38x10^{-16}$, $2.78x10^{-12}$, $4.86x10^{-11}$ and $2.30x10^{-11}$ mol/(m.s.Pa). Among these materials, glass was found as the least permeable material and LDPE the most permeable, thus indicating glass is the best choice for the reactor material based on permeability. Apart from permeability, glass is also more advantageous in terms of mechanical strength and durability; it has been reported that the LDPE reactor tubes used in a previous study (Boran et al., 2010, 2012a) had to be changed every year and the contribution of these tubes to the operating cost was around 65% (Urbaniec & Grabarczyk, 2014).

As the reactor volume increases, product-gas collection also becomes a problem. It has been observed that as the reactor headspace pressure increased, hydrogen productivity decreased (Li et al., 2011). Therefore, it is important to maintain the total gas pressure in the headspace as low as possible, which will also promote lower retention of the produced gas, thereby decreasing the loss of hydrogen through the walls due to permeation as discussed above.

Mixing is promoted in PBRs in order to increase the mass transfer rate, to reduce nutrient gradients, to eliminate cell sedimentation and to facilitate the separation of the

produced gas from the liquid culture. On the other hand, there appears to be an optimum mixing power value, above which productivity starts to decline. Though the reasons for the decrease of productivity at elevated mixing power values are unclear, one possibility is that shear stress, which depends on Reynolds number, induces cell damage. In a study aimed to probe the effects of mixing, the performances of reactors shaken at 40, 80, 120 and 160 rpm were monitored and the average productivity was found to be the highest 2.7 mol $H_2/(m^3.h)$ when the shaking velocity was 120 rpm (Flickinger, 2013). This value was significantly higher than that of the control experiment with no shaking, reported as 1.86 mol $H_2/(m^3.h)$ (Li et al., 2011). In tubular PBRs, it has also been reported that hydrogen production is affected by the volumetric flow rate of recirculation that is used to promote mixing (Jakub Gebicki et al., 2010). When the Reynolds number was varied from 10 to 6000, the highest productivity was observed for a Reynolds number of 240. No hydrogen production was observed when the volumetric flow rate was larger than 2400. However, these experiments were carried out with a manifold type of PBR where flow distribution among the channels changed significantly with the Reynolds number. Consequently, the optimum Reynolds number for other systems should be obtained individually for other geometries. A flow model is especially useful in this regard, to obtain more insight into how the velocity distribution depends on the geometry.

Finally, economics is still the main obstacle, preventing the application of such photofermentative hydrogen production systems in industrial scale. The large ground area required for a manifold type tubular PBR by photofermentation was the reason of capital cost of photofermentation being several times larger than dark fermentation. Therefore, the ground area for the PBR should be reduced (Urbaniec & Grabarczyk, 2014).

Based on the factors discussed up to this point, it can be argued that tubular reactors offer superior characteristics with respect ease of mixing. Thus, in this work, a pilot-scale manifold type glass stacked U-tube PBR was designed, built and operated. An

upright orientation was selected to ensure small ground area to volume ratio with a large illuminated surface area, and the reactor material was chosen as glass for durability and low permeability to hydrogen and air. In designing the tubular PBR geometry, a hydrodynamic model was used to assess whether a low overall pressure drop and a uniform velocity distribution could be achieved throughout the reactor and the dimensions of the reactor was based on the results of the model. The PBR was then constructed and run with and without bacteria, the latter grown using a molasses solution as a complex substrate.

3.1.2 Method of Attack

While designing the PBR, the following procedure was followed.

- The reactor geometry was selected. Tubular reactors were found more advantageous, since it is easy to mix the reactor contents. Tubular reactors are also easier to scale up when compared with the panel type reactors. As discussed in the literature survey part, tubular PBRs also seem to be more advantageous in terms of durability and ease of cooling.
- Manifolds are preferred to distribute the flow.
- The design parameters were selected for a manifold type reactor. Diameter to length ratio of the manifolds, tube pitch, tube length and the volumetric flow rate were the parameters that are widely studied in literature for designing manifolds.
- A flow model was solved for the manifold type tubular reactor (stacked U-tube PBR) via COMSOL Multiphysics 4.4.
- The velocity and pressure profile of the reactor was determined from the model.
- The dimensions of the reactor were determined from the model which gave the most uniform flow distribution among the tubes.

- The reactor materials used for PBRs were investigated. The ideal reactor material should have low hydrogen and air permeability. It should have low cost, and it should be durable in outdoor conditions. The most appropriate material meeting these needs was found as glass.
- The stacked U-tube PBR was constructed.
- The reactor was operated in September 2014 and in July 2015 utilizing *Rhodobacter Capsulatus* YO_3 on 5 mM sucrose containing molasses as the feedstock.

The results of the hydrodynamic model are given in 'Chapter 3' under 'Effect of Design Parameters on Velocity and Pressure Distribution'. The details of the construction and operation are given in 'Chapter 4'. The experimental results and discussion are given in Chapter 5.

3.2 Methods

The steady-state single phase laminar flow module in COMSOL 4.4 was used. The single phase fluid flow interface in COMSOL is based on the Navier – Stokes equations, which is given in Equation 3.2. Equation 3.1 is the continuity equation, which represents the conservation of mass. Equation 3.2 (vector equation) describes the conservation of momentum. Equation 3.3 represents the conservation of energy (Comsol, 2012b).

$$\frac{\partial \rho}{\partial t} + \nabla.(\rho \mathbf{u}) = 0 \tag{3.1}$$

$$\rho \frac{\partial \mathbf{u}}{\partial t} + \rho(\mathbf{u}.\nabla)\mathbf{u} = \nabla.[-p\mathbf{I} + \tau] + \mathbf{F} \tag{3.2}$$

$$\rho C_p \left(\frac{\partial T}{\partial t} + (\mathbf{u}.\nabla)\, T\right) = -(\nabla.\mathbf{q}) + \boldsymbol{\tau}:\mathbf{S} - \frac{T}{\rho}\left.\frac{\partial \rho}{\partial T}\right|_{P} \left(\frac{\partial p}{\partial t} + (\mathbf{u}.\nabla)p\right) + \dot{Q} \tag{3.3}$$

where ρ is the density (kg/m^3) , $\mathbf{u}$ is the velocity (m/s), p is the pressure (Pa), $\boldsymbol{\tau}$ is the viscous stress tensor (Pa), $\mathbf{F}$ is the volume force vector (N/m^3), C_p is the specific heat capacity at constant pressure (J/kg.K), T is the absolute temperature (K), $\mathbf{q}$ is the heat flux vector (W/m^2), $\dot{Q}$ is the heat sources (W/m^3), $\mathbf{I}$ is the identity tensor and S is the strain – rate tensor (Comsol, 2012b).

$$\mathbf{S} = \frac{1}{2}(\nabla \mathbf{u} + (\nabla \mathbf{u})^T) \tag{3.4}$$

The double dot product ":" used in Equation 3.3 is defined in Equation 3.5.

$$\mathbf{a}:\mathbf{b} = \sum_n \sum_m a_{nm} b_{nm} \tag{3.5}$$

In order to solve Equations 3.1, 3.2 and 3.3, constitutive equations relating the viscous stress tensor to the velocity field are needed. In this model, water is used as the working fluid in the reactor; therefore, the fluid is Newtonian. The constitutive equation (Equation 3.6) is defined by the Newtonian fluid assumption and Stokes' assumption (Comsol, 2012b).

$$\tau = 2\mu\mathbf{S} - \frac{2}{3}\mu(\nabla.\mathbf{u})\,\mathbf{I} \tag{3.6}$$

where μ is the dynamic viscosity (Pa.s).

Equations 3.1, 3.2 and 3.3 are applicable in both turbulent and laminar flow. However, they are defined under the Laminar flow interface in COMSOL, since the mesh resolution needed for the turbulent flow problems is hard to apply to this interface (Comsol, 2012b).

In this model, the temperature is assumed to be constant at 30ºC. For isothermal flow, Equation 3.3 is not solved simultaneously with Equation 3.1 and 3.2. For isothermal flow, the density change becomes nearly constant. With the incompressible flow assumption, Equation 3.1 becomes

$$\rho\nabla.\mathbf{u} = 0 \tag{3.7}$$

If stress tensor (Equation 3.4) and viscous stress tensor (Equation 3.6) are put into conservation of momentum equation (Equation 3.2), Equation 3.8 is obtained.

$$\rho\frac{\partial\mathbf{u}}{\partial t} + \rho(\mathbf{u}.\nabla)\mathbf{u} = \nabla.\left[-p\mathbf{I} + \mu(\nabla\mathbf{u} + (\nabla\mathbf{u})^{T}) - \frac{2}{3}\mu(\nabla.\mathbf{u})\,\mathbf{I}\right] + \mathbf{F} \tag{3.8}$$

With the incompressible flow and steady-state assumption, Equation 3.8 becomes

$$\rho(\mathbf{u}.\nabla)\mathbf{u} = \nabla.[-p\mathbf{I} + \mu(\nabla\mathbf{u} + (\nabla\mathbf{u})^{T})] + \mathbf{F} \tag{3.9}$$

All of these assumptions are listed below.

- Newtonian fluid
- Isothermal flow
- Incompressible flow
- Steady-state

The final equations used to model 3 dimensional system in COMSOL 4.4 are given in Equation 3.7 and Equation 3.9. In order to solve these equations, boundary conditions

are needed. 3 boundary conditions given below are enough to solve the equations. No slip boundary condition was applied to all the solid boundaries (Equation 3.10). At the inlet, the fluid velocity was fixed (Equations 3.11 and 3.12). The flow at the inlet is assumed to laminar and fully developed. At the outlet, pressure was assumed to be zero (Equation 3.13). The mathematical formulations of the boundary conditions are given in Equations 3.10 – 3.13, where n is the normal unit vector pointing out of the domain (Comsol, 2012b).

$$\mathbf{u_{wall}} = 0 \tag{3.10}$$

$$\mathbf{u}_{inlet} = 2 \cdot \mathbf{u}_{ave} \cdot \left(1 - \frac{r^2}{R^2}\right) \tag{3.11}$$

$$\mathbf{u_{ave}} = -\,u_0\mathbf{n} \tag{3.12}$$

$$p_{out} = 0 \tag{3.13}$$

where $\mathbf{u_{wall}}$ is the velocity at the tube wall (m/s), $\mathbf{u_{inlet}}$ is the inlet velocity (m/s), $\mathbf{u_{ave}}$ is the average velocity (m/s), R is the pipe radius and r is the distance from the center, u_0 is the velocity magnitude at the inlet (m/s), **n** is the normal unit vector pointing out of the domain, and p_{out} is the outlet gauge pressure (Pa).

COMSOL utilizes the finite element method while solving partial differential equations. The finite element method is a numerical technique which discretize the domain into smaller units called 'mesh elements'. Set of equations defined by the Physics interface are solved for all the mesh elements using a numerical analysis technique. Then, individual element equations are linked to obtain a global solution. (Comsol, 2012b).

While solving a multiphysics problem, fully coupled or segregated approach could be utilized. Fully coupled method is suggested while solving Navier-Stokes' equations by COMSOL Multiphysics. The fully coupled solution approach uses either a damped

version of Newton's method or a double dogleg method. The damped version of Newton's method was preferred in this model. The default values of Newton's method in COMSOL 4.4 were used. They are shown in Table 3.1.

Table 3.1: The default values of Newton's method

The initial damping factor	0.01
Minimum damping factor	$1x10^{-6}$
Restriction step size update	10
Recovery damping factor	0.75

Two different approaches could be used while solving the linear system of equations: Direct and Iterative. Direct approach computes the solution in a finite number of steps. In this model, iterative solution technique is used. Iterative solution technique starts from an initial guess and make successive approximations until the solution converges to a value within the error margin. There are different iteration methods in COMSOL such as conjugate gradient, GMREs, FGMRES, BiCStab, and geometric multigrid. All these methods use preconditioners. A preconditioner solves all the equations in a coarser mesh. Then, the solution obtained is used as the initial guess for the real problem.

In this model, the problem gave no solution when the maximum number of iterations were reached before the convergence criteria had been met. GMREs (generalized minimum residual method), which is the default solution technique for laminar flow interface, was used. (Comsol, 2012a & Comsol, 2012b). The tolerance factor was set to 0.001, which indicates that when the error between the iterations reach %0.1, COMSOL gives a result.

The staked U-tube PBR geometry solved via COMSOL Multiphysics 4.4 is shown in Figure 3.1. The tube pitch and tube length were changed for different models.

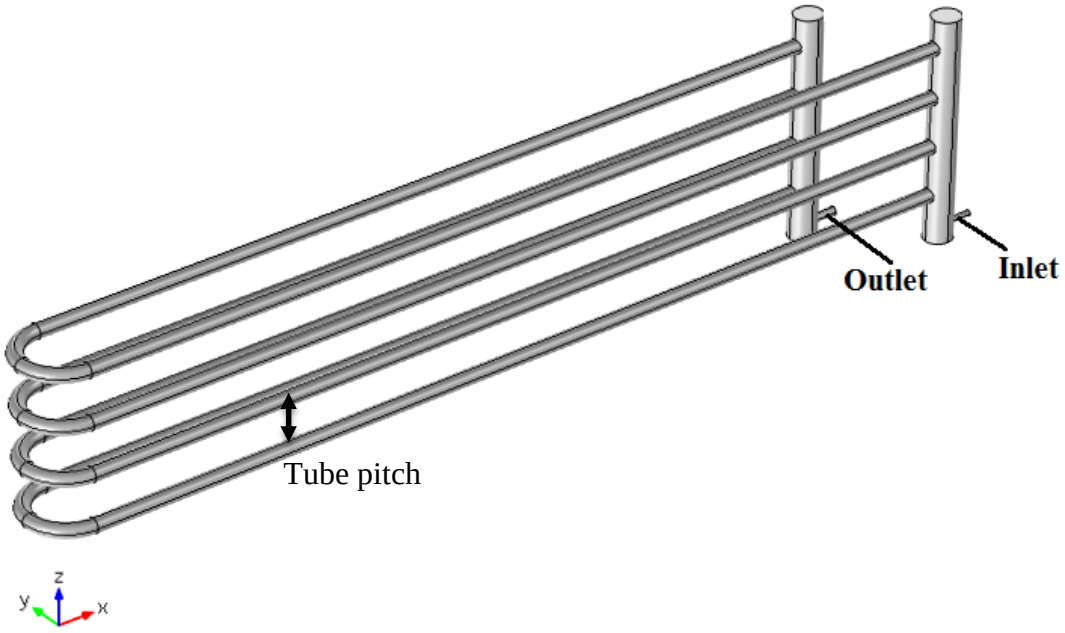

Figure 3.1: The stacked U-tube PBR geometry solved via COMSOL Multiphysics 4.4. The tube pitch is 10.5 and the tube length is 4.0 m.

3.3. Mesh Convergence Study

Meshes were distributed around the inlet and outlet manifolds (Figure 3.2), around inlet and outlet tubes (Figure 3.3), along the inlet and outlet tubes (Figure 3.4) and around the tubes (Figure 3.5). First, the number of meshes distributed around the tube inlet and outlet (Distribution 4) was increased. Then, the number of meshes was increased by using fine, finer, extra fine and extremely fine meshes. The details of all the runs were given in Table 3.2. Mass balance was checked for all these runs, and the results were also shown in Table 3.2. Volumetric flow rate at the inlet was calculated by surface integration of velocity. The calculation was performed by COMSOL. Then, the sum of the volumetric flow rates in the pipes was computed by COMSOL by surface integration of the velocities. The volumetric flow rate in the pipes and at the inlet were compared and the error in between was reported as the '% Error for mass balance' in Table 3.2. For all the runs, mass balance was satisfied with an error less than 2.5%.

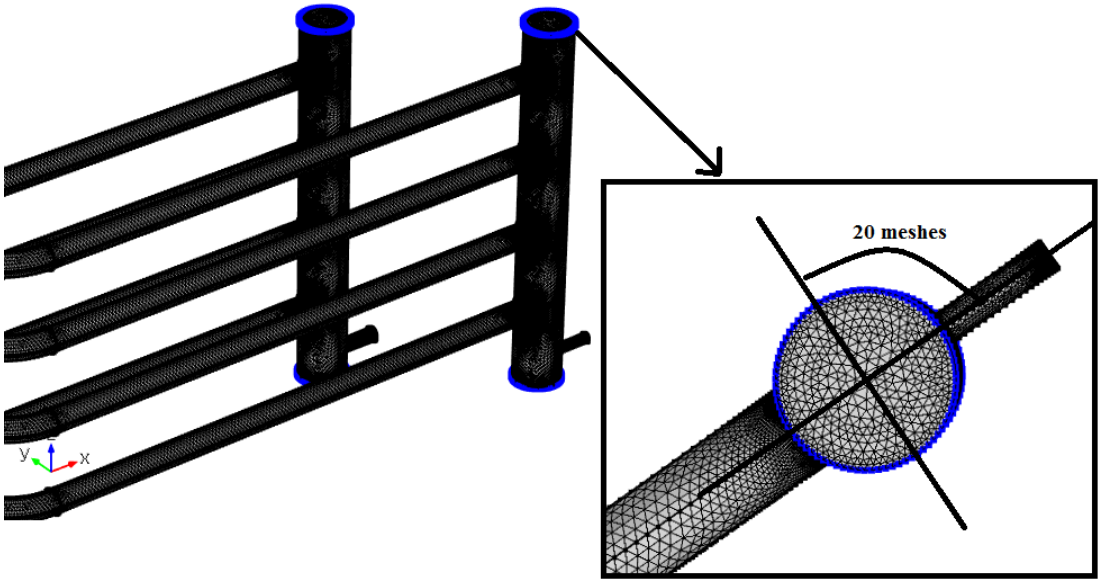

Figure 3.2: Twenty meshes distributed around the manifolds (Distribution 1).

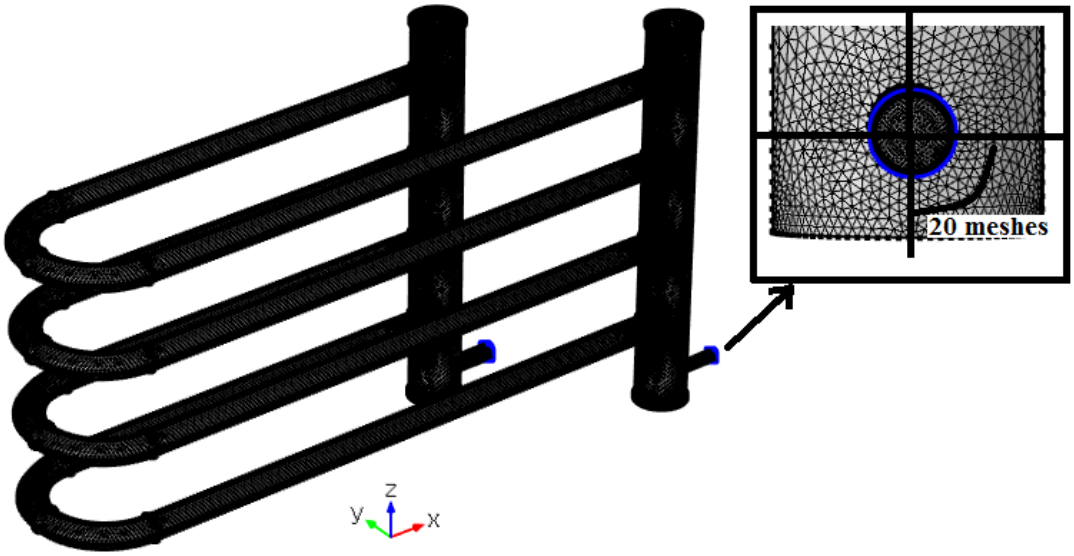

Figure 3.3: Twenty meshes distributed around the inlet and outlet pipes (Distribution 2).

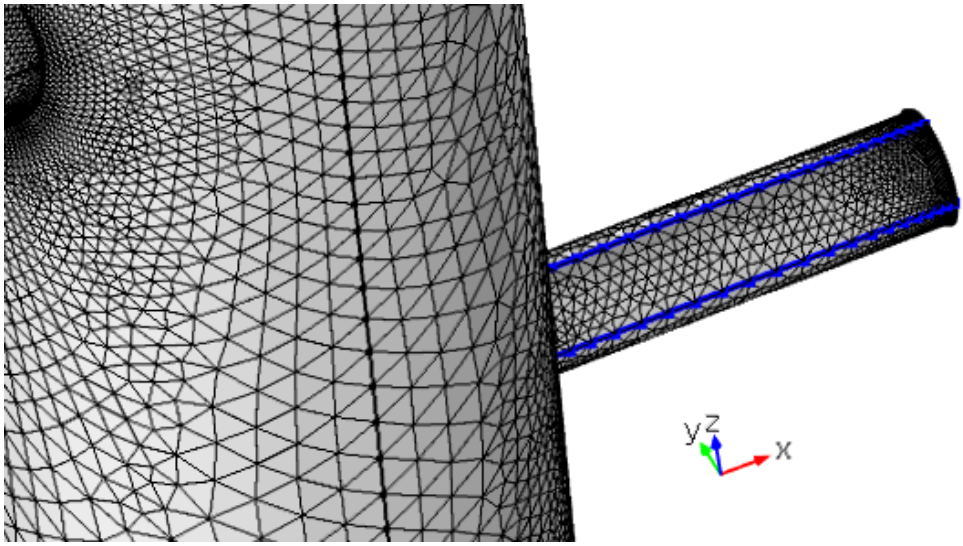

Figure 3.4: Twenty meshes were distributed along the inlet pipe (Distribution 3).

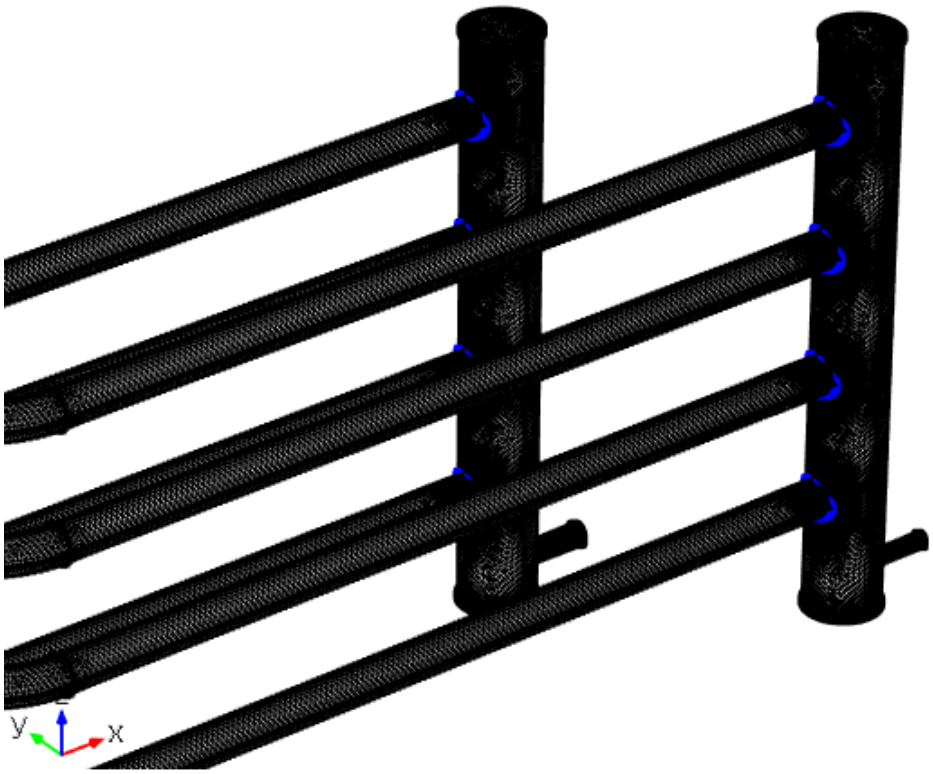

Figure 3.5: Twenty meshes were distributed around the tubes (Distribution 4).

Table 3.2: Details of runs done for the mesh convergence study. The volumetric flow rate was 25 L/h (Ret=92), the tube pitch was 10.5 cm and the tube length was 1.4 m.

Run no	Distribution 1	Distribution 2	Distribution 3	Distribution 4	Mesh type	Number of elements	Average element quality	% Error for the mass balance
1	20	20	20	10	Extremely fine	3120192	0.774	0.65
2	20	20	20	10	Extra fine	1147689	0.767	1.37
3	20	20	20	10	Finer	677020	0.770	1.34
4	20	20	20	10	Fine	429589	0.759	3.03
5	20	20	20	20	Extremely fine	4830079	0.773	0.64
6	20	20	20	20	Extra fine	2043152	0.769	1.35
7	20	20	20	20	Finer	1311929	0.770	1.40
8	20	20	20	20	Fine	839940	0.763	2.21
9	20	20	20	30	Extremely fine	7251606	0.773	0.82
10	20	20	20	30	Extra fine	3160800	0.770	1.37
11	20	20	20	30	Finer	2070471	0.770	1.29
12	20	20	20	30	Fine	1316951	0.764	2.03
13	5	5	5	5	Extremely fine	2600023	0.774	0.48
14	5	5	5	5	Extra fine	609805	0.767	0.89

A mesh convergence study was carried out by comparing the velocities in all the tubes separately. The volumetric flow rates in different tubes were compared and reported in

Table 3.3. While calculating the volumetric flow rate, the velocity data computed by the program was exported. Then, the volumetric flow rate was calculated as shown in Equation 3.14. For the numerical integration, trapezoidal rule for non-uniform grid was utilized.

$$Q = \int_0^{2\pi} \int_0^R V_z r dr d\theta \tag{3.14}$$

where Q is the volumetric flow rate, V_z is the velocity in the z direction, r is the distance from the center, θ is the angle and R is the radius of the tube.

The difference between the extra fine and extremely fine mesh was below 5% for all the runs with different distribution of meshes. Therefore, extra fine mesh was selected for further studies.

For all the runs, volumetric flow rate was 25 L/h (Re_t=92). When the volumetric flow rate was increased, COMSOL was not able to find a solution when the distributed number of meshes exceeds 5. The reason behind this problem was about the solution technique that the COMSOL utilizes. As the more mesh elements were distributed, the preconditioner cannot coarsen the mesh. Therefore, the number of mesh elements were restricted to 5 so that the preconditioner converges and the program finds a solution. The difference in volumetric flow rates between the Run 10 and Run 14 was found to be less than 3%, indicating that the reduction in the number of meshes from 30 to 5 in the distribution 4 did not affected the result significantly. It can be concluded that distribution 5 was a proper choice for further studies.

The model was solved with a mesh number of 609805. The total difference was found to be less than 5% when the mesh number was increased from 609805 to 2600023.

Table 3.3: Results of mesh convergence study

Pipe no	Volumetric flow rate (x10^6 m^3/s)				Percent Error		
	Extremely fine	Extra fine	Finer	Fine			
	Distribution 4 = 10						
	Run 1	**Run 2**	**Run 3**	**Run 4**	**Run 1- Run 2**	**Run 2 - Run 3**	**Run 3 - Run 4**
1	1.90	1.95	1.83	1.79	2.6	6.2	2.7
2	1.89	1.85	1.81	1.80	1.9	2.6	0.2
3	1.84	1.82	1.79	1.70	1.2	1.2	5.3
4	1.83	1.79	1.74	1.66	1.9	3.4	4.8
	Distribution 4 = 20						
	Run 5	**Run 6**	**Run 7**	**Run 8**	**Run 5 - Run 6**	**Run 6 - Run 7**	**Run 7- Run 8**
1	1.99	1.91	1.88	1.66	4.1	1.7	13.7
2	1.86	1.85	1.76	1.76	0.4	5.3	0.1
3	1.80	1.84	1.74	1.69	2.1	5.7	2.9
4	1.79	1.81	1.73	1.66	1.5	4.8	4.0
	Distribution 4 = 30						
	Run 9	**Run 10**	**Run 11**	**Run 12**	**Run 9 - Run 10**	**Run10- Run11**	**Run 11- Run 12**
1	1.94	1.96	1.88	1.80	1.4	4.6	4.2
2	1.87	1.83	1.78	1.80	2.2	2.6	0.8
3	1.83	1.80	1.77	1.74	1.4	1.6	2.3
4	1.81	1.78	1.74	1.57	1.7	2.3	10.3
	Distribution 4 = 5						
	Run 13	**Run 14**			**Run13 -Run14**	**Run 9- Run 13**	**Run 10- Run 14**
1	1.88	1.83			3.0	5.9	2.9
2	1.82	1.76			3.6	6.3	2.6
3	1.79	1.74			3.0	5.3	2.3
4	1.77	1.73			2.7	4.7	2.0

3.3 Effect of Design Parameters on Velocity and Pressure Distribution

Within the scope of this work, the effect of tube length, tube pitch (i.e., the spacing between the parallel tubes measured from the center of one tube to the center of the next one), and volumetric flow rate on the flow distribution were studied. For convenience, the results were interpreted by introducing the fractional volumetric flow rate, defined for the i^{th} tube, as shown in Equation 2.2. If the flow distribution is uniform among the tubes, then β would be 0.25 for all the tubes for a manifold with 4 channels.

Recall:

$$\beta_i = \frac{Q_i}{Q_0} \tag{2.2}$$

where Q_i and Q_0 represents the volumetric flow rate (m^3/s) in the i^{th} tube and total volumetric flow rate, respectively.

In the first part of the model studies, 3 different tube lengths were investigated: 1.4 m, 2.0 m and 3.8 m, while maintaining the volumetric flow rate as 25.0 L/h, and the tube pitch as 10.5 cm. The comparison of flow distribution among the tubes in terms of tube length is displayed in Figure 3.6. Tubes were counted from the bottom (i.e. Tube 1 is closest to the ground) to the top.

The flow non-uniformity parameter (Φ, defined in Equation 2.1) was calculated as 2.1% for both 1.4 m and 2.0 m long tubes, but found to be 1.5% for 3.8 m long tubes, indicating more uniform velocity in the latter. As the tube length is increased, resistance to flow increases in all of the tubes. The flow distribution is considerably affected by the tube length when the frictional forces in the tubes are larger than the

frictional forces in the manifolds. This behavior was also noted in a previous study; although there, the flow resistance due to channel length was found to be small compared to the flow resistance in the manifolds, thus reducing the effect of tube length (Ahn et al., 1998). For PBRs, it is inconvenient to further increase the tube length, as very long tubes result in high residence times which is undesirable, increase the likelihood of leakage and are difficult to maintain at a selected temperature. The pressure drop between the inlet and outlet was found as 0.30, 0.34 and 0.49 Pa for tube lengths of 1.4 m, 2.0 and 3.6 m, respectively.

The second parameter investigated in the model was the tube pitch. Three tube pitches, 8.0, 10.5 and 13.0 cm, were studied while other parameters were kept constant. The volumetric flow rate and tube length were 25.0 L/h and 1.4 m, respectively. The most uniform flow distribution was obtained for a tube pitch of 10.5 cm (Figure 3.7).

As the tube pitch increases, the diameter to height ratio of the distribution and collection manifolds decreases in this geometry. The effect of this ratio on the flow distribution was previously studied for other manifold models (Ahn et al., 1998; J. Wang, 2011). The diameter to height ratio for the distribution manifold has previously been stated as the 'main governing parameter' in design, whereas the same ratio for the combination manifold was found as a controlling parameter (Ahn et al., 1998). This behavior could be easily interpreted via the effective forces in such manifolds. In general, for horizontal manifolds, the flow distribution is determined by the wall friction and momentum change. As the manifold diameter to height ratio decreases for the distribution manifold, friction becomes the dominant force, whereas for larger diameter to length ratios, momentum effects are dominant. In the collection manifold, both the momentum and friction effects work in the same direction, as the fluid moves towards the outlet. (Acrivos et al., 1959; J. Wang, 2011). In addition to these forces, for vertical manifolds, gravity also affects the flow distribution. Therefore, there is an optimum diameter to length ratio when these forces balance each other. In this work,

the optimum tube pitch was found as 10.5 cm. The pressure drops were found as 0.30, 0.30 and 0.29 Pa for 8, 10.5 and 13 cm tube pitches respectively.

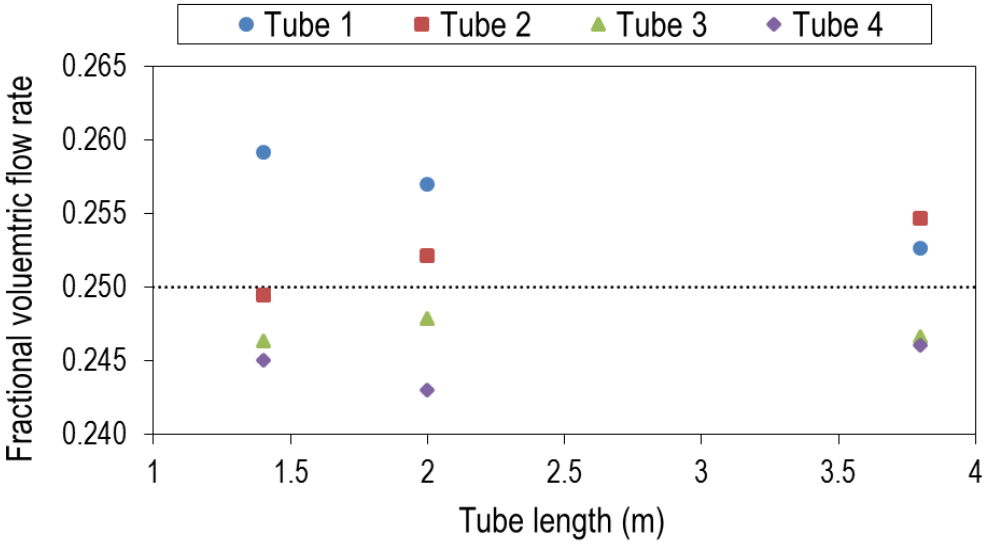

Figure 3.6: Effect of tube length on the fractional volumetric flow rate for a volumetric flow rate of 25.0 L/h (Re_t=92) and tube pitch 10.5 cm

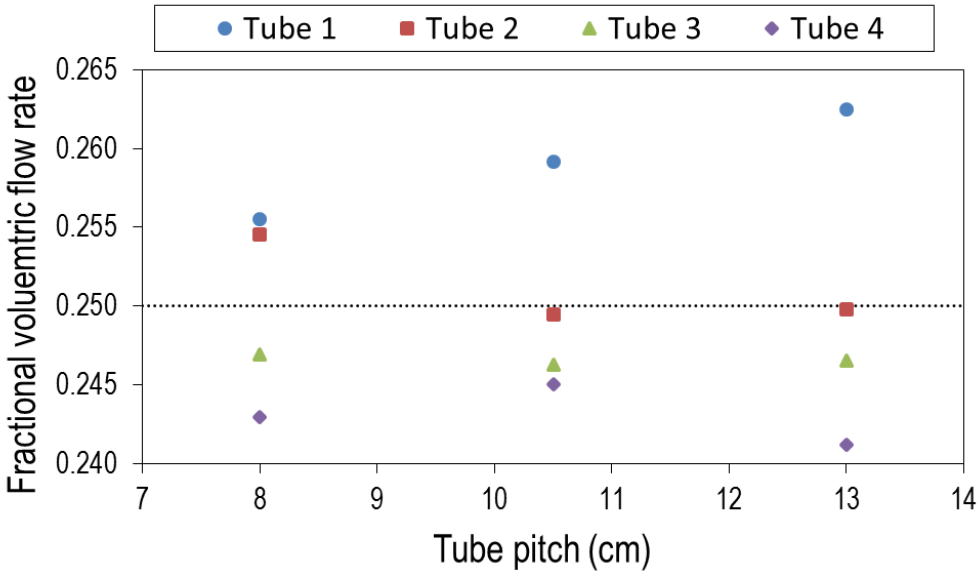

Figure 3.7: Effect of tube pitch for a volumetric flow rate of 25.0 L/h and a tube length of 1.4 m

The volumetric flow rate was increased from 25 L/h to 250 L/h with 25 L/h increments. For these cases, the tube pitch was 10.5 cm and tube length was 1.4 m. It is more convenient to report the volumetric flow rates in terms of Reynolds number (Equation 3.14).

$$\mathrm{Re} = \frac{\rho \cdot u \cdot D}{\mu} \tag{3.14}$$

where ρ is the density (kg/m^3), u is the velocity (m/s), D is the diameter (m), and μ is the viscosity (Pa.s)

In this study, fractional volumetric flow rate was compared using the tube Reynolds number, $\mathrm{Re_t}$. It should be noted that $\mathrm{Re_t}$ is not the actual Reynolds number in the tubes computed from the model, but rather a hypothetical number, that gives a sense about what would have been the Reynolds number in the tubes if the flow was distributed uniformly to all the tubes.

Figure 3.8 indicates that increasing the volumetric flow rate (Re_t) did not change the flow distribution. More fluid tended to go from the lowest tube for all the volumetric flow rates. This result revealed that both gravitational and momentum effects were higher compared to frictional effects in the distribution manifold. Still, looking at the the flow non-uniformity parameter changing between 2.1% and 2.3% for different flow rates, it could be concluded that a uniform flow distribution was achieved.

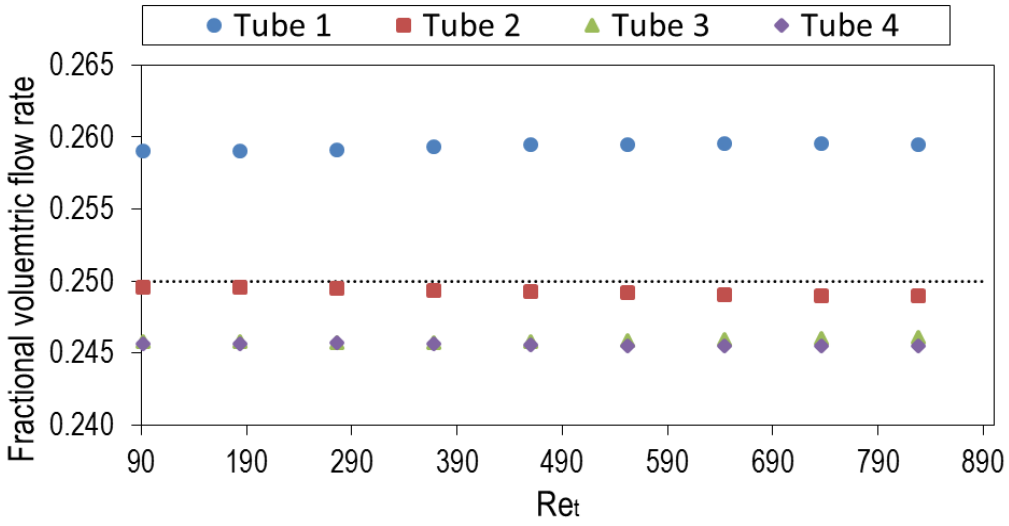

Figure 3.8: Effect of fractional volumetric flow rates for tube pitch and tube lengths of 10.5 and 1.4 m, respectively.

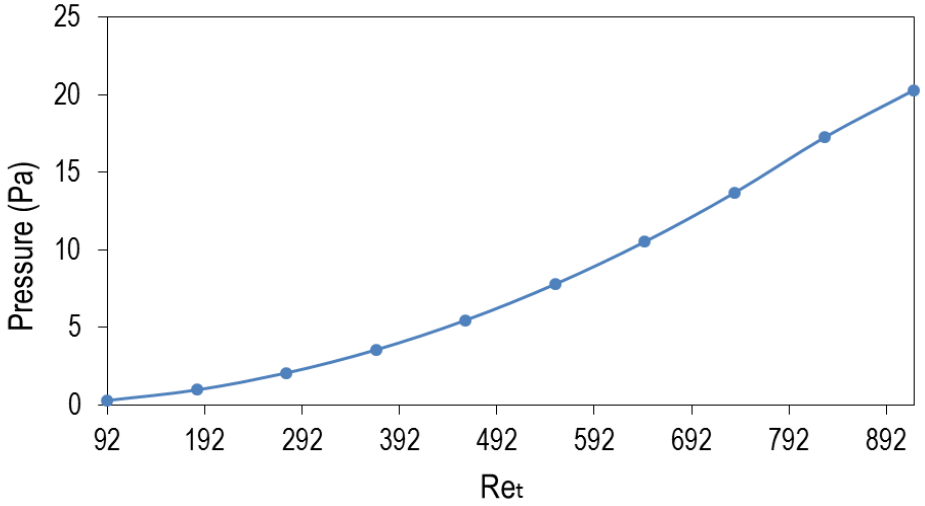

Figure 3.9: Pressure drop with respect to volumetric flow rate. The tube pitch and lengths are 10.5 cm and 1.4 m.

The pressure difference between the inlet and outlet of the reactor with respect to Re_t is plotted in Figure 3.9. The pressure drop increased as Re_t increased, as expected. The values were low; however, even for the highest volumetric flow rate (250 L/h) for which the pressure difference between the inlet and outlet of the reactor was only 20.3 Pa. The summary of the parameters studies are shown in Table 3.4.

Table 3.4: The summary of the parameters studied and corresponding non-uniformity parameter.

Tube length (m)	**Tube pitch (cm)**	**Overall volumetric flow rate (L/h)**	**Re_t**	**Φ (%)**
1.4	10.5	25.0	92.0	2.1
2.0	10.5	25.0	92.0	2.1
3.8	10.5	25.0	92.0	1.5
1.4	8	25.0	92.0	2.1
1.4	13	25.0	92.0	3.1
1.4	10.5	50.0	184.0	2.2
1.4	10.5	75.0	276.0	2.2
1.4	10.5	100.0	368.0	2.2
1.4	10.5	125.0	460.0	2.3
1.4	10.5	150.0	552.0	2.3
1.4	10.5	175.0	644.0	2.3
1.4	10.5	200.0	736.0	2.3
1.4	10.5	225.0	828.0	2.3
1.4	10.5	250.0	920.0	2.3

3.4 Evaluation and Final Selection

The issues related with the design discussed above are summarized below:

- Tubular reactors are more advantageous due to ease of mixing and cooling.

- The ground area per volume of the tubular reactors should be reduced as much as possible for tubular reactors.
- The flow distribution should be uniform to obtain the same flow regime and same residence time in all of the channels.
- Pressure drop should be less to protect the bacteria.
- Light should be distributed inside the reactor properly.
- The residence time of hydrogen should be small. Gas should go to the gas collection unit as soon as it is produced.
- Reactor material should have low permeability to hydrogen and air.
- The reactor should be durable in outdoor conditions.
- Reactor geometry should be proper for an efficient cooling.

The proposed vertical stacked U-tube PBR design meets these needs. The most uniform flow distribution (the non-uniformity parameter is 1.5 %) was obtained when the tube length, tube pitch and the volumetric flow rate were 3.8 m, 10.5 cm and 25 L/h, respectively. Accordingly, the tube length for the final design of the stacked U-tube PBR was chosen as 4 m, and the tube pitch was chosen as 10.5 cm.

CHAPTER 4

CONSTRUCTION AND OPERATION

4.1 Materials and Methods

4.1.1 The Bacterial Strain

Rhodobacter capsulatus YO$_3$ (hup$^-$) strain, previously mutated from the wild-type by Dr. Yavuz Öztürk (GMBE, TUBITAK MAM-Gebze) by deleting the gene coding for uptake hydrogenase enzyme (hup$^-$) of *Rhodobacter capsulatus* MT1131 (Öztürk et al., 2006) was used in this study.

4.1.2 Culture Media

4.1.2.1 Solid Media

Bacteria kept at -80 ºC were activated using a solid media. Solid media were also used to detect contamination. While preparing solid media, agar (3% w/v) was added to the growth media. After the media was autoclaved and cooled to around 40 ºC, it was poured into the agar plates. After solidification of the media, bacteria were inoculated to the agar plates. The plates were wrapped by an aluminum foil to keep them dark, and they were kept in an incubator at 30 ºC until visible colonies were obtained.

4.1.2.2 Growth Media

The Biebl and Pfennig (1981) medium containing 20 mM acetate and 10 mM glutamate as carbon and nitrogen sources respectively, was used for bacterial growth (Biebl & Pfennig, 1981). After all chemicals were dissolved in distilled water, pH was

adjusted to 6.4 – 6.5 by using NaOH solution. The medium was autoclaved for 20 minutes at 121 ^{0}C (Prior Clave). After the medium was cooled to room temperature, trace elements, iron citrate and vitamin solutions were added to the medium in a sterile cabin. The detailed recipes of the BP medium, trace elements, iron citrate and vitamin solutions are given in Appendix A.

4.1.2.3 Sucrose Adaptation Media

Bacteria need to be adapted to sucrose before being inoculated to the hydrogen production media. Therefore, the bacteria were transferred to a sucrose adaptation medium containing 20 mM acetate, 10 mM glutamate and 5 mM sucrose besides Biebl and Pfennig (1981). The bacteria stayed in sucrose adaptation media until its OD reached 1.0 – 1.5 at 660 nm. Then, bacteria were transferred to a second sucrose adaptation media which contains 5 mM sucrose, 10 mM glutamate and the Biebl and Pfennig (1981) medium.

4.1.2.4 Hydrogen Production Media Containing Molasses

Molasses bought from Ankara sugar factory was used as the hydrogen production medium. In this work 5 mM sucrose containing molasses was used as the hydrogen production medium. In order to control pH, 30 mM KH_2PO_4 solution was used as buffer. Initial pH was adjusted to 7.5 with 5 M NaOH solution. After preparing the buffer solution, molasses was added. 10 % (v/v) bacteria were inoculated to the hydrogen production medium. In RUN 092014, Fe and Mo were not added. However, in RUN 072015-R2, Fe and Mo were added to the molasses so that the final amount of Fe and Mo in the feedstock was 0.1 mM and 0.16 μM, respectively.

4.1.2.5 Defined Hydrogen Production Medium

Bacteria which were grown in BP medium containing 40 mM acetate and 20 mM glutamate medium were transferred to hydrogen production medium which contained 40 mM acetate, 2 mM glutamate and Biebl and Phennig medium. The initial concentration was adjusted to OD_{660} of 0.55-0.65. As a buffer, 22mM KH_2PO_4 was used. The initial pH was adjusted to 6.3-6.4 by 5 mM NaOH addition.

4.1.2.6. Preparation of Inoculum

First, one colony of bacteria was inoculated to the 1.5 ml growth media. After the OD value reached to 1.0 – 1.5 at 660 nm, 1.5 ml bacteria was inoculated to 15 ml growth media. Anaerobic conditions were obtained by flushing the media with argon (99.9 % purity) for 2 minutes. Then, the same procedure (10 %, v/v inoculation of bacteria) was applied until the desired amount of culture was obtained.

4.1.2.6 Storage

For long term storage of the bacteria, the medium was mixed with sterile glycerol (40 % v/v) and put into cryogenic vials. The vials were stored in -80 ºC refrigerator. To store the bacteria for about a mount, the bacteria grown in Biebl and Pfennig (1981) medium containing 20 mM acetate and 10 mM glutamate was kept at +4ºC in a refrigerator. The bacteria kept in +4 ºC were activated before use.

4.1.3. Analyses

4.1.3.1.Molasses Analyses

Density and sugar content of molasses together with analysis of some elements (Na, K, Ca, Mg, Fe, Mn and Zn) were reported by Ankara Sugar Factory, Turkey. The

results provided by Ankara Sugar Factory are shown in Table B.1 in Appendix B. Total amino acids and minerals (Fe, Mo, S, K) were analyzed by Düzen Norwest Laboratory, Ankara, Turkey. The results of the analysis are given in Table B.2 and Table B.3, respectively. Amino acids and sucrose are the sources of nitrogen and carbon in molasses, respectively. Moreover, the necessary nutrients for bacterial growth such as Fe and Mo are also present in molasses. However, since the molasses needs to be diluted to adjust the sucrose content, glutamate, Fe and Mo need to be added to obtain the desired amounts necessary for bacterial growth.

4.1.3.2.Sugar Content Analysis

The sugar content in the samples was analyzed by two different methods. (only sucrose is expected to be present in the molasses.) In RUN 092015, sucrose was analyzed using a sucrose kit, provided by Megazyme (Sucrose D-Glucose Assay Kit). The calibration of the sucrose kit was done by using standard solution. -The samples were filtered with 22 μm filters. In RUN 072015, the sucrose content in the samples was measured by HPLC (Shimadzu 20A series). Two detectors (UV and RI) were connected in series. The sucrose content was determined from the results of the RID detector. The column was Alltech IOA-1000 (300 mm x 7.8 mm). 0.0085 M H_2SO_4 was used as the mobile phase. The oven temperature was kept at 60 ºC. A low gradient pump (Shimadzu LC-20AT) with a degasser (Shimadzu DGU-20A5) was used to keep the flow rate at 0.4 ml/min. 10 μL samples were injected to the system with the help of an auto sampler (Shimadzu SIL-10AC). RI (refractive index) detector (Shimadzu RID-20A) was used to determine sugar content. The retention times and peak areas were recorded automatically. Calibration was done using the standard solutions.

4.1.3.3.Organic Acid Analysis

Organic acids were analyzed by an HPLC (Shimadzu 20A series). The method used was the same as the method used for sugar content analysis with HPLC except for the

detector type. A UV detector (Shimadzu SPD-20A) whose absorbance set at 210 nm was used for the detection of organic acids. The calibration was done by using standard solutions for organic acids. Lactic acid, acetic acid, propionic acid and butyric acid were the organic acids measured.

4.1.3.4. pH Analyses

The pH of the samples was measured with a pH meter (Ezdo MP-103). Three measurements were taken from each sample and an average was reported. Before usage, the pH of the standard solutions was measured. If the accuracy was less than 95%, pH meter was calibrated.

4.1.3.5.Cell Concentration

The cell concentration was measured by a UV spectrophotometer (Shimadzu UV-1201). The absorbance was set at 660 nm. Distilled water was used as a blank solution. The dry cell weights were determined from absorbance values. The calibration factor was 0.4656 for *Rhodobacter capsulatus YO*$_3$ (Öztürk, 2005).

4.1.3.6.Light Intensity

Light intensity was measured with a luxmeter (Lutron LX-105 Light Meter) for indoors. The PBRs which were kept in an incubator (Nüve) was illuminated by 100 W tungsten lamps. The light intensity on the surface of the PBRs was adjusted to 2000 lux.

The light intensity for RUN 092014 was recorded by a pyranometer (HOBO-S-LIB-M003) which was connected to an online weather station (HOBO® U30 ETH).

The light intensity values were recorded for RUN 072015-R1 and RUN072015-R2 by a weather station (Davis Vantage Pro2 Weather Station equipped with a solar radiation sensor) which was mounted near the reactors.

4.1.3.7.Temperature Measurements

The temperature measurements were taken with thermocouples (Fe-constant J type) which are connected to an online data logger (Ordel UDL100). 12 temperature measurements were taken from RUN 092014 and RUN 072015-R1. The ports in which thermocouples were inserted are shown in Figure 4.6. For RUN 092014, cooling water inlet and outlet temperatures were also measured. 2 temperature measurements were taken from RUN 072015-R2 (T4 and T12). Air temperature was also measured with J type thermocouple for RUN 092014. Air temperature data for RUN 072014-R1 and RUN 072014-R2 were measured by the weather station (Davis Vantage Pro2 Weather Station).

4.1.3.8.Gas Analysis

The gas composition was determined by using a gas chromatography (Agilent Technologies 6890N) equipped with a Supelco Carboxen 1010 column. A thermal conductivity detector was used. 100 µL samples were injected to the gas chromatography with a gas-tight syringe (Hamilton, 22 GA 500µL). Argon was used as the carrier gas. The flow rate of Argon gas was 26 mL/min. The oven, injector and detector temperatures were 140, 160 and 170 ºC, respectively.

4.2 Construction

The hydrodynamic model of the PBR was developed and shown in ‘Modelling of Photobioreactor’. The pilot scale reactor was constructed based on the dimensions

obtained from the model. The PBR was made of glass. The details of the PBR dimensions are given below.

4.2.1 Inlet and Outlet Manifolds

The fluid was distributed to the tubes by means of manifolds. Inlet and outlet manifolds were identical. They are made of glass. The diameter of each manifold was 6 cm, and the length was 47.5 cm. The wall thickness of the glass manifolds was 2 mm. At the upper side of the manifold, gas was collected by connecting a polyurethane pipe to the manifold. The inlet manifold has one inlet which has 12 cm diameter, 4 exits with 3 cm outside diameters and a gas exit whose outside diameter was 6 mm. Similarly, the outlet manifold has 4 inlets with 3 cm diameters, 1 outlet which has 18 cm diameter, and 1 gas outlet with 6 mm outside diameter.

In order to keep the temperature of the reactor at the desired values, a spiral glass cooling coil was designed inside the manifolds. Temperature was measured at the bottom and upper side of the manifold by inserting J-type thermocouples. The inlet and outlet manifolds were shown in Figure 4.1.

(a)

(b)

Figure 4.1: Inlet and Outlet manifolds (a) front view (b) side view

4.2.2 Tubing

Hydrogen production mainly occurred in the glass tubes. Glass tubes have 3 main sections for the ease of use. 2 tubes with 1.5 m in length were connected to manifolds. U – Tube was used to connect these tubes (Figure 4.2-a). Tees were used for sampling as shown in Figure 4.2-b. The tube diameter was chosen as 3 cm after the experiments mentioned in Diameter Selection (Appendix C) were performed. The wall thickness of the tubes was chosen as 1.5 mm. Hydrogen production mainly occurred in this part of the reactor. Temperature was measured in the reactor at 3 points by using tees: after the inlet manifold, before U – tube and before outlet manifold. U-tubes were tilted 30 ºC in order to collect the hydrogen gas easily. Connections of the glass tubes were made via silicon pipe.

(a)

(b)

Figure 4.2: a) U – tubes b) Tees for sampling and thermocouples

Polyurethane pipes, which have 5.5 mm inlet diameter and 8 mm outlet diameter, were used between the gas outlet of the manifolds and the gas collection unit.

To provide a secondary cooling capability (in addition to the glass coils in the manifolds) PVC cooling pipes were inserted into each of tube during RUN 092014 in order to keep the temperature of the reactor below 40 ºC in summer. The pipes had an inner diameter of 5 mm and an outer diameter of 7 mm. These pipes were connected to a process water cooler (PNÖSO PSS 6 D). The cooling water temperature ranged between 5 – 10 ºC manually, in order to keep the temperature of the reactor below 40 ºC in summer.

No cooling coils were inserted into the tubes during RUN 072015-R1 and RUN 082015-R2. The temperature was controlled by using a controller system which changed the flow rate of the cooling water to keep the reactor temperature at 30ºC.

4.2.3 Stand

A stand was designed for the PBR by taking into account the approximate weight of the PBR. Inlet and outlet manifolds were put on a metal sheet that was welded on the stand. The inlet manifold stands 30 cm above ground whereas outlet manifold stands on the 38 cm above ground so that U-tubes would be 30ºC tilted. The pipes were fastened with pipe clamps. Wheels were fitted to the stand for ease of movement.

4.3 Pump Selection

It is generally argued that the bacteria cannot stand high shear stresses in pumping and recirculation (Flickinger, 2013; Li et al., 2011). Therefore, the pressure difference created by the pump could become an important parameter in large scale operations. In order to understand the effect of pump type, an experiment was carried out. U-tube PBRs were run parallel with *Rhodobacter Capsulatus YO*$_3$. 5 mM sucrose-containing molasses was used as the hydrogen production medium. The experimental set-up is shown in Figure 4.3.

The growth of the bacteria was compared in two U-tube parallel reactors whose volumes were 3 L. One of the reactors was operated with a centrifugal aquarium pump (referred to simply as the aquarium pump henceforth); whereas the other was operated with a peristaltic pump. A higher biomass concentration was achieved with the peristaltic pump on the first day (Figure 4.1). However, for rest of the 3-day experiment, the order of biomass concentrations in both of the systems became the same (Figure 4.5).

Figure 4.3: U-tube PBRs operated with an aquarium pump (left) and a peristaltic pump (right). The experiment started on December 28, 2014 and lasted 3 days.

While growth was observed to be more or less the same, the peristaltic pump was observed to have several practical advantages over the aquarium pump. It is easy to adjust the flow rate with the peristaltic pump. While the centrifugal pump requires a recycle loop to reduce the flow rates to the targeted Reynolds range, this need is eliminated when a peristaltic pump is used; therefore, there is no need for extra connections. The number of connections in the pilot system should be as few as possible, since every connection brings about a potential leakage problem. Besides, most of the connections are metal in the centrifugal pump, which could affect bacterial growth and hydrogen production (Avcioglu, 2010), whereas peristaltic pump parts do not come directly into contact with the culture medium. Based on these considerations, the peristaltic pump was selected as the suitable pump type for photofermentative hydrogen production. Details of the experimental procedure and the experimental data obtained during the comparison of the pump types are given in Appendix D.

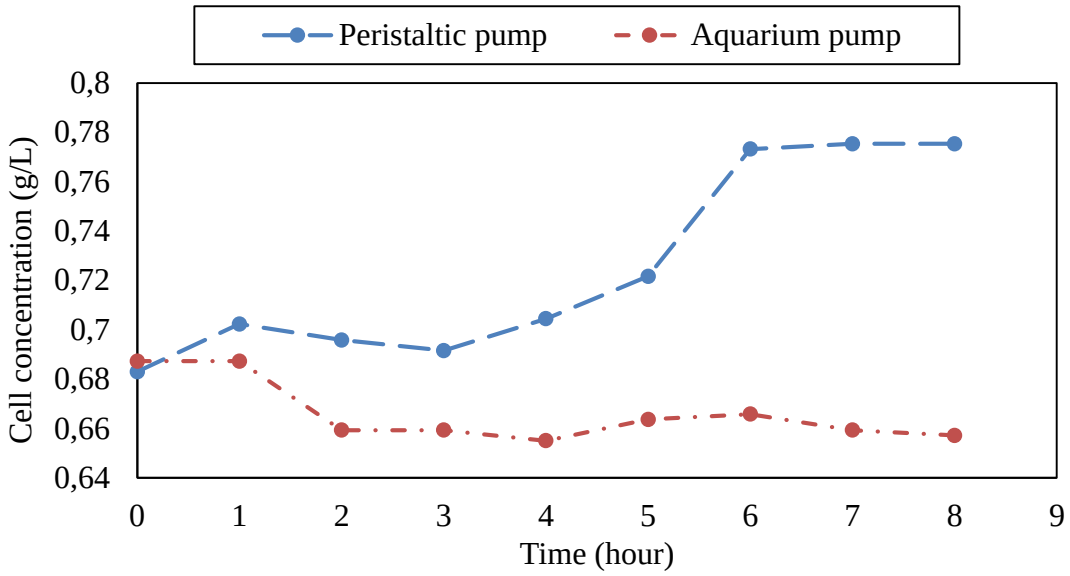

Figure 4.4: Variation in cell concentration for different pump types for the first day. The experiment started on December 28, 2014.

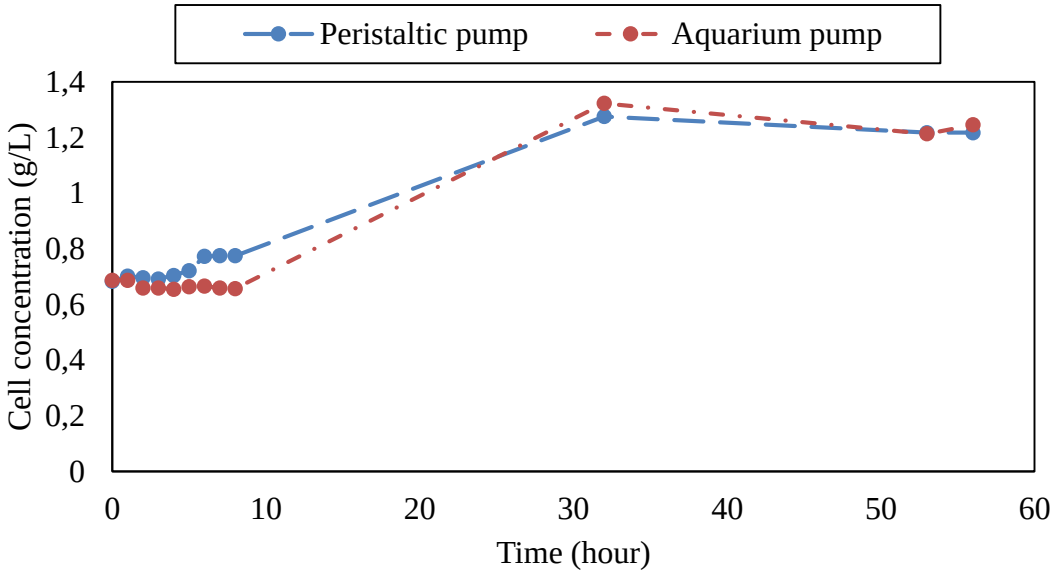

Figure 4.5: Variation in cell concentration for different pump types for 3 days. The experiment started on December 28, 2014.

4.4 Process Flow Diagram

The process flow diagram is shown in Figure 4.6. The liquid culture was circulated by means of a pump. The gas accumulated in the manifolds was collected through check valves (V1 and V2). The check valves opened when the gauge gas pressure inside manifolds reached 1/3 psi. 12 temperature ports were placed on the reactor, shown as T1-T12 in Figure 4.6. During continuous feeding, 1 L feed was given to the reactor and at the same time an equal volume of reactor liquid was discharged to maintain a constant reactor volume. The feed was given to the reactor by means of the valve, V5 on the feed line. At the same time, V3 was opened to discharge the reactor contents. 4 sampling ports were available on the reactor. If otherwise was stated, the samples were taken from the sampling port on the 2^{nd} tube. The cooling was achieved by water circulation from the cooling coils inserted into the manifolds.

In RUN 092014, an aquarium pump was used. A recycle around the pump was necessary while adjusting the flow rate to protect the pump. The flow rate at the inlet was adjusted by means of V6 and V7. In RUN 092014, 12 temperature measurements were taken from the reactor.

In RUN 072015-R1 and RUN 072015-R2, a peristaltic pump with two drive heads was used. Therefore, the recycle line containing V6 was discarded. In RUN 072015-R1, 12 temperature measurements were taken from the reactor. In RUN 072015-R2, 2 temperature measurements were taken from the ports T4 and T12.

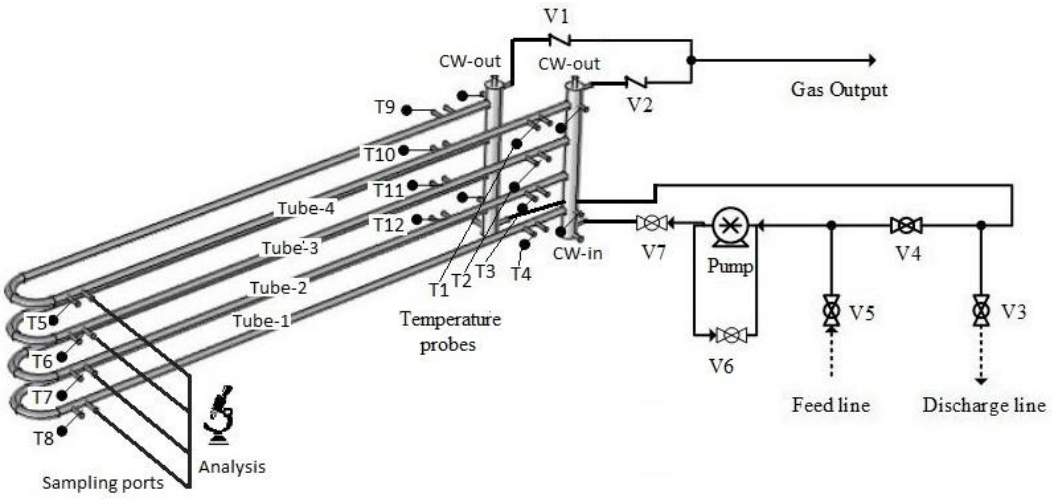

Figure 4.6: Process flow diagram of the stacked U-tube PBR. T1 – T12 are the temperature probes. V1 and V2 are check valves (1/3 psi), V4, V5, V6 and V7 are ball valves. CW-in and CW-out are cooling water inlet and outlet, respectively.

4.5 Operation

4.5.1 Sterilization and Leakage Test

The reactor was filled with 3 % hydrogen peroxide (H_2O_2) solution and the solution was circulated for 24 hours. Then the hydrogen peroxide solution inside the reactor was emptied, and the reactor was flushed with distilled water for 2 - 3 times in order to make sure that all the hydrogen peroxide solution was removed from the reactor.

4.5.2 Inoculation

The reactor was filled with inoculated culture media as soon as the sterilization and cleaning was complete. The reactor was filled until air was left only at the top of the inlet and outlet manifolds. While filling the reactor, the gas outlet was left open to the air. When the reactor was filled, the gas outlet was connected to a check valve (HAMLET 1/3 psi). The valve was connected to the gas collection unit as shown in Figure 4.6.

4.5.3 Continuous Feeding

In RUN 092015, the feeding started on the 3rd day of the experiment when the bacterial concentration stabilized. The feeding strategy was modified several times during this experiment, as discussed in detail in the 'Results and Discussion' part. A photograph taken during RUN 092015 is shown in Figure 4.7.

In RUN 072015-R1 (where acetate was the carbon source), the feeding was started when the cell density stabilized around an OD_{660} of 1.5 on the 4th day of the experiment. The feeding strategy was to keep the acetic acid concentration at 40 mM.

Figure 4.7: A photograph of the experimental set up (RUN 091025). The experiment performed with *R. capsulatus YO3* on molasses.

Each morning, as mentioned previously, 1 L fresh medium was fed in exchange for 1 L of reactor medium discharged. The acetic acid concentration in the feed was adjusted so that its concentration within the reactor remained around 40 mM. The feed also contained 2 mM sodium glutamate, vitamins, trace elements and Fe-citrate. The concentrations of vitamin, trace elements and Fe-citrate solutions were adjusted by taking into account the amounts added to 1 L basal medium. The contents of the solutions are given in Appendix A. A picture of the reactor is given as Figure 4.8.

Figure 4.8: Side views of the Reactor 1. Experiment performed with *R. capsulatus YO*$_3$ on acetic acid (RUN 072015 – R1)

In RUN 072015-R2 (with molasses as the carbon source), the feeding was started on the 5th day (17.07.2015). Every morning, 1 L of feed containing molasses was fed to the reactor while 1 L of the reactor contents was discharging. The feeding strategy was to keep the sucrose concentration at 5 mM in the reactor. The sucrose concentration of the feed was adjusted accordingly every day. The feed was supplied with molybdenum (0.16 μM) and iron (0.1 mM) by the addition of sodium molybdate ($Na_2MoO_4.2H_2O$)

and iron (III) citrate ($Fe(C_6H_5O_7)$). The metal concentrations were based on previous studies. A photograph of the reactor operated with *R. capsulatus* on molasses is shown in Figure 4.9. Another picture showing both reactors (RUN 071025-R1 and RUN 072015-R2) is shown in Figure 4.10.

Figure 4.9: Side views of the Reactor 2. Experiment performed with *R. capsulatus* YO_3 on molasses (RUN 072015 – R2).

Figure 4.10: The parallel reactors run in July 2015. (RUN 072015-R1 and RUN 072015-R2).

4.5.4 Sampling

In RUN 092014, 1 or 2 samples were taken every day from tube 2. The average of the samples are reported here. The OD and pH values were measured 3 times for each sample and the average values are given in Appendix F. The OD, pH, organic acid, and sucrose content in the samples were analyzed daily.

In RUN 072015-R1 and RUN 072015-R2, 2 samples (one in the morning and one in the evening) were taken each day from the 2nd tube (counted from the bottom). 3 measurements for OD and pH for each of the samples were made for each of the samples. The organic acid and sucrose content (only for reactor 2) of the samples were analyzed daily. The biogas content was also measured daily. All raw data are given in ‘Appendix F.

CHAPTER 5

RESULTS AND DISCUSSION

5.1 September 2014 Outdoor Experiment with *Rhodobacter capsulatus YO$_3$* (hup$^-$) on Molasses (Run 092014)

The experiment with *R. capsulatus YO$_3$* was conducted between September 9 and September 29, 2014. The reactor was cooled intermittently, only on days 2, 3, 4 and 6 at noon time, to keep the culture temperature below 40ºC. The temperature variation of the culture along the reactor length is shown in Figure 5.1-a. Temperature did not change significantly along the reactor length when there was cooling. Temperature variation from tube to tube was also insignificant (Figure 5.1-b). However, as expected, the lowest temperature was observed in the lowest tube (T12), when cooling started, since cooling water enters the manifolds from the bottom. The temperature variation according to tube position and length was not appreciable when there was no cooling. (Figure 5.2). It can be observed that the reactor temperature followed the same trend with the air temperature, but it was slightly higher. The daily temperature variation within the reactor is illustrated in Figure 5.3. As expected, the liquid culture temperature was highly affected by the solar radiation. Since most of the time there was no cooling, the temperature of the reactor was mainly driven by solar radiation.

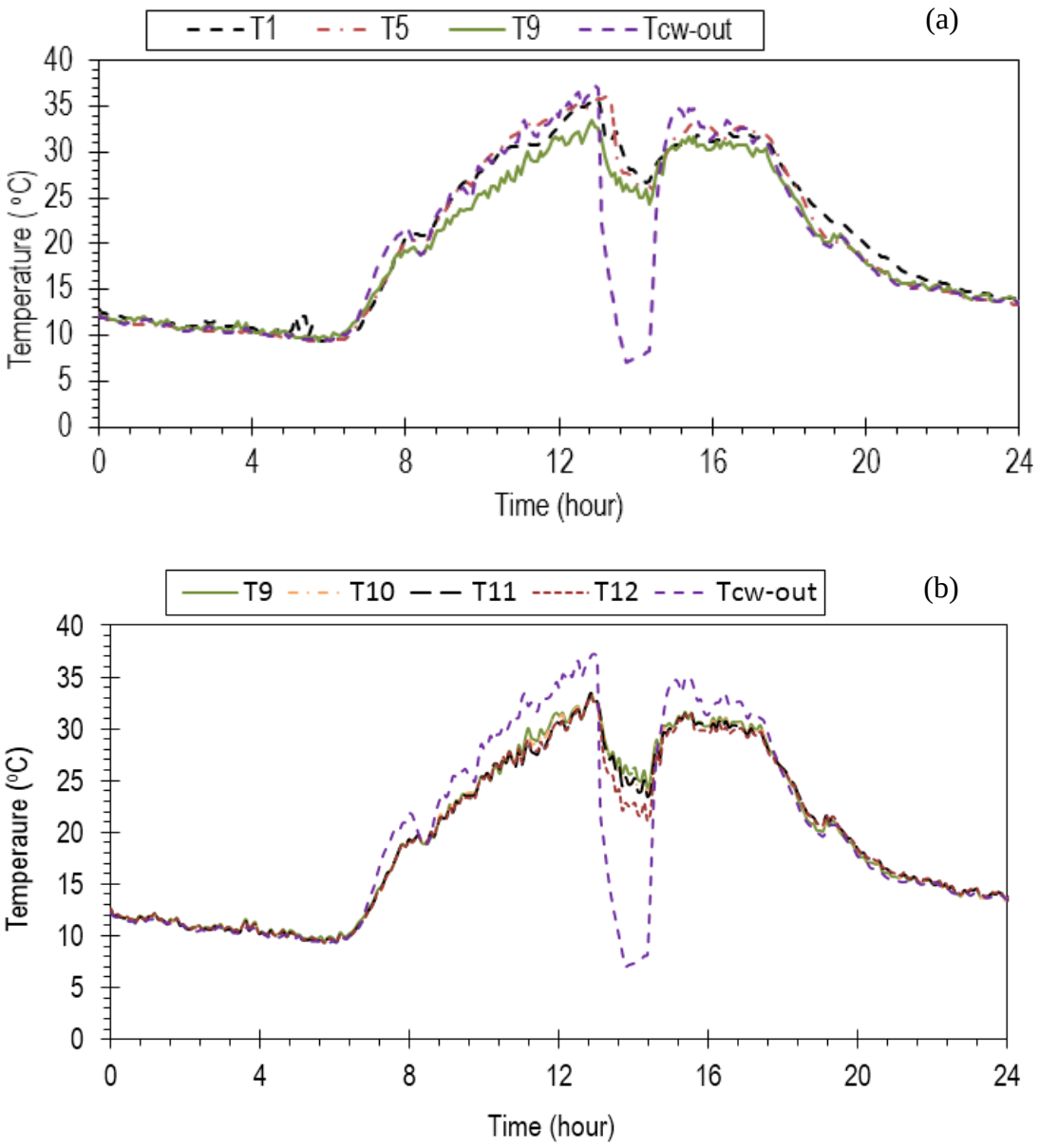

Figure 5.1: (a) Comparison of temperature variation with time for different tubes on the 6th day of the experiment (T1, T5 and T9 were measured from the entrance, midpoint and exit ports in tube 4, respectively) (b) Comparison of temperatures along the length of the PBR on the 6th day of the experiment. The experiment started on September 9, 2014. (T9, T10, T11 and T12 were measured from the exit ports of tube 4, tube 3, tube 2 and tube 1, respectively.)

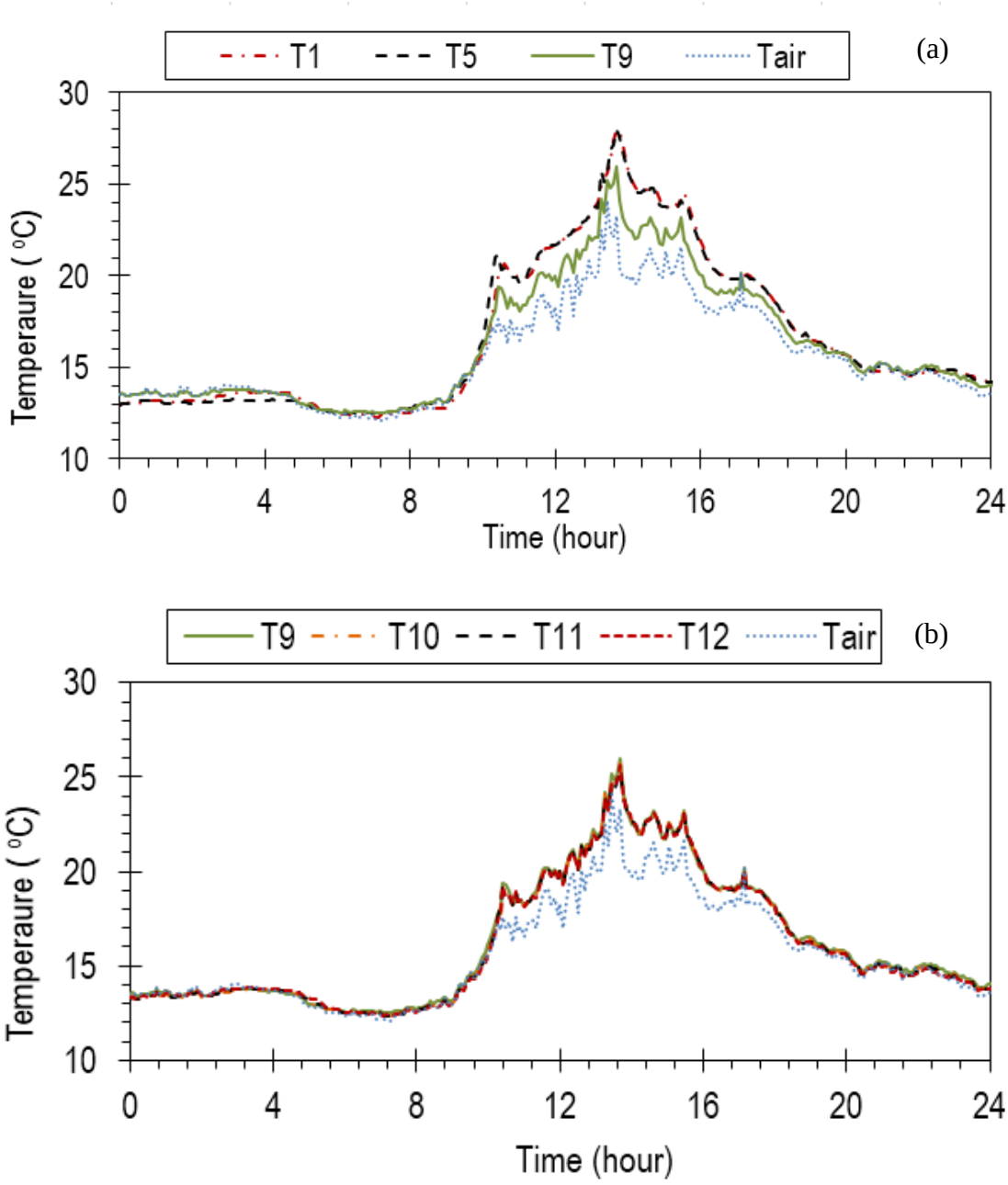

Figure 5.2: (a) Comparison of temperature change along the length of the PBR on the 10th day of the experiment. (T1, T5 and T9 were measured from the entrance, midpoint and exit ports in tube 4, respectively.) (b) Comparison of temperature change for different tubes on the 10th day of the experiment. Experiment started on September 9, 2014. (T9, T10, T11, T12 were measured from the exit ports of tube 4, tube 3, tube 2 and tube 1, respectively.)

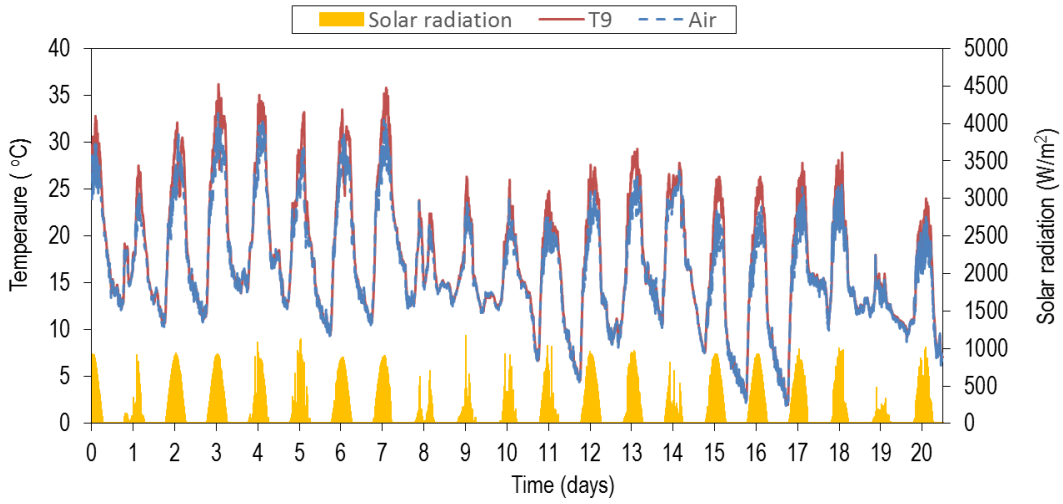

Figure 5.3: Relation between the temperature change and the daily solar radiation for RUN072015-R1. T9 is measured from the exit port of the tube 4. Experiment started on September 9, 2014.

The feeding strategy was based on the work of Sağır (2012). The highest hydrogen production was found with *R. capsulatus YO*$_3$ with 5 mM sucrose containing molasses in a batch PBR (Sağır, 2012). However, due to the fact that the observed sucrose consumption rate of the present study was found to deviate considerably from indoor results, a more variable strategy had to be adopted based on the culture response in order to maintain the nutrients and reactor conditions close to optimal conditions. The 'phases' of this feeding strategy were given in Table 5.1 and are explained further below.

The initial sucrose concentration of molasses was adjusted to 5 mM. The cell concentration stabilized at the 3rd day of the experiment (Phase I) and the sucrose concentration decreased to very low values (around 0.5 mM). To increase the cell concentration, Phase II, involving continuous feeding of molasses, was started on the 4th day.

Table 5.1: The feeding strategy

Phase	**Sucrose Concentration in Molasses (Feed)**	**pH (Feed)**	**Feed Rate**
I	5 mM	7.5	40 mL/day
II	5 mM	7.5	1 L/day
III	100 mM	7.5	1 L/day
IV	-	-	No feeding
V	50 mM	7.5	1 L/day
VI	-	-	No feeding
VII	50 mM	11-12	1 L/day

During Phase II, the organic acid content was below 4 mM (Figure 5.4). At the end of 10 days, cell concentration dropped to 0.12 gdcw/L due to the rapid depletion of carbon source (Figure 5.5), requiring a substantial addition of sucrose to maintain cell viability. Thus, in Phase III, 100 mM sucrose containing molasses were fed to the reactor, which led to a significant increase in the organic acid content, in turn, resulting in a decrease of pH (Figure 5.4). Although the bacteria finally reached optimal levels of cell concentration for hydrogen production (around 0.5 gdcw/L), no hydrogen production was observed, probably due to the low pH. It could be speculated that the metabolism of the bacteria had shifted to other modes after Phase III, based on the increase in lactic and acetic acid concentrations. In Phase IV, feeding was stopped for two days, resulting in stabilized organic acid content in the reactor on the 13^{th} and 14^{th} days of the experiment. As a result, the cell concentration was increased to its highest value (1.0 gdcw/L) on the 14^{th} day of the experiment (Figure 5.6). 1 L of 50 mM sucrose containing molasses was fed to the reactor on the 15^{th} day (Phase V). In the following day, no feeding was done (Phase VI). At the last phase (Phase VII), 1L of 50 mM sucrose containing molasses was fed to the reactor daily. In the feed, pH was adjusted to 11- 12 with addition of NaOH solution. During this phase, all the organic acids' concentration was decreased; however, pH was stabilized around 5 and the reactor was shut down.

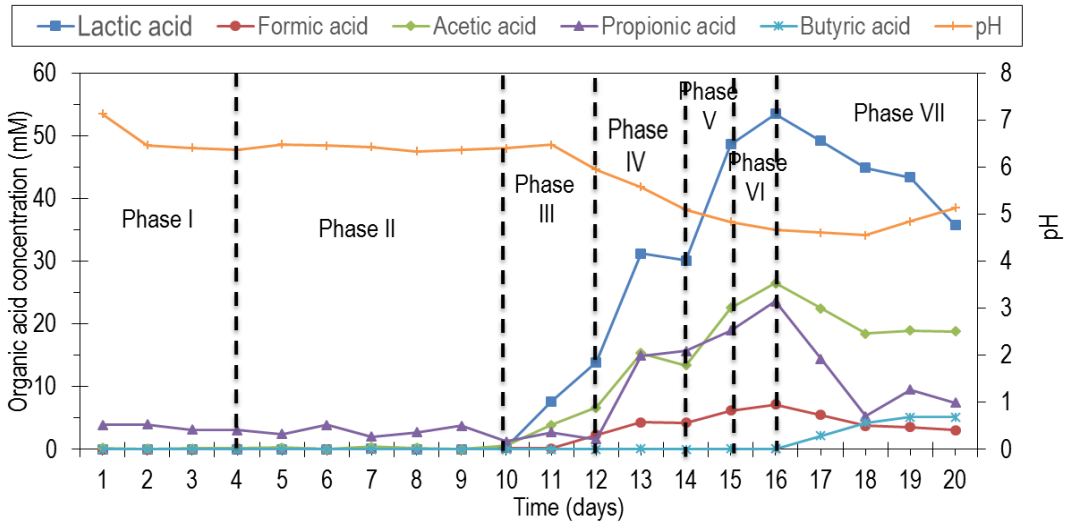

Figure 5.4: Organic acid and pH variation in the reactor. Experiment started on September 9, 2014.

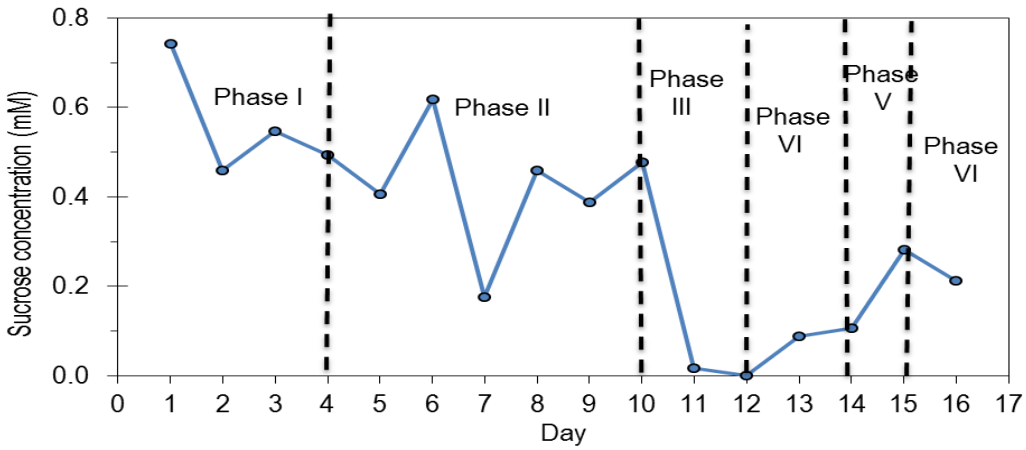

Figure 5.5: Daily sucrose concentration change. Daily sucrose concentration change. Experiment started on September 9, 2014.

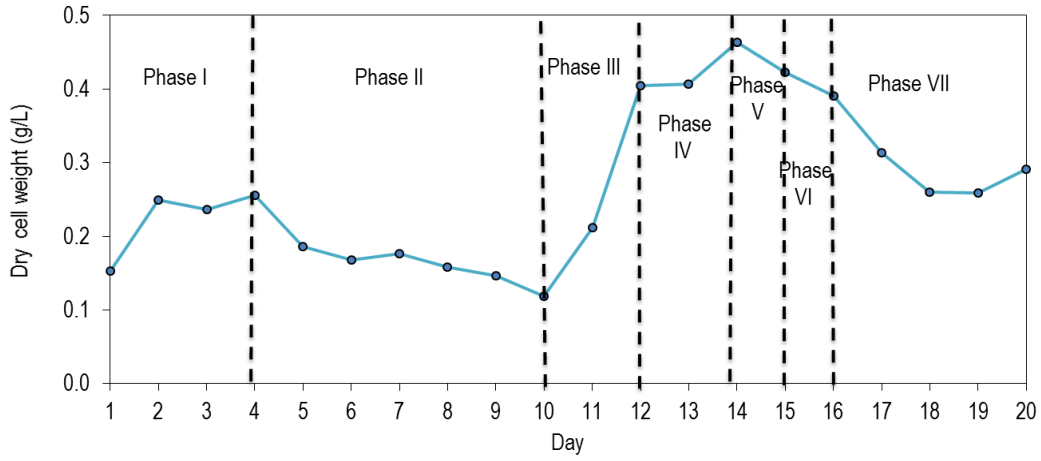

Figure 5.6: Daily cell concentration change. Experiment started on September 9, 2014.

5.2 July 2015 Outdoor Experiments with *Rhodobacter capsulatus YO$_3$* (hup$^-$) (Run 072015)

Two reactors were run in parallel with *Rhodobacter capsulatus YO$_3$* (hup$^-$) in July 2015. Reactor 1 (R1) initially contained 40 mM acetic acid and 2 mM sodium glutamate, whereas Reactor 2 initially contained 5 mM sucrose containing molasses. Details of the experimental operation of the reactors were given previously under the 'Operation' part of Chapter 4.

Both of the reactors were operated at the same recirculation flow rate: 80.4 L/h (Re_t=296) between July 12 and July 16, 2015, and 100 L/h (Re_t=368) between July 16 and July 24, 2015. The flow rate was increased at July 16, because cooling was not sufficient with 80.4 L/h. By increasing the recirculation flow rate, convective cooling was improved. Besides, the residence time of the culture in the tubes was decreased. Therefore, the cooling become more effective in the reactor.

A temperature controller was installed to the reactor system to keep the reactor temperature about 30ºC. The cooling water temperature was set manually between 5 and 10ºC, though it was fixed at 10ºC most of the time. The controller varied the

cooling water flow rate to maintain the set point. The temperature of Reactor 1 was measured from the port T11, and the cooling water flow rate was adjusted accordingly for both reactors.

5.2.1 Run 072015-R1: Outdoor Experiment with *Rhodobacter capsulatus YO$_3$* (hup$^-$) on Artificial Medium

The experiment with *R. capsulatus YO$_3$* was carried on with artificial medium between July 12 and July 21, 2015. The volume of the reactor (Reactor 1) was 11 L. Both reactors were cooled solely from the cooling coils inserted into the manifolds. It was observed that the flow rate of the reactor had an effect on the temperature profile. At the extreme case, at which flow was completely stopped, the temperature just before the collection manifold (T9, T10, T11, and T12) would be higher than the air temperature presumably due to metabolic activity and absorption of radiation. This behavior was also observed previously in RUN 092014, when there was no cooling (Figure 5.2). Additionally, the temperature of the tube closer to the ground was significantly lower than the temperature of higher ones, since the cooling water entered the manifolds from the bottom. In order to make sure that the reactor was efficiently cooled, the temperature of the reactor was checked at several locations. The temperature difference along the reactor length was noted and the corresponding results are displayed in Figure 5.7-a. Figure 5.7-a indicates that the temperature gradient was acceptable. The temperature difference along the length of the PBR remained below 5ºC.

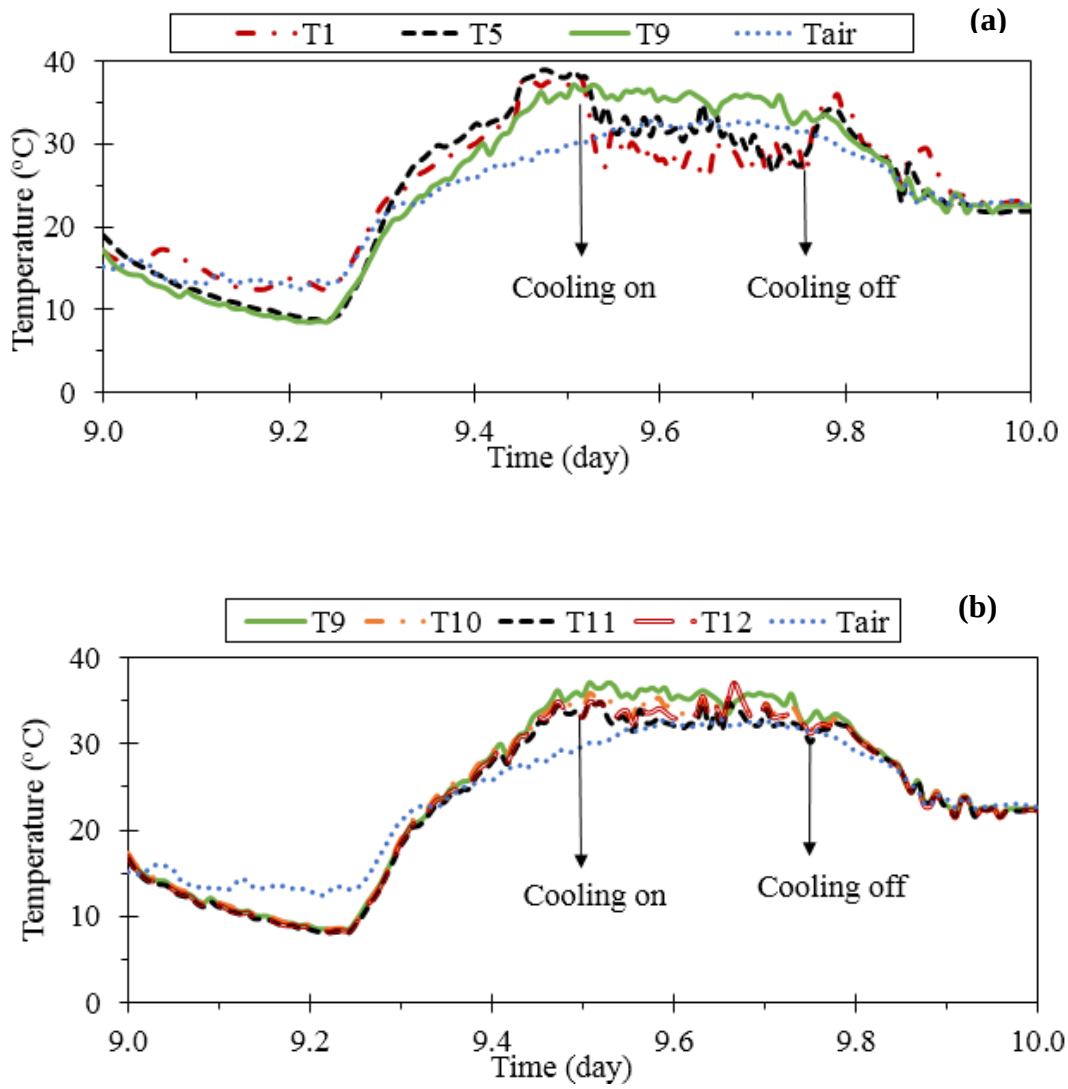

Figure 5.7: (a) Comparison of temperature variation with time for different tubes on the 9th day of the experiment (T1, T5 and T9 were measured from the entrance, midpoint and exit ports in tube 4, respectively) (b) Comparison of temperatures along the length of the PBR (RUN072015-R1) on the 9th day of the experiment. Experiment started on July 12, 2015. (T9, T10, T11, T12 were measured from the exit ports of tube 4, tube 3, tube 2 and tube 1, respectively.)

T1 was the closest thermocouple to the distribution manifold. During cooling, T1 was the lowest temperature. It was followed by T5 and T9, as expected. T9 was measured on the tube 4, just before the collection manifold. Therefore, its temperature was the highest. Air temperature was also reported as reference point. Temperature differences

between the tubes were also compared in Figure 5.7-b. Again, T9 was found as the highest temperature. There was not a significant temperature gradient between the tubes. The temperature in all of the tubes (T5, T6, T7 and T8) was maintained around 35ºC. Therefore, an effective cooling was achieved. The changes in reactor (T9) and the air temperature and solar radiation during the experiment were shown in Figure 5.8.

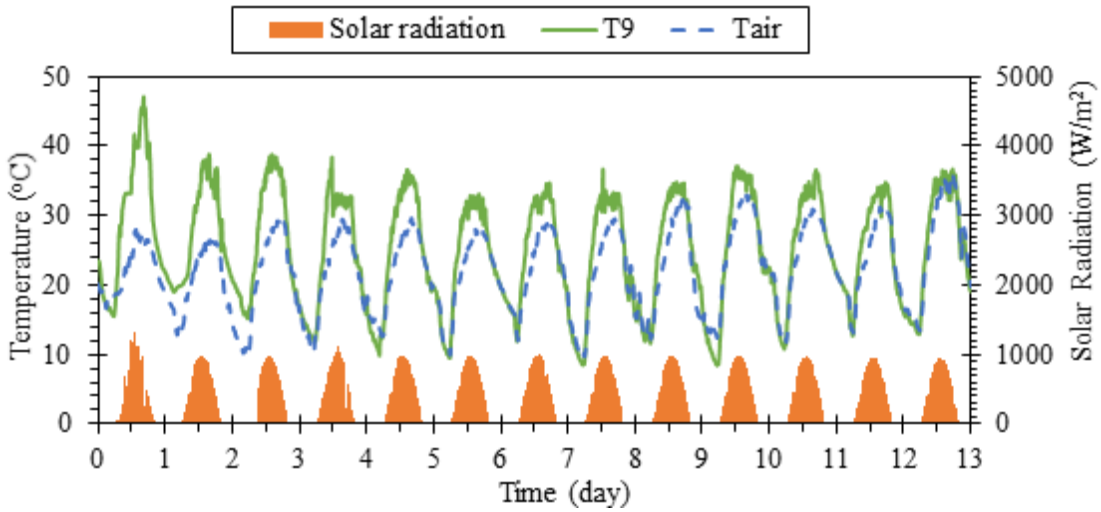

Figure 5.8: Relation between the temperature change and the daily solar radiation for RUN072015-R1. T9 is measured from the exit port of the tube 4. The experiment was started on July 12, 2015.

The dry cell weight and hydrogen production was shown in Figure 5.9-a and Figure 5.9-b, respectively. The maximum cell concentration was observed on the 3rd day as 0.748 gdcw/L. After the feeding started on the 4th day, the cell concentration was stabilized in between 0.5 and 0.6 gdcw/L.

The average hydrogen productivity was found as 0.077 mol H_2/(m^3.h). The highest productivity, 0.144 mol H_2/(m^3.h), was observed on the 2nd day of the experiment (Figure 5.9). A sample calculation for the productivity is given in Appendix K.1. In comparison, Boran (2010) performed an outdoor experiment with *R. capsulatus YO*$_3$ on an artificial medium containing acetate, reporting the average and maximum

productivity as 0.20 and 0.40 mol $H_2/(m^3.h)$, respectively (Boran et al., 2012a). The feed was not autoclaved in this run to simulate industrial scale applications. However, this probably caused a decrease in productivity.

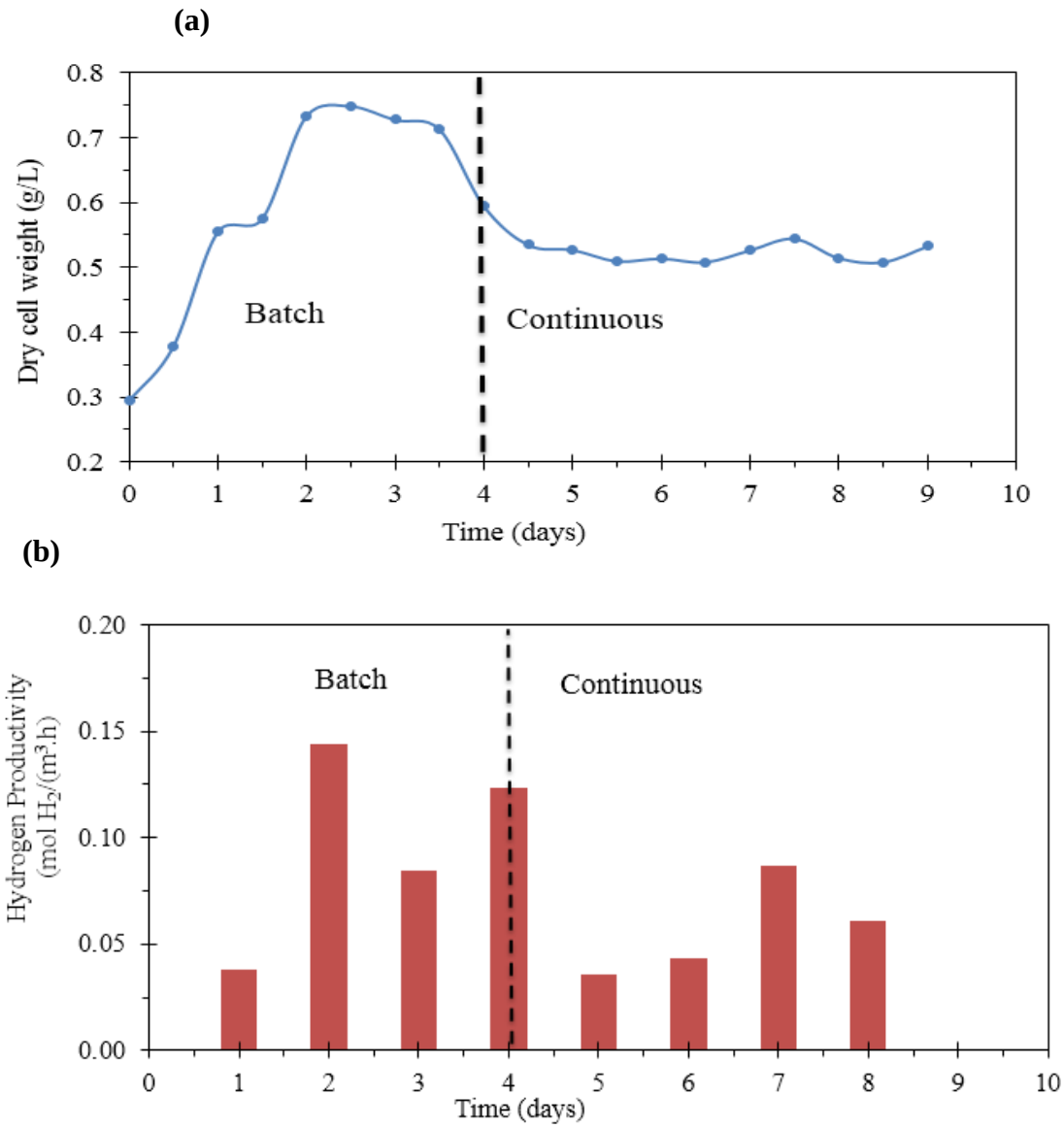

Figure 5.9: (a) Variation in cell concentration (b) Daily hydrogen production in outdoors with *R. capsulatus YO3* on artificial medium under non-sterile conditions (RUN072015-R1).

The starting date of the experiment was July 12, 2015. Feeding started on the 4th day In Table 5.2, total gas produced and the gas percentages are shown. Substrate

conversion efficiency and light conversion efficiency are also given in Table 5.2. The maximum substrate conversion efficiency was found 17.5 % on the 3rd day of the experiment. The maximum light conversion efficiency was found as 0.027 % on the 2nd day of the experiment. The sample calculations for the substrate conversion efficiency and the light conversion efficiency are given in Appendix K.2 and K.3, respectively. The average substrate conversion efficiency was calculated (excluding the last day) as 9.2%. In another outdoor study, the substrate conversion efficiency was calculated as 15% when *R. capsulatus YO3* on acetic acid was utilized (Boran et al., 2012b). The maximum substrate conversion efficiency in this study was found higher than that is found by Boran et al (2012b). When acetic acid in the dark fermenter effluent of thick juice was utilized with the same bacteria, the substrate conversion efficiency was found as 9 % (Boran et al., 2012a, 2012b).

Table 5.2: The experimental results of hydrogen in outdoors with *R. capsulatus YO3* on artificial medium under non-sterile conditions (RUN072015-R1).

Date	**Gas content**		**Total gas (mL)**	**H_2 productivity (mol H_2/(m^3.h)**	**Light conversion efficiency, %**	**Substrate conversion efficiency %**
	H_2 %	**CO_2 %**				
13.07.2015	96.8	3.2	171	0.038	0.007	5.1
14.07.2015	96.5	3.5	643	0.144	0.027	8.5
15.07.2015	97.6	2.4	372	0.084	0.016	17.5
16.07.2015	95.8	4.2	556	0.123	0.021	12.5
17.07.2015	93.0	7.0	486	0.035	0.006	7.0
18.07.2015	78.7	21.3	239	0.044	0.007	8.3
19.07.2015	87.2	12.8	429	0.087	0.015	8.2
20.07.2015	87.5	12.5	301	0.061	0.010	6.7
21.07.2015	6.5	93.5	2	0.000	0.000	0.0

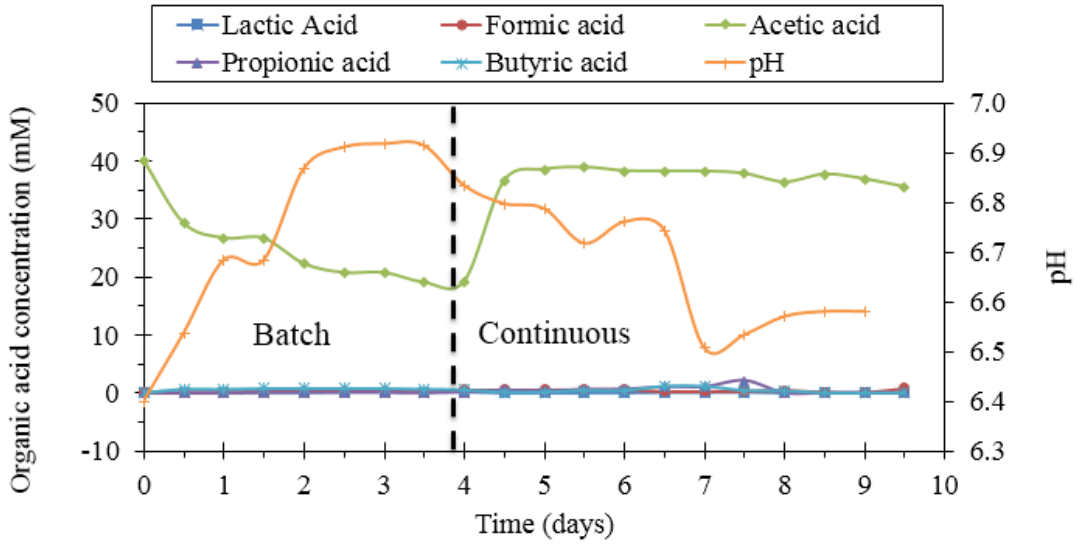

Figure 5.10: Variation in pH and organic acid concentration in outdoors with *R. Capsulatus YO₃* on artificial medium under non-sterile conditions (RUN072015-R1). The starting date of the experiment was 12.07.2015. Feeding started on the 4th day.

The variation in organic acid concentration and pH are shown in Figure 5.10. Acetic acid concentration decreased to around 20 mM during the batch phase. When the feeding started, acetic acid concentration was adjusted to 40 mM every day in the morning. Lactic acid, formic acid, propionic acid and butyric acid concentrations remained under 1 mM (11 mmol). After the continuous feeding started, 2-3 mM (22-33 mmol) acetic acid was consumed daily. The pH of the culture was between 6.4 and 7.0 throughout the experiment.

5.2.2 Run 072015-R2: Outdoor Experiment with *Rhodobacter capsulatus YO₃* (hup⁻) on Molasses in July

The experiment with *R. capsulatus YO₃* on molasses (RUN 092014) was repeated between July 12 and July 24, 2015. The reactor was operated under the same conditions as RUN 072015-R1. Apart from the medium, the only difference between the two reactors (R1 and R2) was the volume. R1 was 11 L; whereas R2 was 9 L because of the difference in their headspaces.

The temperature of Reactor 2 (R2) was measured with thermocouples, T4 and T12, which were both located on the tube closest to the ground (Tube 1). The thermocouple, T4 was just after the distribution manifold, and T12 was located at the end of the same tube, just before the collection manifold. The temperature along the tube length for Reactor 2 did not change significantly (Figure 5.11). Therefore, it can be concluded that efficient cooling was also achieved in Reactor 2 as in Reactor 1.

In order to have a closer look at the temperature difference between the two reactors, Figure 5.12 was plotted. The temperatures measured from the thermocouples T12 for both of the reactors were very similar throughout the experiment.

Daily variations in sucrose concentration for RUN072915-R2 are shown in Figure 5.13. Daily, the sucrose concentration in the reactor was adjusted to 5 mM after the continuous feeding started. The measurements were taken each day, in the morning before feeding and in the evening. In the actual case, the sucrose concentration went as high as 5 mM every day in the morning, and almost all of the sucrose was consumed daily. In comparison, under indoor conditions the bacteria consumed 47 % of the sucrose during 200 hours (~8days) (Sağır, 2012). It is obvious that there is a great difference in the sucrose consumption rate in indoor and outdoor experiments. This makes it difficult to find a proper feeding strategy, since the sucrose consumption rate is also related with some of the uncontrolled and fluctuating parameters in outdoors such as light intensity and temperature. The kinetics of the sucrose consumption rate and its relation with the light intensity should be investigated further to find the best feeding strategy.

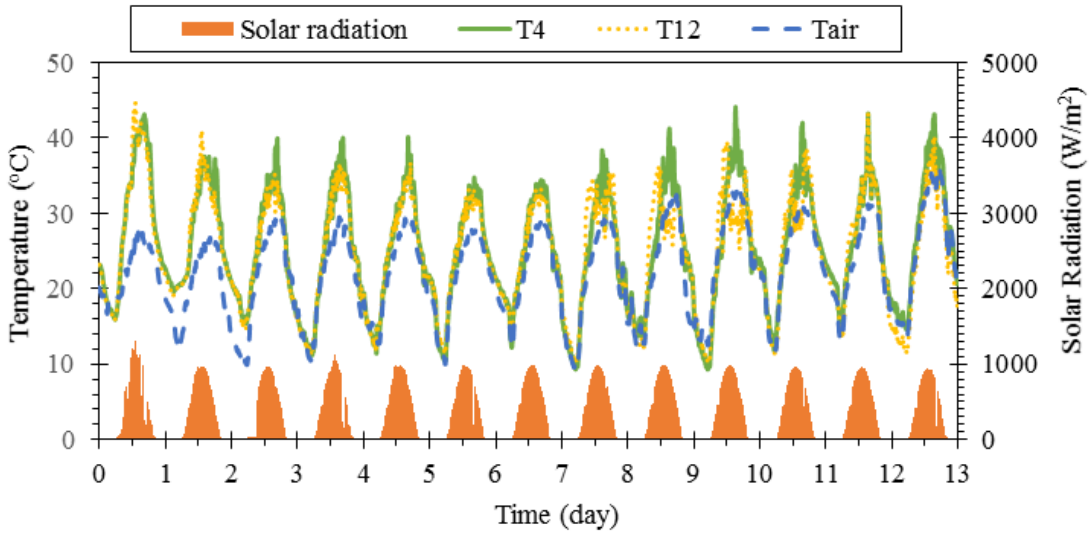

Figure 5.11: Relation between the temperature change and the daily solar radiation for RUN072015-R2. T4 and T12 were measured from after the distribution manifold and before the combination manifold, respectively. Both of them were on the Tube 1. Experiment started on July 12, 2015.

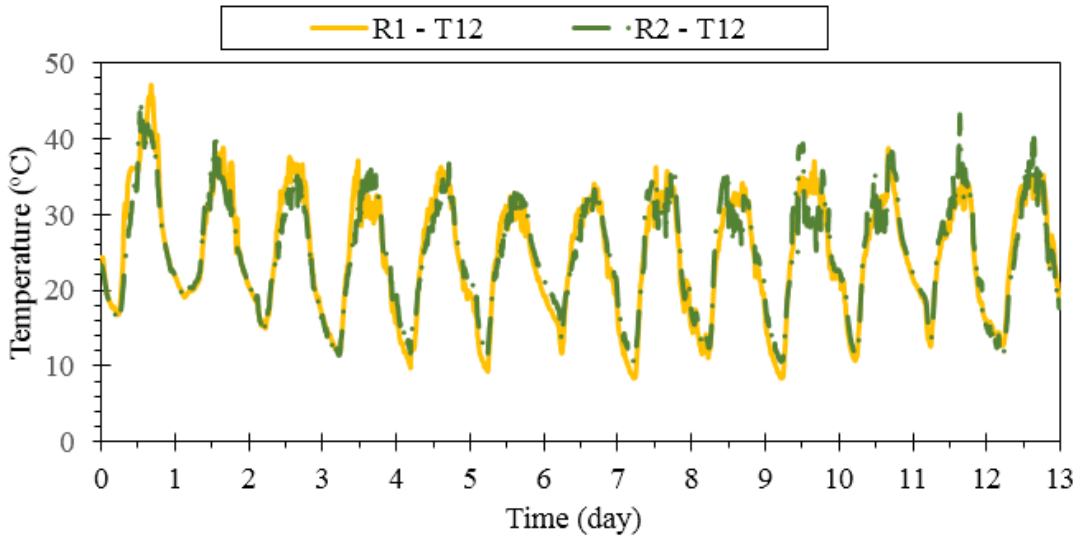

Figure 5.12: The comparison of the temperatures for RUN072015-R1 and RUN072015-R2. R1-T12 and R2-T12 were measured on the Tube 1 just before the combination manifold. Experiments started on July 12, 2015.

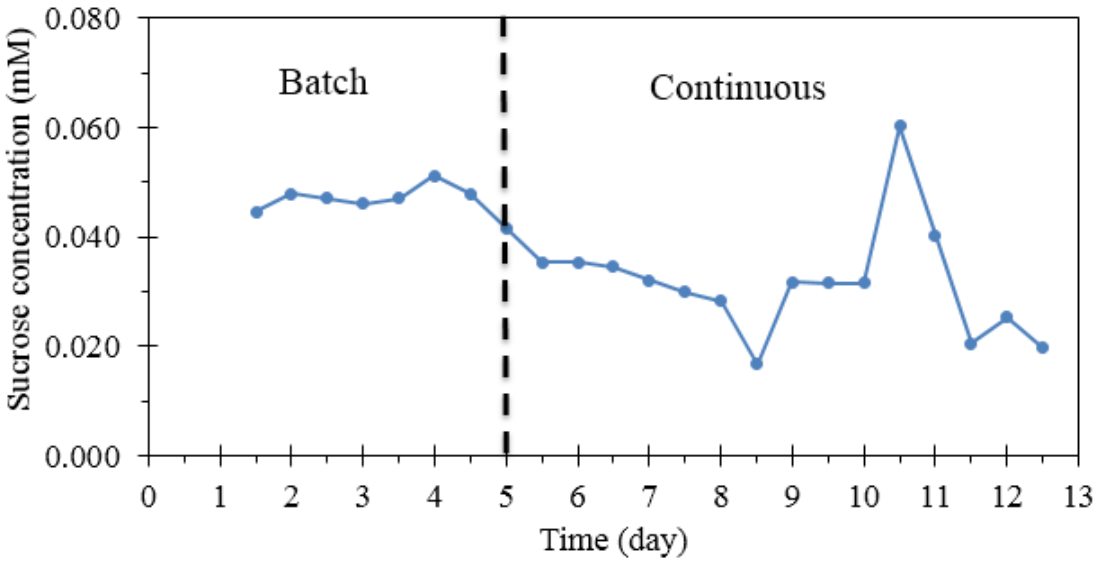

Figure 5.13: Daily variation in sucrose concentration for RUN 072915-R2. The initial sucrose concentration was 5 mM (data not shown). The starting date of the experiment was July 12, 2015.

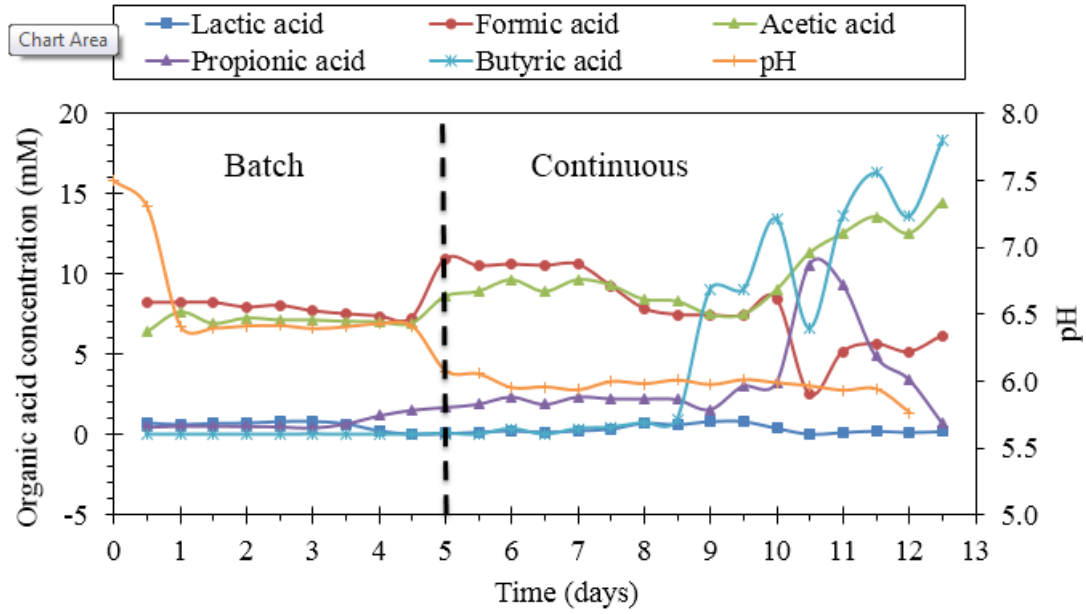

Figure 5.14: Variation in pH and organic acid concentration in outdoors with *R. capsulatus* YO_3 on molasses (RUN072015-R2). The starting date of the experiment was 12.07.2015. Feeding started on the 5th day.

The change in the daily organic acid concentration is shown in Figure 5.14. pH decreased to 5.5 – 6 during the experiment possibly due to the formation of organic acids. After the continuous feeding started, pH decreased even more. Therefore, on the 6th day, the pH of the feed was increased to 9.0 with NaOH addition. The pH of the feed was adjusted to 9.0-10.0 for the following days. After the 6th day, the pH of the culture stabilized around 6.0.

The acetic acid concentration during the entire experiment was in between 5- 15 mM. When the acetic acid pathway is used, 24 moles of hydrogen should be produced from one mole of sucrose. The highest substrate conversion efficiency based on these reactions was determined as 3.7 % on the 10^{th} day of the experiment (Table 5.3) assuming only the acetic acid pathway was used. The average substrate conversion efficiency (excluding the days with no hydrogen production) was calculated as 1.9 %. This is yield is hypothetical, since other organic acids are also produced in the medium. When the pathway differs, theoretical hydrogen production from 1 mol of sucrose also differs.

The dry cell weight and hydrogen production was shown in Figure 5.15 and Figure 5.16, respectively. The dry cell weight changed between 0.4 and 0.6 gdcw/L after the continuous feeding started.

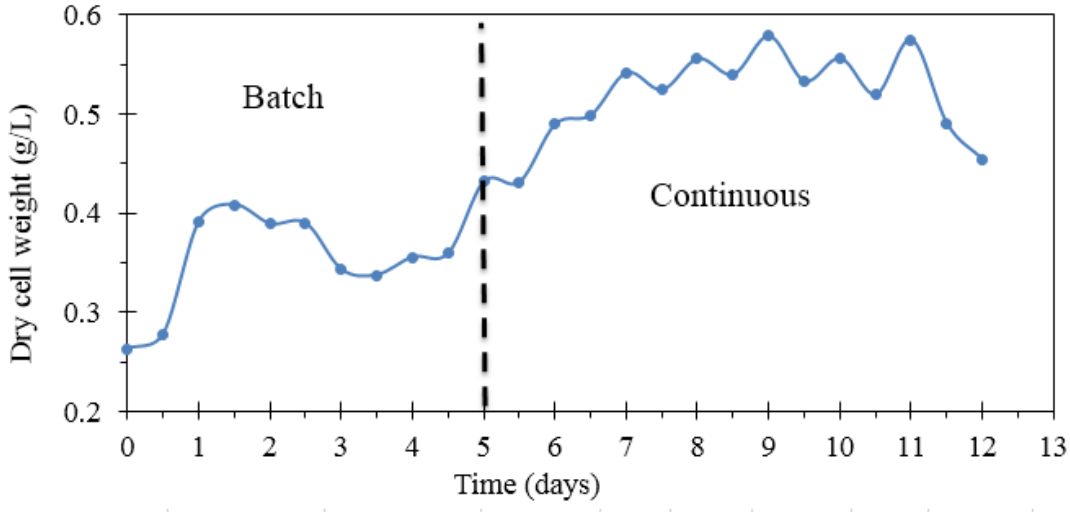

Figure 5.15: Cell concentration and hydrogen production in outdoors with *R. Capsulatus YO3* on molasses (RUN072015-R2). The starting date of the experiment was 12.07.2015.

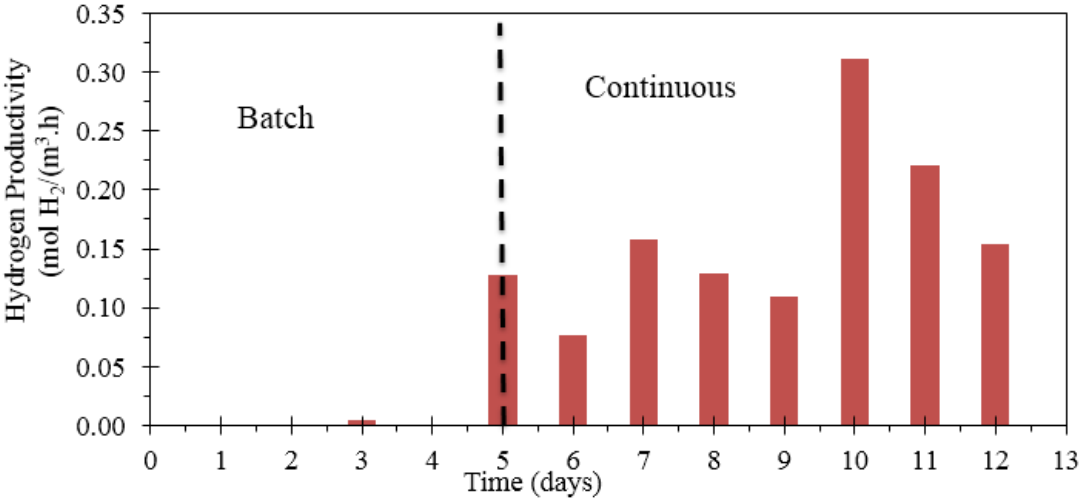

Figure 5.16: Daily hydrogen productivity. The starting date of the experiment was 12.07.2015.

It is known that the optimum pH for hydrogen production is 7.0. Previous studies show that hydrogen production diminish at pH 6.0 and completely stops around pH of 5.0 (Sasikala et al., 1991). During this experiment, the hydrogen production continued even though the pH values got as low as 5.5 - 6.0. The average and the highest productivities were found as 0.108 mol $H_2/(m^3.h)$ and 0.311 mol $H_2/(m^3.h)$,

respectively. Sağır (2012) studied indoors with the same bacteria on 5 mM sucrose containing molasses. He found the productivity as 0.410 mol $H_2/(m^3.h)$. (Sağır, 2012). The productivity found in this study under outdoor conditions was very close to the productivity obtained in the previous indoor study where most of the key parameters such as light intensity and temperature was kept under control. Moreover, with a proper pH controller, this productivity can be increased.

Table 5.3: The experimental results of hydrogen production outdoors with *R. capsulatus YO3* on molasses (RUN072015-R2)

Date	**Gas content**		**Total gas (mL)**	**H_2 productivity (mol $H_2/(m^3.h)$)**	**Light conversion efficiency %**	**Substrate conversion efficiency %**
	H_2%	**CO_2%**				
13.07.2015	0	0	0	0.000	0.000	0.0
14.07.2015	0	0	0	0.000	0.000	0.0
15.07.2015	100	0	18	0.005	0.001	0.0
16.07.2015	0	0	0	0.000	0.000	0.0
17.07.2015	84.7	15.3	532	0.128	0.018	1.5
18.07.2015	53.5	46.5	506	0.077	0.011	0.9
19.07.2015	37.5	62.5	1484	0.158	0.022	1.9
20.07.2015	24.5	75.5	1865	0.129	0.018	1.5
21.07.2015	29.6	70.4	1298	0.109	0.015	1.3
22.07.2015	23.2	76.8	4732	0.311	0.044	3.7
23.07.2015	20.2	79.8	3851	0.220	0.031	2.6
24.07.2015	17.6	82.4	3090	0.155	0.024	1.8

The percent biogas content and hydrogen productivity was shown in Table 5.3. As pH decreased, the hydrogen percentage also decreased after the 5^{th} day of the experiment.

The reason behind the high hydrogen percentages was attributed to the pH range within which the bacteria are capable of hydrogen production. The solubility of CO_2 was 1.45 g/L in distilled water under atmospheric pressure. The aqueous dissociation of CO_2 is shown below. CO_2 acts as weak acid in water (Koku, 2001).

$$CO_2(g) \rightarrow CO_2(aq) + H_2O\ (l) \leftrightarrow H^+ + HCO_3^- \leftrightarrow 2H^+ + CO_3^- \quad (5.1)$$

The dominant species in the pH range between 7.0 and 8.5 is bicarbonate (HCO_3^-) (Figure 5.17). Therefore, most of the carbon dioxide was captured inside the medium as bicarbonate during photofermentation. However, in the pH range of 4.0 and 6.0, the dominant species is the carbon dioxide (Koku, 2001). Therefore, the carbon dioxide percentage in the biogas increased due to the decrease in pH.

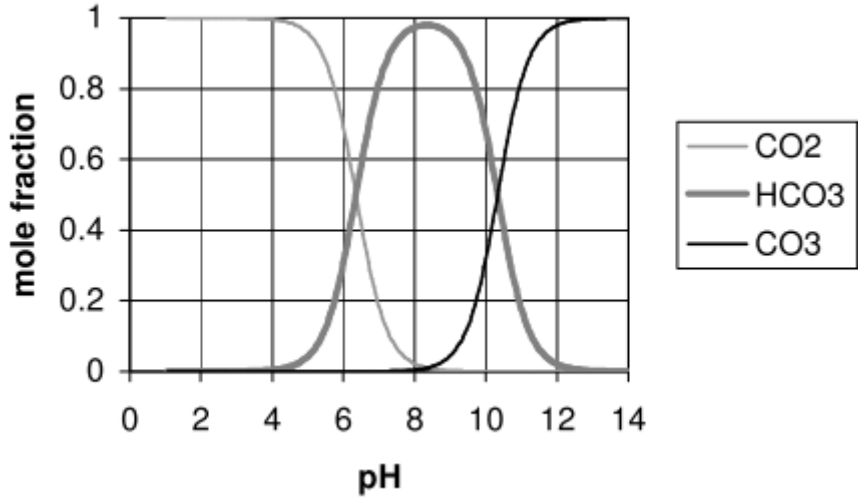

Figure 5.17: Mol fractions of carbon dioxide, carbonate and bicarbonate with respect to pH.

The use of wastes are essential for an economically feasible operation. Up to now, dark fermenter effluents of different industries' wastes were utilized in photofermentation. To the best of our knowledge, the current study is the first outdoor study operated directly with molasses. Previously, Boran (2011) studied with *R. capsulatus YO3* on DFE of molasses. The system was operated in August, 2010. He reported the average and the maximum productivities as 0.05 and 0.12 mol $H_2/(m^3.h)$ (Boran, 2011). In the

current study, the productivity increased significantly, reporting the average and the maximum productivities as 0.16 and 0.31 mol $H_2/(m^3.h)$. Therefore, in the current study the productivity was increased around 3 fold.

5.3 Overall Evaluation of the Stacked U-tube Reactor and the Comparison of Productivities with Other Outdoor Studies

The bottleneck of photofermentation is its high capital and operating costs. The main capital cost item of photofermentation is the rent for large ground area (Urbaniec & Grabarczyk, 2014). With this reactor, the ground area to volume ratio (2.41 m^{-1}) was reduced compared to tubular or nearly tubular PBRs. This ratio can be further reduced with the addition of more tubes to the manifolds. In a recent study, the reason behind the high operational costs for tubular PBRs was found as the LDPE tubes which needs to be changed every year (Urbaniec & Grabarczyk, 2014). Therefore, the material selection is quite important for PBRs. Glass having less permeability of hydrogen and air than LDPE tubes is a good choice for PBR. Moreover, glass is more durable in outdoor conditions, and its life time is much more (~20 years). With stacked U-tube reactor, the capital and operational cost of PBR is reduced.

In this study, molasses was utilized as the feedstock for photofermentation for the first time in literature. From the results of RUN 092014, a proper feeding strategy was proposed for outdoor operations when molasses was used as the feedstock. With the light of the information obtained for this run, the stacked U-tube PBR was operated successfully with *R. capsulatus YO3* on molasses between July 12 and July 24, 2015. Another reactor working with *R. capsulatus YO3* on acetate was also run in parallel. The experimental results of these runs were summarized in Table 5.4.

Hydrogen productivity enhanced 3 folds when compared with the outdoor experiment performed with *R. capsulatus YO3* on DFE of molasses (Boran, 2011). Moreover, the

productivity obtained in outdoor conditions was very close to the productivity obtained with the same bacteria on molasses under controlled conditions (Sağır, 2012). The productivity per ground area was increased almost 4 fold compared with the nearly horizontal tubular PBR working with *R. capsulatus YO3* on DFE of molasses (Boran, 2011).

Table 5.4: Summary of the results of experimental results

	RUN 072015-R1	RUN 072015-R2
Experiment duration	July 12 – July 21, 2015	July 12 – July 24, 2015
Reactor volume (L)	11	9
Highest productivity (per volume) (mol $H_2/(m^3.h)$)	0.14	0.31
Average productivity (per volume) (mol $H_2/(m^3.h)$)	0.08	0.16
Highest productivity (per ground area) (mmol $H_2/(m^2.h)$)	7.20	12.73
Average productivity (per ground area) (mmol $H_2/(m^2.h)$)	3.86	6.58
Highest substrate conversion efficiency, %	17.5	3.7
Average substrate conversion efficiency, %	9.2	1.9
Highest light conversion efficiency , %	0.027	0.44
Average light conversion efficiency, %	0.014	0.023

The comparison of the yield and productivities in outdoor studies are shown in Table 5.5 for outdoor studies. The productivities are in the range between 0.130 and 1.120 mol $H_2/(m^3.h)$.

Table 5.5: The comparison of outdoor studies in terms of productivities and substate conversion efficiencies

Reactor type	**Mode of operation**	**Bacteria**	**Reactor volume (L)**	**Substrate**	**Productivity (mol H_2/(m^3.h)**	**Substrate conversion efficiency, %**	**Reference**
Panel - vertical	Batch	*R. sphaeroides B5*	33	Lactate	0.766	69	(Kim, Ito, & Takahashi, 1982)
Panel – 15^o inlination					0.877	78	
Panel	Semi-continuous	*R. sphaeroides B6*	6	Lactate	2.247	–	(Kim, Ito, Izaki, & Takahashi, 1987)
Roux flask	Batch	*R. sphaeroides RV*	0.7	Sodium lactate	0.130	–	(Miyake, Wakayam, Schnackenberg, Arai, & Asada, 1999)
Glass Bottles	Batch	*R. capsulatus DSM 1710*	0.55	Acetate, lactate	0.14	19	(Özgür, Uyar, et al., 2010)
Tubular nearly horizontal	Fed-batch	*R. capsulatus DSM 1710*	80	Acetate	0.74	16	(Boran et al., 2010)

Table 5.5.continued

Reactor type	Mode of operation	Bacteria	Reactor volume (L)	Substrate	Productivity (mol $H_2/(m^3.h)$	Substrate conversion efficiency, %	Reference
Panel	Batch	*R. sphaeroides O.U.001 (DSM 5864)*	6.5	Malate	0.225 - 0.449	10 - 77	(Eroğlu, Tabanoğlu, Gündüz, Eroğlu, & Yücel, 2008)
				Acetate	0.36	30	
				Lactate / Olive mill wastewater	0.090 / 0.135	13	
Outdoor	Fed-batch	*R. capsulatus JP91*	4	DFE of thick juice	1.12	—	(Özkan et al., 2012)
Panel	Fed-batch	*R. capsulatus DSM 155*	25L x 4	Acetate, lactate	0.94	—	(Jacub Gebicki, Modigell, Schumacher, Van Der Burg, & Roebroeck, 2009)

Table 5.5.continued

Reactor type	**Mode of operation**	**Bacteria**	**Reactor volume (L)**	**Substrate**	**Productivity (mol H_2/(m^3.h)**	**Substrate conversion efficiency, %**	**Reference**
Tubular, nearly horizontal	Fed - batch	*R. capsulatus hup - (YO3)*	90	Acetic acid - DFE of thick juice	0.4	9	(Boran et al., 2012a)
Tubular, nearly horizantal	Fed - batch	*R. capsulatus hup - (YO3)*	90	Acetic acid - DFE of thick juice	0.27	10	(Boran et al., 2012b)
				Acetic acid	0.74	15	
Outdoor	Fed-batch	*Rp. palustris 420L*	50	malate	0.48	10	(Adessi et al., 2012)
Outdoor	Fed-batch	*R. capsulatus YO3 (hup-)*	90	Acetate	0.4	12	(Boran et al., 2012b)
Outdoor	Fed-batch	*R. capsulatus DSM 1710*	90	DFE of thick juice	0.27	12	

Table 5.5.continued

Reactor type	**Mode of operation**	**Bacteria**	**Reactor volume (L)**	**Substrate**	**Productivity (mol H_2/(m^3.h)**	**Substrate conversion efficiency, %**	**Reference**
Panel	Fed-batch	*R. capsulatus YO3 (hup-)*	8	Acetate	0.30	—	(Androga, Özgür, Eroglu, Gündüz, & Yücel, 2011)
Panel	Fed-batch	*R. capsulatus YO3 (hup-)*	4	Acetate	0.51	—	(Androga, Ozgur, Gunduz, Yucel, & Eroglu, 2011)
Panel	Fed - batch	*R. capsulatus YO3 (hup-)*	4	DFE of molasses	0.67	78	(Avcıoglu et al., 2011)
		R. capsulatus DSM 1710			0.50	50	

CHAPTER 6

CONCLUSIONS AND RECOMMENDATIONS

A new stacked-tubular design was proposed in this study with the goal of addressing problems with scale up of PBRs for hydrogen production. A hydrodynamic model for this design was developed utilizing COMSOL Multiphysics 4.1. The effects of tube pitch, tube length and volumetric flow rate on the flow distribution were investigated in the model. The most uniform flow distribution with a non-uniformity parameter of 1.5% was obtained for a tube pitch of 10.5 cm, a tube length of 3.8 m and a volumetric flow rate of 25 L/h. Then, the stacked U-tube PBR was constructed. The dimensions of the PBR (10.5 cm tube pitch and 4 m tube length) were based on the model results. In view of its lower long-term material costs and low permeability to hydrogen and air, glass was chosen as the reactor material. The illuminated surface area to ground area of the reactor was found as 5:1, a high value for tubular-type reactors. Moreover, the volume to ground area ratio (2.44 m^{-1}) is very high compared to other tubular reactors. The PBR proposed in this thesis is a much more suitable one for photofermentative hydrogen production compared to the panel or slightly inclined horizontal tubular reactors.

The tube diameter was selected based on the photon counts and absorbencies of molasses at different depths. The tube diameter was selected as 3 cm for photofermentative hydrogen production purposes under outdoor conditions.

Centrifugal and peristaltic pump types were compared in terms of bacterial growth in the greenhouse utilizing U-tubes. Although there was not a significant difference in bacterial growth between the pumps, the peristaltic pump was preferred for the pilot-scale experiments, since it is easier to control the flow rate with a peristaltic pump.

A proper feeding strategy is essential to test the stacked U-tube PBR. An experiment (RUN 092014) was carried out in September 2014 using molasses as the carbon source and *Rhodobacter capsulatus YO3* (Hup^-) as the microorganism. The PBR was tested in outdoor conditions with *R. capsulatus* YO_3 on molasses in September, 2014. Evaluation of the sucrose consumption rate and organic acid production rate gave an insight about the feeding strategy for future applications. From the results of this run, it has been concluded that the sucrose content in the reactor should be maintained above 5 mM, and acetic acid and lactic acid content should be kept below 40 mM. These values lead to establish the feeding strategy for the succeeding experiments.

Two experiments were run successfully in parallel in July 2015. RUN 072015-R1 was run with *Rhodobacter capsulatus* YO_3 (hup^-) on acetate. The feeding strategy was to keep the acetic acid concentration 40 mM in the reactor. The maximum substrate conversion efficiency was calculated on the 3rd day of the experiment as 17.5%. Average substrate conversion efficiency was found as 9.2%. The highest light conversion efficiency was found on the 2nd day as 0.021%. The highest and the average productivity was found as 0.144 and 0.077 mol $H_2/(m^3.h)$, respectively. The highest productivity was observed on the 2nd day before continuous feeding started. Another reactor containing *Rhodobacter capsulatus* YO_3 (hup^-) was operated with molasses (RUN 072015-R2). This is the first time that molasses was utilized directly for photofermentation in outdoor conditions. The feeding strategy was based on the previous experimental results. The maximum substrate conversion efficiency was found as 3.65% on the 10th day of the experiment. The average substrate conversion efficiency was found as 1.89%. The highest light conversion efficiency of this reactor was 0.044 % on the 10th day. Hydrogen production observed mainly after continuous

feeding started. The highest and the average productivity was found as 0.311 and 0.161 respectively. It has been concluded that hydrogen productivity is higher with molasses used as substrate compared to acetate. Therefore single stage photofermentation with molasses is more advantageous compared to two-stage biological hydrogen production; dark fermentation followed by photofermentation.

Some recommendations for future studies are listed below.

- A kinetic analysis is necessary to figure out the sucrose consumption rate and organic acid production rates and to suggest a better feeding strategy.
- Productivity was decreased due to low pH values in the PBR operating with molasses. Therefore, a pH control system should be adopted for the reactor.
- All of the sucrose supplied by molasses was consumed every day in RUN 072015-R2. Therefore, sucrose content can be increased up to 10 mM or more for higher productivities. However, without a proper pH controller, increasing the sucrose concentration in molasses will result in a decrease in pH.
- Most of the biogas is produced in the tubes. In order to collect the gas accumulated in the tubes, the flow rate of the reactor could be increased for a while. Since the bacteria cannot withstand the stress created by turbulent flow regime, the maximum flow rate should be adjusted such that Reynolds number in the tubes will be at most 2100. The duration should be equal to or more than the residence time to collect all the gas properly.
- If such as reactor is to be operated in much larger scale, the number of connections should be reduced to prevent the risk of leakage. However, while welding glass, there can be some small errors in dimensions if the glass pieces is not cast in mold. If all glass pieces is to be welded, the system loses its flexibility, and it gets harder to connect the glass pieces to the stand. Moreover, glass breaks easily during construction. It is easier to change the pieces, if they are not all welded. Considering these issues, the optimum number of connections should be determined for larger volume systems.

- More tubes can be added to the reactor to increase the reactor volume. By this way, the illuminated area to ground area ratio will get higher. However, the flow model of such systems should also be investigated to obtain the most uniform flow distribution.

REFERENCES

Abdul, P. M., Md. Jahim, J., Harun, S., Markom, M., Hassan, O., Mohammad, A. W., & Asis, A. J. (2013). Biohydrogen production from pentose-rich oil palm empty fruit bunch molasses: A first trial. *International Journal of Hydrogen Energy*, *XXX*, 1–7.

Ablanque, N., Oliet, C., Rigola, J., Pérez-Segarra, C. D., & Oliva, A. (2010). Two-phase flow distribution in multiple parallel tubes. *International Journal of Thermal Sciences*, *49*, 909–921.

Abo-Hashesh, M., Ghosh, D., Tourigny, A., Taous, A., & Hallenbeck, P. C. (2011). Single stage photofermentative hydrogen production from glucose: An attractive alternative to two stage photofermentation or co-culture approaches. *International Journal of Hydrogen Energy*, *36*(21), 13889–13895.

Acrivos, A., Babcock, B. D., & Pigford, R. L. (1959). Flow distributions in manifolds. *Chemical Engineering Science*, *10*(1-2), 112–124.

Adessi, A., Torzillo, G., Baccetti, E., & De Philippis, R. (2012). Sustained outdoor H2 production with Rhodopseudomonas palustris cultures in a 50 L tubular photobioreactor. *International Journal of Hydrogen Energy*, *37*(10), 8840–8849.

Afsar, N., Özgür, E., Gürgan, M., Akköse, S., Yücel, M., Gündüz, U., & Eroglu, I. (2011). Hydrogen productivity of photosynthetic bacteria on dark fermenter effluent of potato steam peels hydrolysate. *International Journal of Hydrogen Energy*, *36*(1), 432–438.

Ahn, H., Lee, S., & Shin, S. (1998). Flow Distribution in manifolds for low Reynolds number flow. *KSME International Journal*, *12*(1), 87–95.

Akkerman, I., Janssen, M., Rocha, J., & H, W. R. (2002). Photobiological hydorgen production: photochemical efficiency and bioreactor design. *International Journal of Hydrogen Energy*, *27*(11-12), 1195–1208.

Androga, D. D. (2009). *Biological hydrogen production on acetate in continuous panel photobioreactors using Rhodobacter capsulatus*. M. Sc Thesis submitted to Chemical Engineering Department of Middle East Technical University.

Androga, D. D. (2014). *Modelling and simulation of photobioreactors for biological hydrogen production*. PhD. Thesis submitted to Department of Biotechnology of Middle East Technical University.

Androga, D. D., Ozgur, E., Gunduz, U., Yucel, M., & Eroglu, I. (2011). Factors affecting the longterm stability of biomass and hydrogen productivity in outdoor photofermentation. *International Journal of Hydrogen Energy*, *36*(17), 11369–11378.

Androga, D. D., Özgür, E., & Eroglu, I. (2012). Amelioration of photofermentative hydrogen production from molasses dark fermenter effluent by zeolite-based removal of ammonium ion. *International Journal of Hydrogen Energy*, *37*(21), 16421–16429.

Androga, D. D., Özgür, E., Eroglu, I., Gündüz, U., & Yücel, M. (2011). Significance of carbon to nitrogen ratio on the long-term stability of continuous photofermentative hydrogen production. *International Journal of Hydrogen Energy*, *36*(24), 15583–15594.

Androga, D. D., Özgür, E., Eroglu, I., Gündüz, U., & Yücel, M. (2012). Photofermentative Hydrogen Production in Outdoor Conditions. In D. Minic (Ed.), *Hydrogen Energy - Challenges and Perspectives*. InTech.

Ángel, M.-D. J., Manuel, O.-R. J., Omar, J.-S., Antonio, Z.-A. M., & Armando, E.-O. (2013). Analysis of Flow and Heat Transfer in a Flat Solar Collector with Rectangular and Cylindrical Geometry Using CFD. *Ingeniería, Investigación Y Tecnología*, *14*(4), 553–561.

Argun, H., & Kargi, F. (2010a). Effects of light source, intensity and lighting regime on bio-hydrogen production from ground wheat starch by combined dark and photo-fermentations. *International Journal of Hydrogen Energy*, *35*(4), 1604–1612.

Argun, H., & Kargi, F. (2010b). Photo-fermentative hydrogen gas production from dark fermentation effluent of ground wheat solution: Effects of light source and light intensity. *International Journal of Hydrogen Energy*, *35*(4), 1595–1603.

Argun, H., & Kargi, F. (2011). Bio-hydrogen production by different operational modes of dark and photo-fermentation: An overview. *International Journal of Hydrogen Energy*, *36*(13), 7443–7459.

Argun, H., Kargi, F., & Kapdan, I. K. (2009). Effects of the substrate and cell concentration on bio-hydrogen production from ground wheat by combined dark and photo-fermentation. *International Journal of Hydrogen Energy*, *34*(15), 6181–6188.

Asada, Y., Tokumoto, M., Aihara, Y., Oku, M., Ishimi, K., Wakayama, T., … Kohno, H. (2006). Hydrogen production by co-cultures of Lactobacillus and a photosynthetic bacterium, Rhodobacter sphaeroides RV. *International Journal of Hydrogen Energy*, *31*(11), 1509–1513.

Avcioglu, S. G. (2010). *Scale up of panel photobioreactors for hydrogen production by PNS bacteria*. M.Sc. Thesis submitted to Chemical Engineering Department of Middle East Technical University

Avcıoglu, S. G., Özgur, E., Eroglu, I., Yücel, M., & Gündüz, U. (2011). Biohydrogen production in an outdoor panel photobioreactor on dark fermentation effluent of molasses. *International Journal of Hydrogen Energy*, *36*(17), 11360–11368.

Ball, M., & Wietschel, M. (2009). The future of hydrogen - opportunities and challenges. *International Journal of Hydrogen Energy*, *34*(2), 615–627.

Barbosa, M. J., Rocha, J. M. S., Tramper, J., & Wijffels, R. H. (2001). Acetate as a carbon source for hydrogen production by photosynthetic bacteria. *Journal of Biotechnology*, *85*(1), 25–33.

Basak, N., & Das, D. (2009). Photofermentative hydrogen production using purple non-sulfur bacteria Rhodobacter sphaeroides O.U.001 in an annular photobioreactor: A case study. *Biomass and Bioenergy*, *33*(6-7), 911–919.

Benemann, J. R., Berenson, J. a, Kaplan, N. O., & Kamen, M. D. (1973). Hydrogen evolution by a chloroplast-ferredoxin-hydrogenase system. *Proceedings of the National Academy of Sciences of the United States of America*, *70*(8), 2317–2320.

Biebl, H., & Pfennig, N. (1981). Isolation of members of the family Chloroflexaceae. In H. G. Starr, Mortimer P.; Stolp, Heinz; Trüper, Hans G.; Balows, Albert; Schlegel (Ed.), *The Prokaryotes* (pp. 267–273). Springer-Verlag.

Boran, E. (2011). *Process development for continuous photofermentative hydrogen production*. Middle East Technical University. M.Sc. Thesis submitted to Chemical Engineering Department of Middle East Technical University

Boran, E., Özgür, E., Van Der Burg, J., Yücel, M., Gündüz, U., & Eroglu, I. (2010). Biological hydrogen production by Rhodobacter capsulatus in solar tubular photo bioreactor. *Journal of Cleaner Production*, *18*(SUPPL. 1), S29–S35.

Boran, E., Özgür, E., Yücel, M., Gündüz, U., & Eroglu, I. (2012a). Biohydrogen production by Rhodobacter capsulatus Hup− mutant in pilot solar tubular photobioreactor. *International Journal of Hydrogen Energy*, *37*(21), 16437–16445.

Boran, E., Özgür, E., Yücel, M., Gündüz, U., & Eroglu, I. (2012b). Biohydrogen production by Rhodobacter capsulatus in solar tubular photobioreactor on thick juice dark fermenter effluent. *Journal of Cleaner Production*, *31*, 150–157.

Brentner, L. B., Peccia, J., & Zimmerman, J. B. (2010). Challenges in developing biohydrogen as a sustainable energy source: implications for a research agenda. *Environmental Science & Technology*, *44*(7), 2243–2254.

Chen, C., Lee, C., & Chang, J. (2006). Feasibility study on bioreactor strategies for enhanced photohydrogen production from Rhodopseudomonas palustris WP3-5 using optical-fiber-assisted illumination systems. *International Journal of Hydrogen Energy*, *31*(15), 2345–2355.

Chen, C. Y., & Chang, J. S. (2006). Enhancing phototropic hydrogen production by solid-carrier assisted fermentation and internal optical-fiber illumination. *Process Biochemistry*, *41*(9), 2041–2049.

Chen, C. Y., Lee, C. M., & Chang, J. S. (2006). Hydrogen production by indigenous photosynthetic bacterium Rhodopseudomonas palustris WP3-5 using optical fiber-illuminating photobioreactors. *Biochemical Engineering Journal*, *32*(1), 33–42.

Chen, C. Y., Yang, M. H., Yeh, K. L., Liu, C. H., & Chang, J. S. (2008). Biohydrogen production using sequential two-stage dark and photo fermentation processes. *International Journal of Hydrogen Energy*, *33*(18), 4755–4762.

Chen, C. Y., Yeh, K. L., Lo, Y. C., Wang, H. M., & Chang, J. S. (2010). Engineering strategies for the enhanced photo-H2 production using effluents of dark fermentation processes as substrate. *International Journal of Hydrogen Energy*, *35*(24), 13356–13364.

Chen, C.-H., Jung, S.-P., & Yen, S.-C. (2007). Flow distribution in the manifold of PEM fuel cell stack. *Journal of Power Sources*, *173*, 249–263.

Cheng, J., Su, H., Zhou, J., Song, W., & Cen, K. (2011). Hydrogen production by mixed bacteria through dark and photo fermentation. *International Journal of Hydrogen Energy*, *36*(1), 450–457.

Comsol. (2012a). COMSOL Multiphysics Reference Guide, 569–613. Retrieved from http://www.comsol.com/

Comsol. (2012b). Comsol Multiphysics User's Guid. Retrieved from http://www.comsol.com/

Das, D., & Veziroglu, T. N. (2001). Hydrogen production by biological processes: a survey of literature. *International Journal of Hydrogen Energy*, *26*(1), 13–28.

Dasgupta, C. N., Jose Gilbert, J., Lindblad, P., Heidorn, T., Borgvang, S. a., Skjanes, K., & Das, D. (2010). Recent trends on the development of photobiological processes and photobioreactors for the improvement of hydrogen production. *International Journal of Hydrogen Energy*, *35*(19), 10218–10238.

Datar, R., Huang, J., Maness, P. C., Mohagheghi, A., Czernik, S., & Chornet, E. (2007). Hydrogen production from the fermentation of corn stover biomass pretreated with a steam-explosion process. *International Journal of Hydrogen Energy*, *32*(8), 932–939.

Ding, J., Liu, B. F., Ren, N. Q., Xing, D. F., Guo, W. Q., Xu, J. F., & Xie, G. J. (2009). Hydrogen production from glucose by co-culture of Clostridium Butyricum and immobilized Rhodopseudomonas faecalis RLD-53. *International Journal of Hydrogen Energy*, *34*(9), 3647–3652.

Eroglu, E., Gunduz, U., Yucel, M., & Eroglu, I. (2011). Effect of iron and molybdenum addition on photofermentative hydrogen production from olive mill wastewater. *International Journal of Hydrogen Energy*, *36*(10), 5895–5903.

Eroglu, I., Özgür, E., Eroglu, E., Yücel, M., & Gündüz, U. (2014). Applications of photofermentative hydrogen production. In D. Zannoni & R. De Philippis (Eds.), *Microbial Bioenergy: Hydrogen Production* (pp. 237–267). Springer.

Eroğlu, I., Tabanoğlu, A., Gündüz, U., Eroğlu, E., & Yücel, M. (2008). Hydrogen production by Rhodobacter sphaeroides O.U.001 in a flat plate solar bioreactor. *International Journal of Hydrogen Energy*, *33*(2), 531–541.

Fan, J., Shah, L. J., & Furbo, S. (2007). Flow distribution in a solar collector panel with horizontally inclined absorber strips. *Solar Energy*, *81*, 1501–1511.

Fang, H. H. P., Zhu, H., & Zhang, T. (2006). Phototrophic hydrogen production from glucose by pure and co-cultures of Clostridium butyricum and Rhodobacter sphaeroides. *International Journal of Hydrogen Energy*, *31*(15), 2223–2230.

Fernandez-Sevilla, J. M., Acien-Fernandez, F. G., & Molina-Grima, E. (2014). Photobioreactors design for hydrogen production. In D. Zannoni & R. De Philippis (Eds.), *Microbial Bioenergy: Hydrogen Production*. Springer.

Flickinger, M. C. (2013). *Upstream Industrial Biotechnology, 2 Volume Set*. John Wiley & Sons.

Gebicki, J., Modigell, M., Schumacher, M., Van Der Burg, J., & Roebroeck, E. (2009). Development of photobioreactors for anoxygenic production of hydrogen by purple bacteria. *Chemical Engineering Transactions*, *18*, 363–366.

Gebicki, J., Modigell, M., Schumacher, M., Van Der Burg, J., & Roebroeck, E. (2010). Comparison of two reactor concepts for anoxygenic H2 production by

Rhodobacter capsulatus. *Journal of Cleaner Production*, *18*(SUPPL. 1), S36–S42.

Ghosh, D., Sobro, I. F., & Hallenbeck, P. C. (2012). Optimization of the hydrogen yield from single-stage photofermentation of glucose by Rhodobacter capsulatus JP91 using response surface methodology. *Bioresource Technology*, *123*, 199–206.

Guo, C. L., Zhu, X., Liao, Q., Wang, Y. Z., Chen, R., & Lee, D. J. (2011). Enhancement of photo-hydrogen production in a biofilm photobioreactor using optical fiber with additional rough surface. *Bioresource Technology*, *102*(18), 8507–8513.

Guo, W. Q., Ren, N. Q., Wang, X. J., Xiang, W. S., Meng, Z. H., Ding, J., … Zhang, L. S. (2008). Biohydrogen production from ethanol-type fermentation of molasses in an expanded granular sludge bed (EGSB) reactor. *International Journal of Hydrogen Energy*, *33*(19), 4981–4988.

Hallebeck, P. C. (2014). Bioenergy from Microorganisms: An Overview. In D. Zannoni & R. De Philips (Eds.), *Microbial Bioenergy: Hydrogen Production* (pp. 3–21). Springer.

Hallenbeck, P. C., & Benemann, J. R. (2002). Biological hydrogen production; Fundamentals and limiting processes. *International Journal of Hydrogen Energy*, *27*(11-12), 1185–1193.

Hallenbeck, P. C., & Ghosh, D. (2009). Advances in fermentative biohydrogen production: the way forward? *Trends in Biotechnology*, *27*(5), 287–297.

Hawkes, F. R., Dinsdale, R., Hawkes, D. L., & Hussy, I. (2002). Sustainable fermentative hydrogen production: Challenges for process optimisation. *International Journal of Hydrogen Energy*, *27*(11-12), 1339–1347.

International Energy Agency. (2015). *Energy and climate change*. Paris.

Jeong, T. Y., Cha, G. C., Yoo, I. K., & Kim, D. J. (2007). Hydrogen production from waste activated sludge by using separation membrane acid fermentation reactor and photosynthetic reactor. *International Journal of Hydrogen Energy*, *32*(5), 525–530.

Kataoka, N., Miya, A., & Kiriyama, K. (1997). Studies on hydrogen production by continuous culture system of hydrogen-producing anaerobic bacteria. *Water Science and Technology*, *36*(6-7), 41–47.

Keskin, T., & Hallenbeck, P. C. (2012). Hydrogen production from sugar industry wastes using single-stage photofermentation. *Bioresource Technology*, *112*, 131–136.

Kim, J. S., Ito, K., Izaki, K., & Takahashi, H. (1987). Production of molecular hydrogen by a semi-continuous outdoor culture of Rhodopseudomonas sphaeroides. *Agricultural and Biological Chemistry*, *51*(4), 1173–1174.

Kim, J. S., Ito, K., & Takahashi, H. (1982). Production of molecular hydrogen in outdoor batch cultures of Rhodopseudomonas sphaeroides. *Agricultural and Biological Chemistry*, *46*(4), 937–941.

Koku, H. (2001). *Hydrogen metabolism and factors affecting hydrogen production in Rhodobacter Sphaeroides*. M.Sc Thesis submitted to Chemical Engineering Department of Middle East Technical University.

Kothari, R., Buddhi, D., & Sawhney, R. L. (2008). Comparison of environmental and economic aspects of various hydrogen production methods. *Renewable and Sustainable Energy Reviews*, *12*(2), 553–563.

Lay, C. H., Wu, J. H., Hsiao, C. L., Chang, J. J., Chen, C. C., & Lin, C. Y. (2010). Biohydrogen production from soluble condensed molasses fermentation using anaerobic fermentation. *International Journal of Hydrogen Energy*, *35*(24), 13445–13451.

Li, X., Wang, Y., Zhang, S., Chu, J., Zhang, M., Huang, M., & Zhuang, Y. (2011). Effects of light/dark cycle, mixing pattern and partial pressure of H2 on biohydrogen production by Rhodobacter sphaeroides ZX-5. *Bioresource Technology*, *102*(2), 1142–1148.

Liao, Q., Wang, Y. J., Wang, Y. Z., Zhu, X., Tian, X., & Li, J. (2010). Formation and hydrogen production of photosynthetic bacterial biofilm under various illumination conditions. *Bioresource Technology*, *101*(14), 5315–5324.

Liu, B. F., Ren, N. Q., Tang, J., Ding, J., Liu, W. Z., Xu, J. F., … Xie, G. J. (2010). Bio-hydrogen production by mixed culture of photo- and dark-fermentation bacteria. *International Journal of Hydrogen Energy*, *35*(7), 2858–2862.

Lo, Y. C., Chen, C. Y., Lee, C. M., & Chang, J. S. (2011). Photo fermentative hydrogen production using dominant components (acetate, lactate, and butyrate) in dark fermentation effluents. *International Journal of Hydrogen Energy*, *36*(21), 14059–14068.

Manish, S., & Banerjee, R. (2008). Comparison of biohydrogen production processes. *International Journal of Hydrogen Energy*, *33*(1), 279–286.

Marbán, G., & Valdés-Solís, T. (2007). Towards the hydrogen economy? *International Journal of Hydrogen Energy*, *32*(12), 1625–1637. http://doi.org/10.1016/j.ijhydene.2006.12.017

Miyake, J., Wakayama, T., Schnackenberg, J., Arai, T., & Asada, Y. (1999). Simulation of the daily sunlight illumination pattern for bacterial photo-hydrogen production. *Journal of Bioscience and Bioengineering*, *88*(6), 659–663. http://doi.org/10.1016/S1389-1723(00)87096-6

Nakada, E., Asada, Y., Arai, T., & Miyake, J. (1995). Light penetration into cell suspensions of photosynthetic bacteria and relation to hydrogen production. *Journal of Fermentation and Bioengineering*, *80*(1), 53–57. http://doi.org/10.1016/0922-338X(95)98176-L

Nath, K., & Das, D. (2004). Biohydrogen production as a potential energy resource – Present state-of-art. *Journal of Scientific & Industrial Research*, *63*(September), 729–738.

Nath, K., Muthukumar, M., Kumar, A., & Das, D. (2008). Kinetics of two-stage fermentation process for the production of hydrogen. *International Journal of Hydrogen Energy*, *33*(4), 1195–1203. http://doi.org/10.1016/j.ijhydene.2007.12.011

Ntaikou, I., Gavala, H. N., Kornaros, M., & Lyberatos, G. (2008). Hydrogen production from sugars and sweet sorghum biomass using Ruminococcus albus. *International Journal of Hydrogen Energy*, *33*(4), 1153–1163. http://doi.org/10.1016/j.ijhydene.2007.10.053

Ogden, J. M. (1999). Prospects for Building a Hydrogen Energy Infrastructure. *Annual Review of Energy and the Environment*, *24*(1), 227–279. http://doi.org/10.1146/annurev.energy.24.1.227

Ozmihci, S., & Kargi, F. (2010). Bio-hydrogen production by photo-fermentation of dark fermentation effluent with intermittent feeding and effluent removal. *International Journal of Hydrogen Energy*, *35*(13), 6674–6680. http://doi.org/10.1016/j.ijhydene.2010.04.090

Özgür, E., Afsar, N., De Vrije, T., Yücel, M., Gündüz, U., Claassen, P. a M., & Eroglu, I. (2010). Potential use of thermophilic dark fermentation effluents in photofermentative hydrogen production by Rhodobacter capsulatus. *Journal of Cleaner Production*, *18*(SUPPL. 1), S23–S28. http://doi.org/10.1016/j.jclepro.2010.02.020

Özgür, E., Mars, A. E., Peksel, B., Louwerse, A., Yücel, M., Gündüz, U., … Eroğlu, I. (2010). Biohydrogen production from beet molasses by sequential dark and photofermentation. *International Journal of Hydrogen Energy*, *35*(2), 511–517. http://doi.org/10.1016/j.ijhydene.2009.10.094

Özgür, E., & Peksel, B. (2013). Biohydrogen production from barley straw hydrolysate through sequential dark and photofermentation. *Journal of Cleaner Production*, *52*, 14–20. http://doi.org/10.1016/j.jclepro.2013.02.035

Özgür, E., Uyar, B., Öztürk, Y., Yücel, M., Gündüz, U., & Eroğlu, I. (2010). Biohydrogen production by Rhodobacter capsulatus on acetate at fluctuating temperatures. *Resources, Conservation and Recycling*, *54*(5), 310–314. http://doi.org/10.1016/j.resconrec.2009.06.002

Özkan, E., Uyar, B., Özgür, E., Yücel, M., Eroglu, I., & Gündüz, U. (2012). Photofermentative hydrogen production using dark fermentation effluent of sugar beet thick juice in outdoor conditions. *International Journal of Hydrogen Energy*, *37*(2), 2044–2049. http://doi.org/10.1016/j.ijhydene.2011.06.035

Öztürk, Y. (2005). Characterization of the genetically modified cytochrome systems and their application to biohydrogen production in *Rhodobacter capsulatus*. PhD thesis submitted to Department of Biotechnology of Middle East Technical University.

Öztürk, Y., Yücel, M., Daldal, F., Mandaci, S., Gündüz, U., Türker, L., & Eroğlu, I. (2006). Hydrogen production by using Rhodobacter capsulatus mutants with genetically modified electron transfer chains. *International Journal of Hydrogen Energy*, *31*(11), 1545–1552. http://doi.org/10.1016/j.ijhydene.2006.06.042

Panwar, N. L., Kaushik, S. C., & Kothari, S. (2011). Role of renewable energy sources in environmental protection: A review. *Renewable and Sustainable Energy Reviews*, *15*(3), 1513–1524. http://doi.org/10.1016/j.rser.2010.11.037

Perera, K. R. J., Ketheesan, B., Gadhamshetty, V., & Nirmalakhandan, N. (2010). Fermentative biohydrogen production: Evaluation of net energy gain. *International Journal of Hydrogen Energy*, *35*(22), 12224–12233. http://doi.org/10.1016/j.ijhydene.2010.08.037

Pilavachi, P. a., Chatzipanagi, A. I., & Spyropoulou, A. I. (2009). Evaluation of hydrogen production methods using the Analytic Hierarchy Process. *International Journal of Hydrogen Energy*, *34*(13), 5294–5303. http://doi.org/10.1016/j.ijhydene.2009.04.026

Redwood, M., & Macaskie, L. (2006). A two-stage, two-organism process for biohydrogen from glucose. *International Journal of Hydrogen Energy*, *31*(11), 1514–1521. http://doi.org/10.1016/j.ijhydene.2006.06.018

Ren, N., Li, J., Li, B., Wang, Y., & Liu, S. (2006). Biohydrogen production from molasses by anaerobic fermentation with a pilot-scale bioreactor system. *International Journal of Hydrogen Energy*, *31*(15), 2147–2157. http://doi.org/10.1016/j.ijhydene.2006.02.011

Ren, N. Q., Liu, B. F., Zheng, G. X., Xing, D. F., Zhao, X., Guo, W. Q., & Ding, J. (2009). Strategy for enhancing photo-hydrogen production yield by repeated fed-batch cultures. *International Journal of Hydrogen Energy*, *34*(18), 7579–7584. http://doi.org/10.1016/j.ijhydene.2009.07.030

Sağır, E. (2012). Photobiological hydrogen production from sugar beet molasses. M.Sc. Thesis submitted to the Department of Biochemistry of Middle East Technical University.

Sasikala, K., Ramama, C. V., & Raghuveer Rao, P. (1991). Environmental regulation for optimal biomass yield and photoproduction of hydrogen by Rhodobacter sphaeroides O.U.001. *Biotechnology*, *16*(9), 597–601.

Sievert, V. (2003). *Two-phase flow distribution in compact heat exchanger manifolds*. *Norvegian University of Science and Technology*. Retrieved from http://www.mendeley.com/research/twophase-flow-distribution-heat-exchanger-manifolds/

Spruit, C. J. P. (1958). Simultaneous photoproduction of hydrogen and oxygen by Chlorella. *Mededelingen van de Landbouwhogeschool Te Wageningen*, *58*, 1–17. Retrieved from http://www.amazon.co.uk/Simultaneous-photoproduction-Mededelingen-Landbouwhogeschool-Wageningen/dp/B0007J6PKS

Su, H., Cheng, J., Zhou, J., Song, W., & Cen, K. (2009a). Combination of dark- and photo-fermentation to enhance hydrogen production and energy conversion efficiency. *International Journal of Hydrogen Energy*, *34*(21), 8846–8853. http://doi.org/10.1016/j.ijhydene.2009.09.001

Su, H., Cheng, J., Zhou, J., Song, W., & Cen, K. (2009b). Improving hydrogen production from cassava starch by combination of dark and photo fermentation. *International Journal of Hydrogen Energy*, *34*(4), 1780–1786. http://doi.org/10.1016/j.ijhydene.2008.12.045

Sun, Q., Xiao, W., Xi, D., Shi, J., Yan, X., & Zhou, Z. (2010). Statistical optimization of biohydrogen production from sucrose by a co-culture of Clostridium acidisoli and Rhodobacter sphaeroides. *International Journal of Hydrogen Energy*, *35*(9), 4076–4084. http://doi.org/10.1016/j.ijhydene.2010.01.145

Tao, Y., Chen, Y., Wu, Y., He, Y., & Zhou, Z. (2007). High hydrogen yield from a two-step process of dark- and photo-fermentation of sucrose. *International Journal of Hydrogen Energy*, *32*(2), 200–206. http://doi.org/10.1016/j.ijhydene.2006.06.034

UNFCCC COP 21 Paris France - Climate Conference. (2015). Retrieved July 25, 2015, from http://www.cop21paris.org/about/cop21

Urbaniec, K., & Grabarczyk, R. (2014). Hydrogen production from sugar beet molasses - A techno-economic study. *Journal of Cleaner Production*, *65*, 324–329. http://doi.org/10.1016/j.jclepro.2013.08.027

Van Ginkel, S. W., & Logan, B. (2005). Increased biological hydrogen production with reduced organic loading. *Water Research*, *39*(16), 3819–3826. http://doi.org/10.1016/j.watres.2005.07.021

Wang, J. (2008). Pressure drop and flow distribution in parallel-channel configurations of fuel cells: U-type arrangement. *International Journal of Hydrogen Energy*, *33*(21), 6339–6350. http://doi.org/10.1016/j.ijhydene.2008.08.020

Wang, J. (2010). Pressure drop and flow distribution in parallel-channel configurations of fuel cells: Z-type arrangement. *International Journal of Hydrogen Energy*, *35*(11), 5498–5509. http://doi.org/10.1016/j.ijhydene.2010.02.131

Wang, J. (2011). Theory of flow distribution in manifolds. *Chemical Engineering Journal*, *168*(3), 1331–1345. http://doi.org/10.1016/j.cej.2011.02.050

Wang, X. A., & Yu, P. (1989). Isothermal flow distribution in header SYSTEMS. *International Journal of Sustainable Energy*, *7*(3), 159–169. http://doi.org/10.1080/01425918908914252

Wang, Y. Z., Liao, Q., Zhu, X., Tian, X., & Zhang, C. (2010). Characteristics of hydrogen production and substrate consumption of Rhodopseudomonas palustris CQK 01 in an immobilized-cell photobioreactor. *Bioresource Technology*, *101*(11), 4034–4041. http://doi.org/10.1016/j.biortech.2010.01.045

Xie, G. J., Feng, L. B., Ren, N. Q., Ding, J., Liu, C., Xing, D. F., … Ren, H. Y. (2010). Control strategies for hydrogen production through co-culture of Ethanoligenens harbinense B49 and immobilized Rhodopseudomonas faecalis RLD-53. *International Journal of Hydrogen Energy*, *35*(5), 1929–1935. http://doi.org/10.1016/j.ijhydene.2009.12.138

Yokoi, H., Saitsu, A., Uchida, H., Hirose, J., Hayashi, S., & Takasaki, Y. (2001). Microbial hydrogen production from sweet potato starch residue. *Journal of Bioscience and Bioengineering*, *91*(1), 58–63. http://doi.org/10.1016/S1389-1723(01)80112-2

Yokoi, H., Tokushige, T., Hirose, J., Hayashi, S., & Takasaki, Y. (1998a). H2 production from starch by a mixed culture of Clostridium butyricum and Enterobacter aerogenes. *Biotechnology Letters*, *20*(2), 143–147. http://doi.org/10.1023/A:1005372323248

Yokoi, H., Tokushige, T., Hirose, J., Hayashi, S., & Takasaki, Y. (1998b). H2 production from starch by a mixed culture of Clostridium butyricum and Enterobacter aerogenes. *Biotechnology Letters*, *20*(2), 143–147. http://doi.org/10.1023/A:1005372323248

Zeidan, A. a., & van Niel, E. W. J. (2010). A quantitative analysis of hydrogen production efficiency of the extreme thermophile Caldicellulosiruptor

owensensis OLT. *International Journal of Hydrogen Energy*, *35*(3), 1128–1137. http://doi.org/10.1016/j.ijhydene.2009.11.082

Zhang, C., Zhu, X., Liao, Q., Wang, Y., Li, J., Ding, Y., & Wang, H. (2010). Performance of a groove-type photobioreactor for hydrogen production by immobilized photosynthetic bacteria. *International Journal of Hydrogen Energy*, *35*(11), 5284–5292. http://doi.org/10.1016/j.ijhydene.2010.03.085

APPENDIX A

COMPOSITION OF THE GROWTH MEDIA

Table A.1: Growth Media

Component	**Amount**
KH_2PO_4	3 g/l
$MgSO_4.7H_2O$	0.5 g/l
$CaCl_2.2H_2O$	0.05 g/l
Vitamin Solution (from 10X stock) [1]	0.1 ml/l
Iron Citrate Solution (from 50X stock) [2]	0.5 ml/l
Trace Element Solution (from 10X stock) [3]	0.1 ml/l
Na – Glutamate (10 mM)	1.85 g/l
Acetic acid (20 mM)	1.15 ml/l

[1] [2] [3] Vitamin, iron citrate and trace element solutions are added after autoclave. Before aoutoclave pH of the medium was adjusted to 6.3 – 6.4 by using 5 M NaOH solution.

Table A.2: Vitamin Solutions (1X)

Component	**Amount**
Thiamin Chloride Hydrochloride	0.05 g
Niacin (Nicotinic Acid)	0.05 g
D+ Biotin	1.5 mg

The components of vitamin solution were dissolved in 100 ml distilled water. 0.2 µm syringe filter was used to sterilize vitamin solution. It is stored in dark conditions at 4ºC.

Table A.3: Trace Element Solution (1X)

Component	**Amount**
HCl (25% v/v)	1 ml/l
$ZnCl_2$	70 mg/l
$MnCl_2.4H_2O$	100 mg/l
H_3BO_3	60 mg/l
$CoCl_2.6H_2O$	200 mg/l
$CuCl_2.2H_2O$	20 mg/l
$NiCl_2.6H_2O$	20 mg/l
$NaMoO_4.2H_2O$	40 mg/l

Components were dissolved in 1000 ml distilled water and autoclaved. Trace element solution was kept in dark conditions at 4ºC

Table A.4: Iron Citrate Solution (50X)

Component	**Amount**
Fe- Citrate	5 g

Ferric citrate was dissolved in 100 ml distilled water and autoclaved. It was stored in dark conditions at 4ºC.

APPENDIX B

MOLASSES ANALYSES

Table B.1. Molasses Analysis produced in Ankara Sugar Factory in 2013. The analysis were done by Ankara Sugar Factory.

Parameter	**Method**	**Result**
Refractometric dry matter	ICUMSA Method GC 4-13	82.36
Polar sugar (%)	British Sugar Method (CCS Handbook, 213, 2956)	51.52
pH	ICUMSA method GS 1/2/3/4/7(8-23	62.55
Invert sugar (1) (%)	Berlin Institude Method (ICUMSA Sugar Analysis, 55, 1979)	8.62
Invert sugar(1) (g/100 Pol)		0.229
Sucrose (w/w %)	ICUMSA method GS 4/3-7) x 0.95	51.85
Total nitrogen (%)	British sugar method (CCS Handbook, 213, 2956)	1.7
Total nitrogen (g/100Bx)		2.06
Density (g/cm^3)	Density without air	1.272
Na (mg/kg)	Inductively coupled plasma- optical emission spectrometry method	6810
K (mg/kg)		34100
Ca (mg/kg)		2750
Mg (mg/kg)		7
Fe (mg/kg)		15
Mn (mg/kg)		16
Zn (mg/kg)		9

(1) Invert sugar is the mixture of glucose and fructose

Table B.2: Amino acid content of the molasses. The analysis were carried out by Düzen Norwest Laboratory in Ankara

Amino acids	**Units**	**Results**
Aspartic Acid	g/100g	0.358
Glutamic Acid	g/100g	2.541
Asparagine	g/100g	< 0.10 (2)
Serine	g/100g	0.229
Histidine	g/100g	< 0.25 (2)
Glycine	g/100g	0.192
Theronine	g/100g	0.066
Citrulline	g/100g	< 0.07 (2)
Arginine	g/100g	0.08
Alanine	g/100g	0.252
Tyrosine	g/100g	0.191
Cystine	g/100g	< 0.30 (2)
Valine	g/100g	0.139
Methionine	g/100g	< 0.12 (2)
Tryptophan	g/100g	< 0.28 (2)
Isoleucine	g/100g	0.202
Omithine	g/100g	< 0.29 (2)
Lysine	g/100g	0.172
Hydrocproline	g/100g	< 0.27 (2)
Sarcosine	g/100g	< 0.09 (2)
Phenylaline	g/100g	< 0.23 (2)
Prolin	g/100g	0.234
Total Aminoacid	**g/100g**	**4,7**

(2) MDL, Method detection limit

Table B.3: Analysis of some of the elements in molasses. The analysis were carried out by Düzen Norwest Laboratory in Ankara

Parameter	**Units**	**Results**
Iron (Fe)	mg/kg	14.1
Molybdenum (Mo)	mg/kg	0.22
Sulphur (S)	g/kg	1.03
Potassium (K)	g/kg	35.6

APPENDIX C

DIAMETER SELECTION

C.1. Light Intensity Measurements

In order to determine the light intensity at different depths for different sucrose concentrations and for different molasses dilution rates, a luxmeter (Extech HD450) was used. Samples were put into 1 cm thick compartments. Light intensity just in front of the first compartment was adjusted to 4000 lux. In the first run light that is penetrated from the empty compartments were measured for 1 cm, 2 cm, 3 cm, 4 cm and 5 cm thicknesses. Then, solution containing 5 mM sucrose was filled to the compartments, and light intensity was measured at different thicknesses (1 - 5 cm). The same procedure was applied for 7.5 mM, 10 mM, 20 mM sucrose concentrations. Same procedure also applied for different molasses dilution rates (20X, 40X, 60X, 80X and 100X). The results of the experiments are given in Figure C.1, Figure C.2 and Figure C.3.

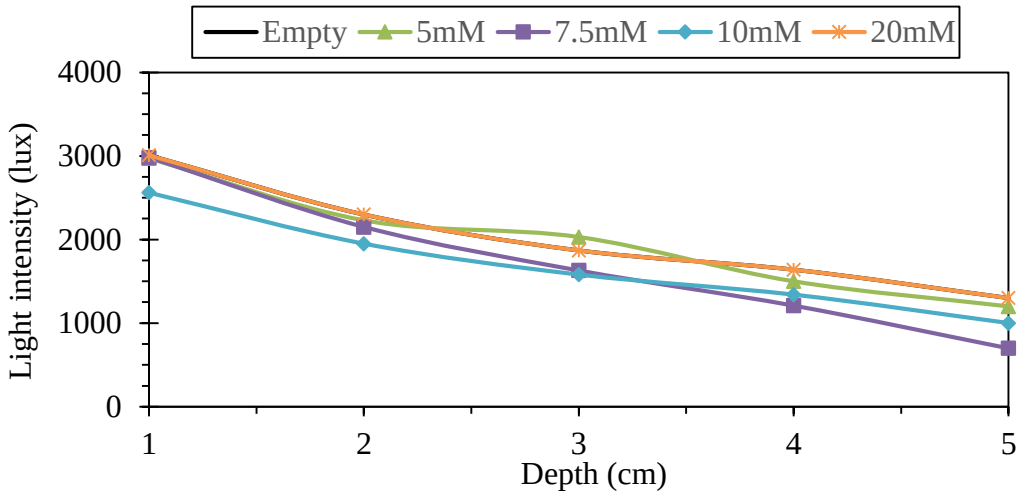

Figure C.1: Light intensity variations at different depths according to different sucrose concentrations. Compartments were filled with pure sucrose at different concentrations

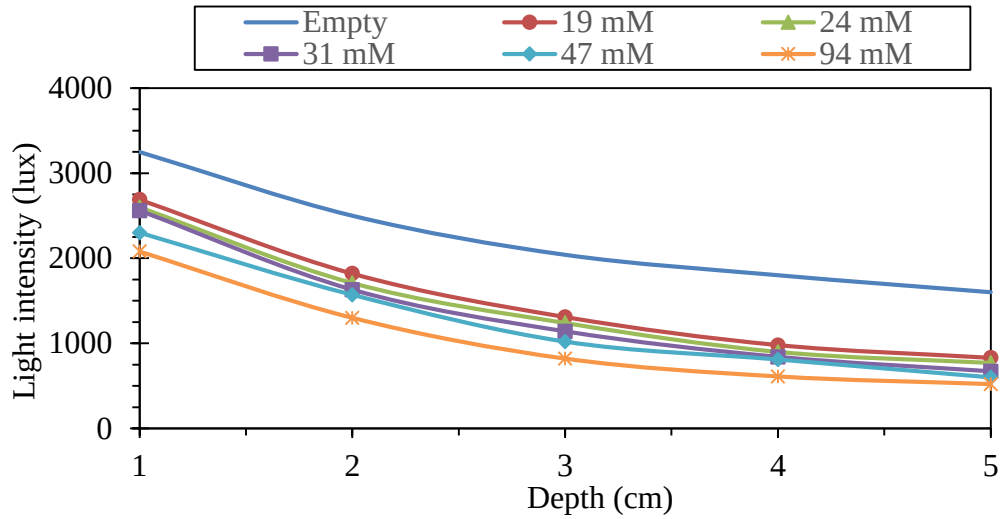

Figure C.2: Light intensity variations at different depths according to different sucrose concentrations. The compartments were filled with diluted molasses containing different amounts of sucrose.

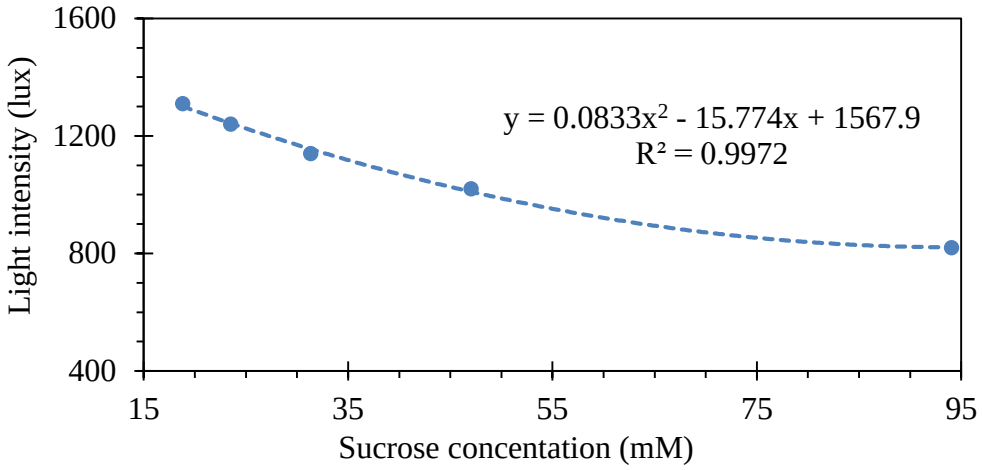

Figure C.3: Light intensity variation for 3 cm depth according to different sucrose concentrations. The compartments were filled with diluted molasses containing different amounts of sucrose.

C.2. Photon Count Measurements

Photon count measurements were done by using a spectroradiometer (Spectrawiz EPP 2000). The detector was connected to the spectroradiometer and the spectroradiometer was connected to a computer as shown in Figure C.4. Data was recorded by the program named SpectraWiz. The parameters of Spectrawiz are given in Table C. 1.

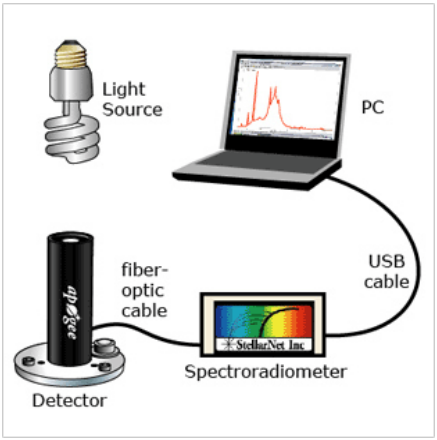

Figure C.4: Schematic representation of the spectroradiometer

Table C. 1: The parameters used for the spectroradiometer

Detector integration period in milliseconds	7
Number of samples averaged	1
Pixel smoothing	1 = 5 pixels
Temperature compensation on/off	off
Timing resolution control	1 = low
Channel	1

Photon count measurements were done for 1 cm, 2 cm, 3 cm, 4 cm and 5 cm thick empty compartments. Then the same procedure was applied for different sucrose concentrations and for different molasses dilution rates. The experimental set – up is shown in Figure C.4. The experiment was performed in a dark room so that the measurements was not affected by the light coming from other sources. The result is given in Figure C.5 and Figure C.7.

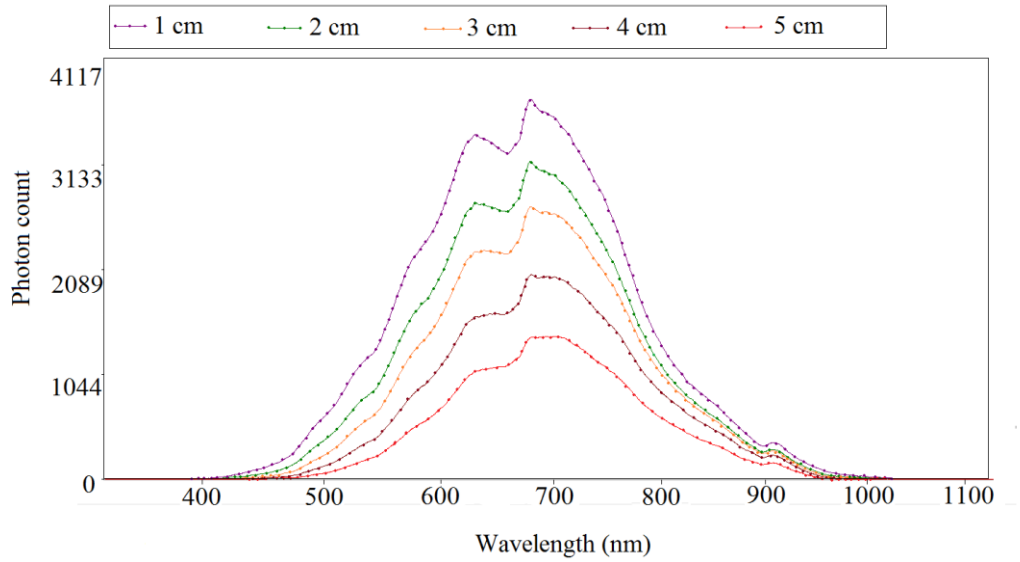

Figure C.5: Photon counts with respect to wavelength for 19 mM sucrose containing molasses at different thicknesses

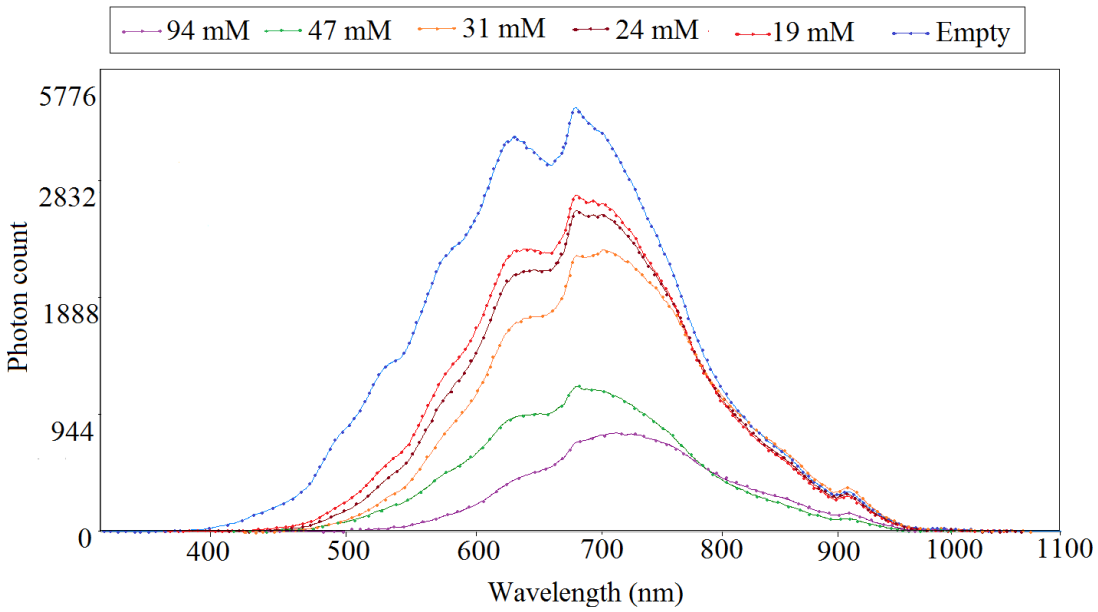

Figure C.6: Photon counts with respect to wavelength for different concentrations of sucrose in molasses.

C.3. Absorbance Experiments

UV – spectrophotometer (Shimadzu UV-1800) was used for absorbance experiments. Quartz compartments were used. Water was used as the blank solution. Samples were scanned with a wavelength range of 190 – 900 nm. The result is given in Figure C.7.

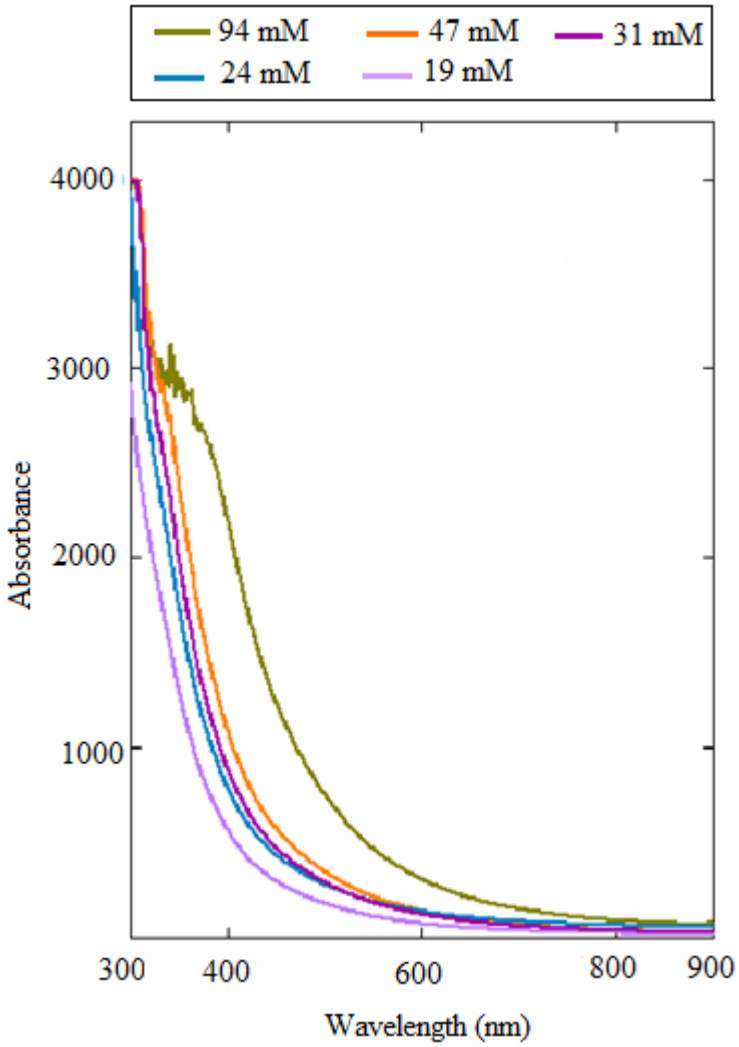

Figure C.7: Comparison of absorbance values for different molasses dilutions

Table C.2: OD of molasses for different dilutions

Dilution	OD at 660 nm
20 X dilution	0.184
40X dilution	0.082
60X dilution	0.073
80X dilution	0.057
100X dilution	0.042

APPENDIX D

PUMP SELECTION

D.1. Experimental Procedure for Pump Selection

The bacteria was grown in Biebl and Pfenning medium (Biebl & Pfennig, 1981), containing 40 mM acetate and 2 mM glutamate. Then the bacteria was adopted to sucrose in indoor conditions. When the concentration of the bacteria reached to around 0.5 gdcw/L, 10% (v/v) bacteria was inoculated to the previously sterilized U-tube reactors. During the first day, pH and cell concentration were measured with 1 hour intervals. 3 measurements for pH and cell concentration were taken, the average values were reported. The experiment was performed in the green house. The starting date of the experiment was in December 12, 2014. It lasted for 3 days.

D.2. pH variation

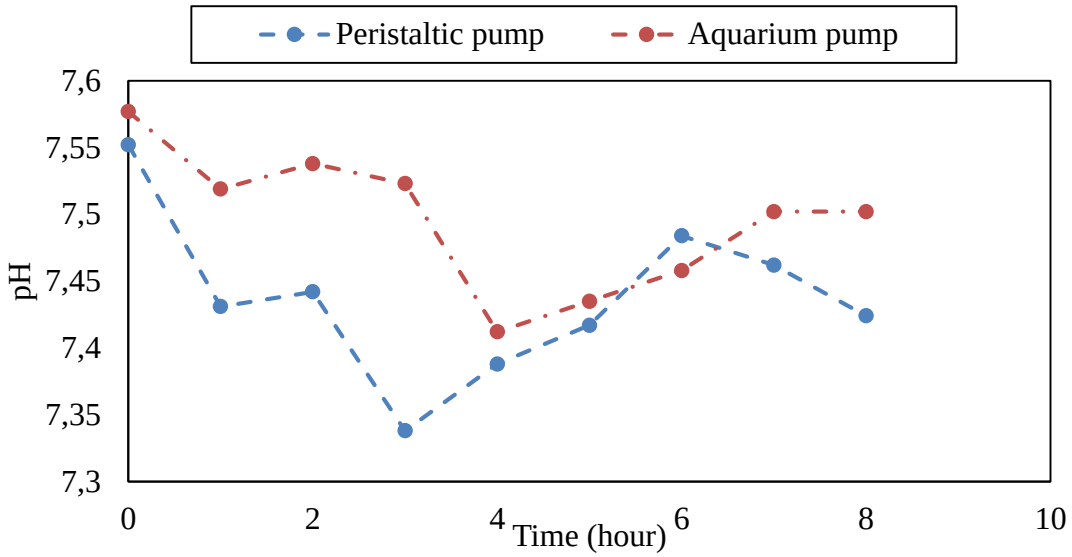

Figure D. 1: pH variation for different pump types for the first day. The starting date of the experiment was Decemeber 12, 2014.

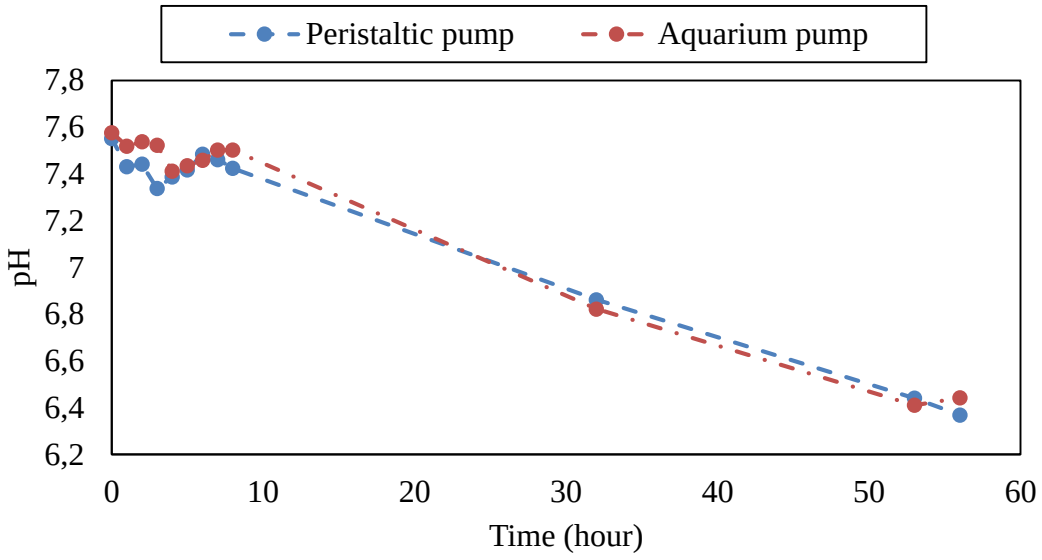

Figure D.2: pH variation for different pump types for the first day. The starting date of the experiment was Decemeber 12, 2014.

D.3. Experimental Data of the Pump Selection

Table D.1: The daily temperature and light intensity change

Date: 28.12.2014			
Time	**Peristaltic pump System Temp. (^{0}C)**	**Aquarium pump System Temp.**	**Light Intensity**
08:30	10.5	11	3.0 Klux
09:30	15.5	15.5	3.6 Klux
10:30	23.5	24	2.3 Klux
11:30	31	31.5	14 Klux
12:30	34	34.5	67 Klux
13:30	29	29	15 Klux
14:30	23.5	23.5	8.5 Klux
15:30	18.5	18	0.37 Klux
16:30	17	16.5	450 Lux
Date: 29.12.2014			
16:30	-	-	-
Date: 30.12.2014			
13:30	18	18	3.25 Klux
16:30	14	13.5	500 Lux

Table D.2: OD, and pH values for peristaltic and centrifugal pump

Date: 28.12.2014								
	System containing peristaltic pump				System containing centrifugal pump			
Time	OD	pH	Average OD	Average pH	OD	pH	Average OD	Average pH
08:30	0.320	7.550	0.318	7.552	0.320	7.592	0.320	7.577
	0.316	7.554			0.320	7.563		
09:30	0.337	7.433	0.327	7.431	0.332	7.484	0.320	7.519
	0.317	7.429			0.308	7.555		
10:30	0.323	7.558	0.324	7.442	0.304	7.553	0.307	7.538
	0.325	7.327			0.310	7.524		
11:30	0.324	7.257	0.322	7.338	0.304	7.533	0.307	7.523
	0.320	7.520			0.310	7.514		
12:30	0.329	7.257	0.328	7.388	0.310	7.446	0.305	7.412
	0.327	7.520			0.300	7.378		
13:30	0.347	7.400	0.336	7.417	0.317	7.428	0.309	7.435
	0.325	7.434			0.301	7.443		
14:30	0.364	7.490	0.360	7.484	0.310	7.456	0.310	7.458
	0.357	7.478			0.310	7.460		
15:30	0.367	7.452	0.361	7.462	0.307	7.518	0.307	7.502
	0.356	7.473			0.308	7.487		
16:30	0.368	7.414	0.361	7.424	0.306	7.518	0.306	7.502
	0.355	7.435			0.309	7.487		
Date: 29.12.2014								
16:30	0.589	6.855	0.594	6.862	0.613	6.834	0.616	6.822
	0.600	6.870			0.620	6.810		
Date: 30.12.2014								
13:30	0.568	6.322	0.567	6.441	0.575	6.423	0.565	6.411
	0.566	6.561			0.555	6.400		
16:30	0.568	6.371	0.567	6.369	0.588	6.337	0.580	6.442
	0.566	6.367			0.573	6.547		

APPENDIX E

CALIBRATION CURVE OF THE DRY CELL WEIGHT

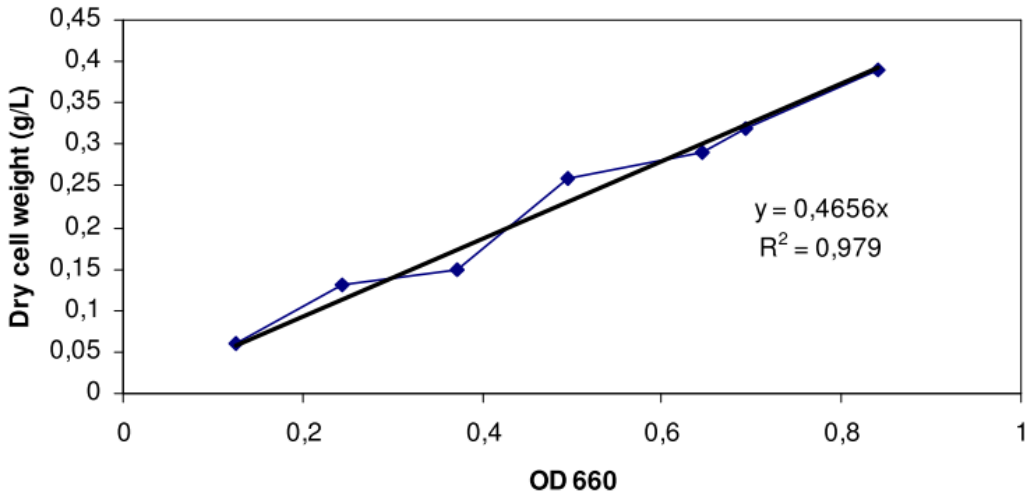

Figure E.1: Calibration curve for the dry cell weight versus OD_{660} of the *Rhodobacter capsulatus YO3* (hup-) (Öztürk, 2005). Optical density of 1.0 at 660 nm corresponds to 0.4656 gdcw/$L_{c.}$

APPENDIX F

LIGHT ABSORPTION SPECTRA OF *Rhodobacter capsulatus YO3* (hup$^-$)

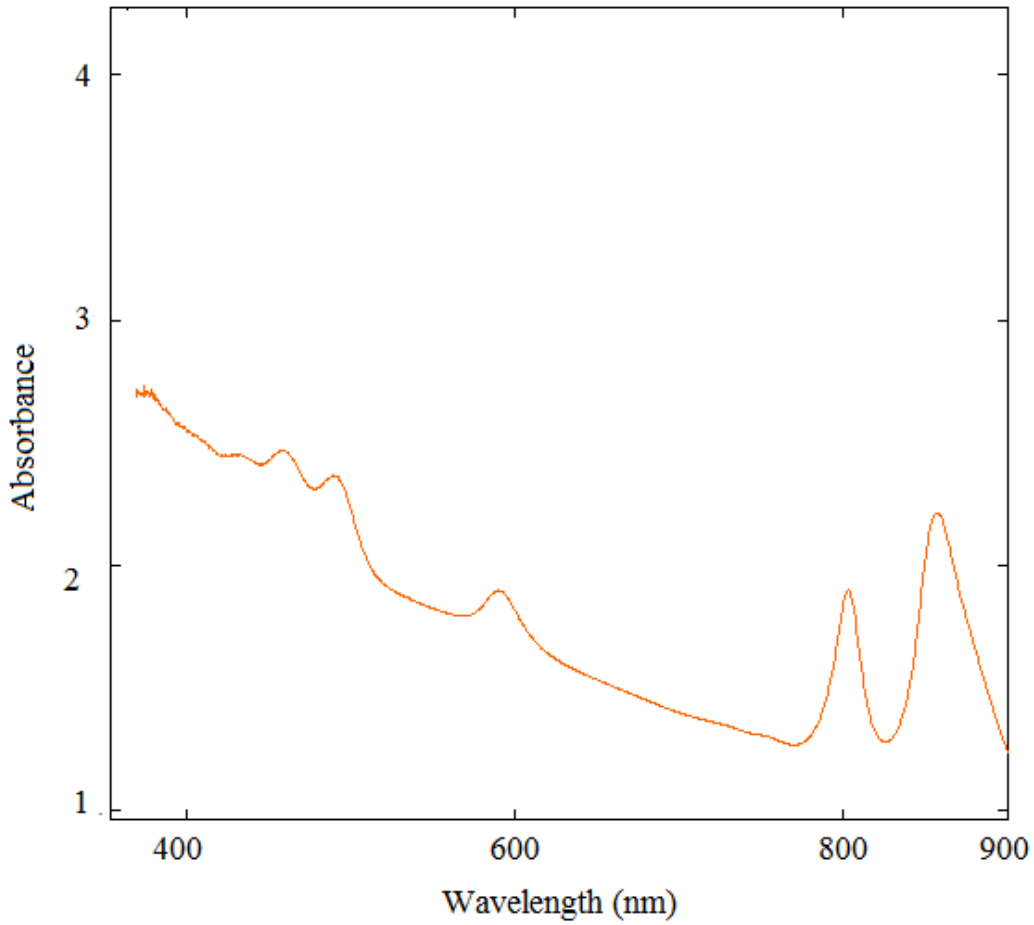

Figure F.1: Light absroption spectra of *Rhodobacter capsulatus YO3* (hup$^-$). Optical density at 660 nm was 1.4.

APPENDIX G

SAMPLE GAS CHROMATOGRAM FOR GAS ANALYSIS

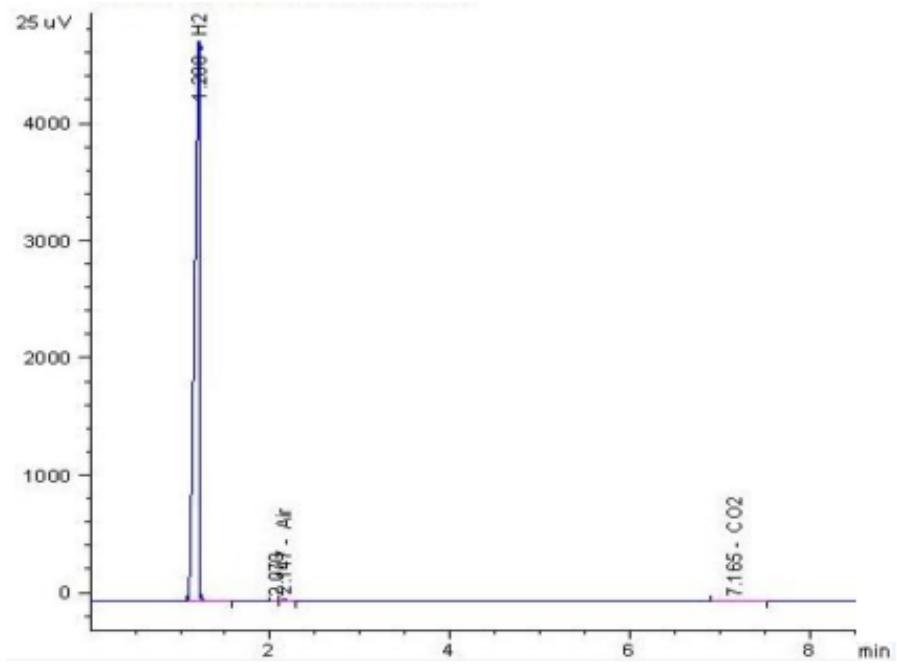

RetTime [min]	Type	Area [25 uV*s]	Amt/Area	Norm %	Grp	Name
1.208	BB	1.78157e4	5.36760e-3	92.790983		H2
2.147	VB	104.16668	4.30476e-2	4.351104		Air
7.165	BB	52.88443	5.56929e-2	2.857913		CO2
Totals :				100.000000		

Figure G.1: A sample gas chromotogram (Androga, 2009)

APPENDIX H

SAMPLE HPLC CHROMATOGRAM AND CALIBRATION CURVES OF ORGANIC ACIDS AND SUCROSE

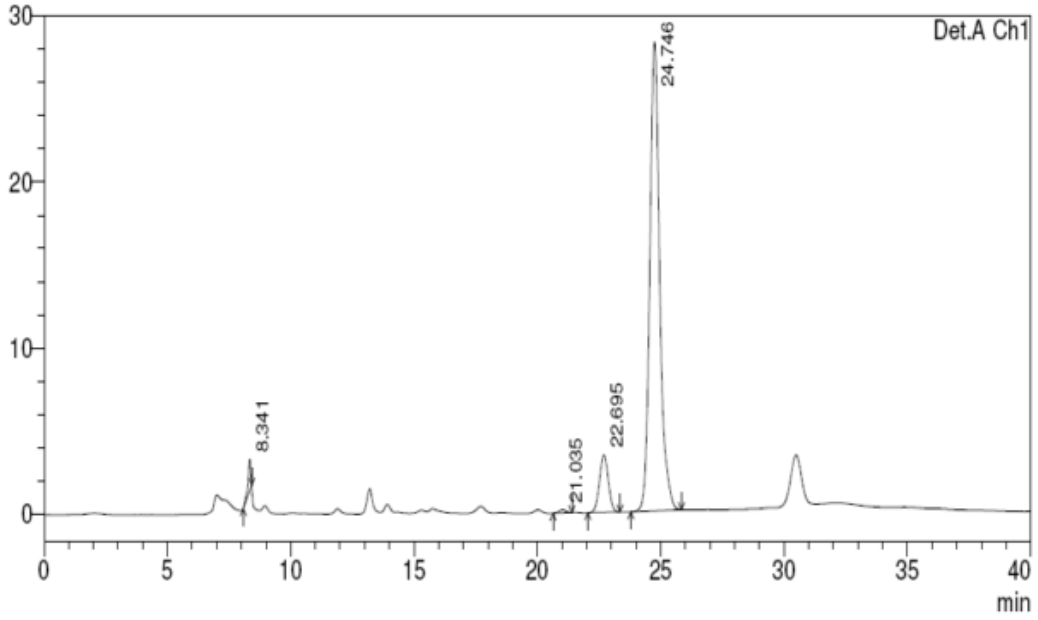

Figure H.1: A sample HPLC chromotogram. (Androga, 2009). Retention times of lactic, formic, acetic, propionic and butyric acid are 22.0, 24.5, 26.5, 31.3 and 38.6 min, respectively.

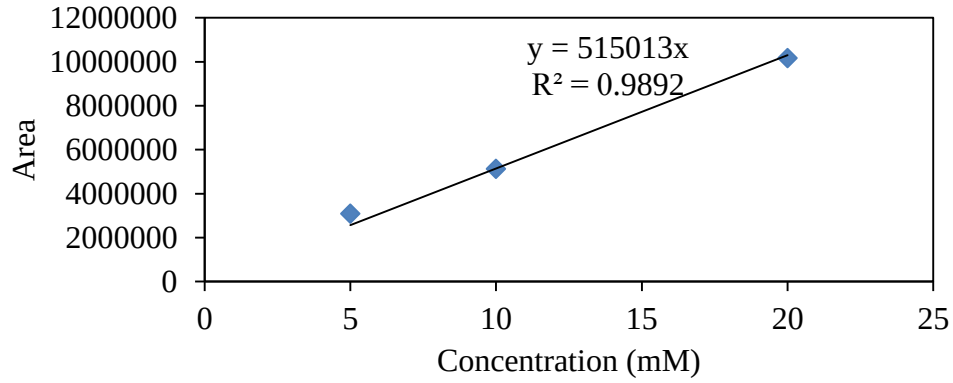

Figure H.2: HPLC calibration for lactic acid

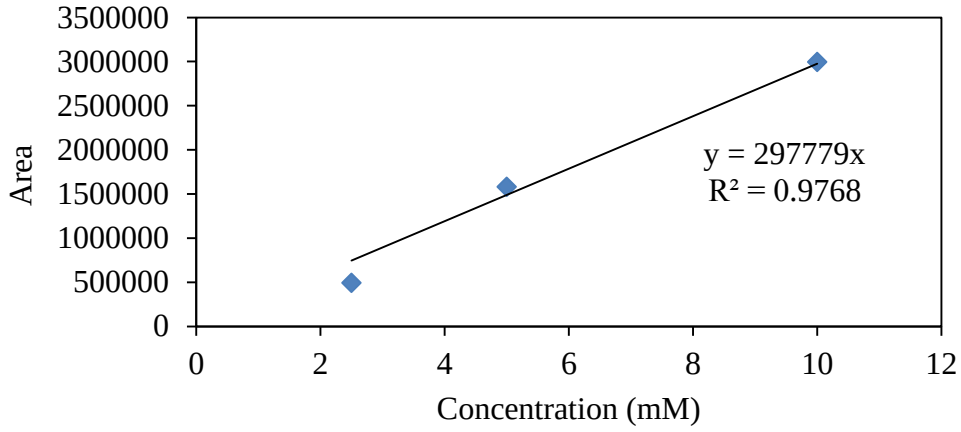

Figure H.3: HPLC calibration for formic acid

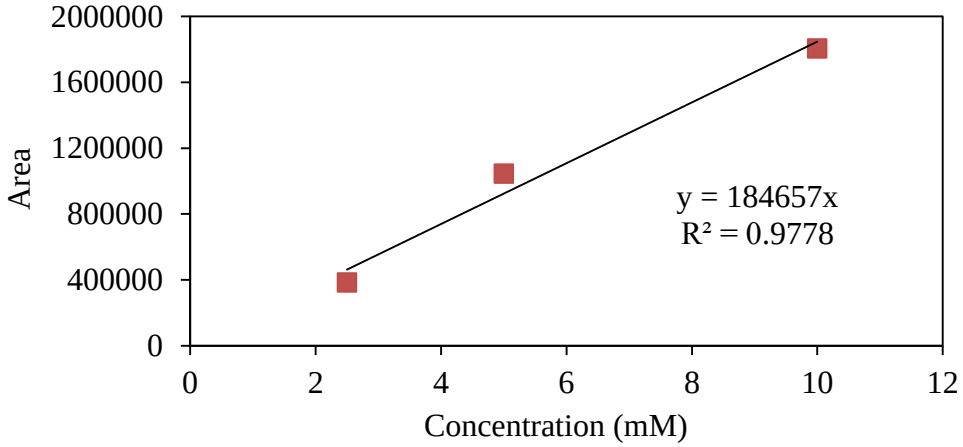

Figure H.4: HPLC calibration for acetic acid

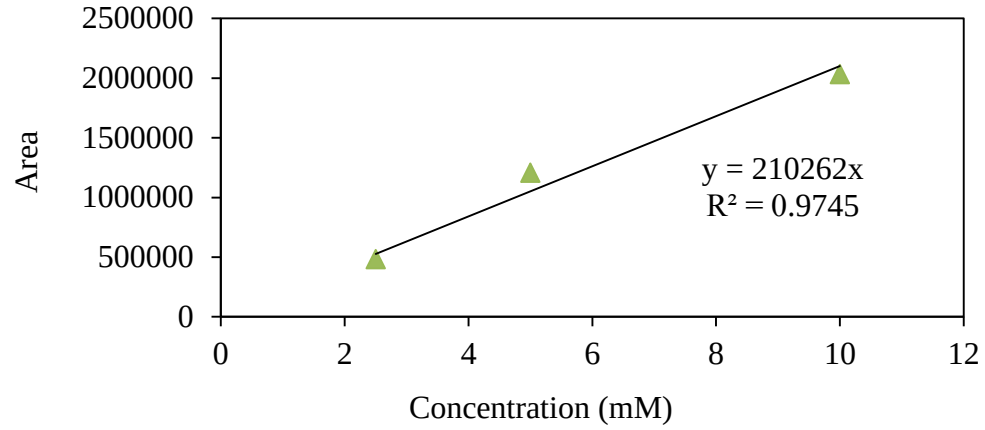

Figure H.5: HPLC calibration for propionic acid

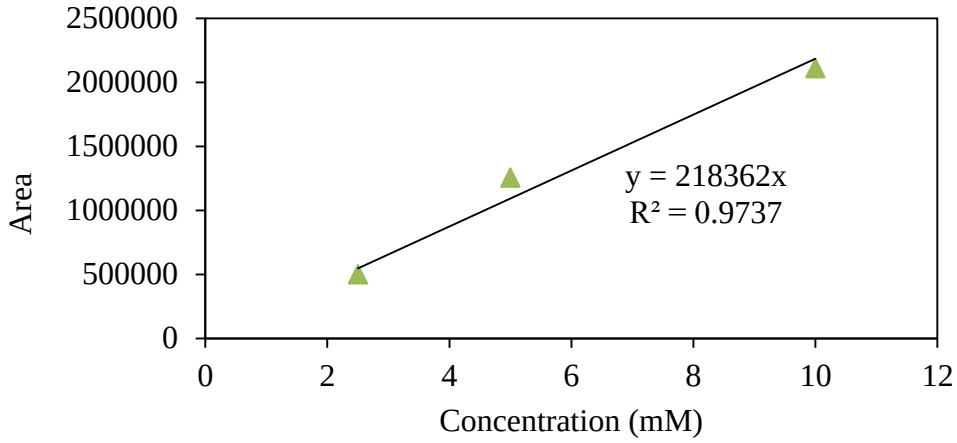

Figure H.6: HPLC calibration for butyric acid

APPENDIX I

MODEL OUTPUTS

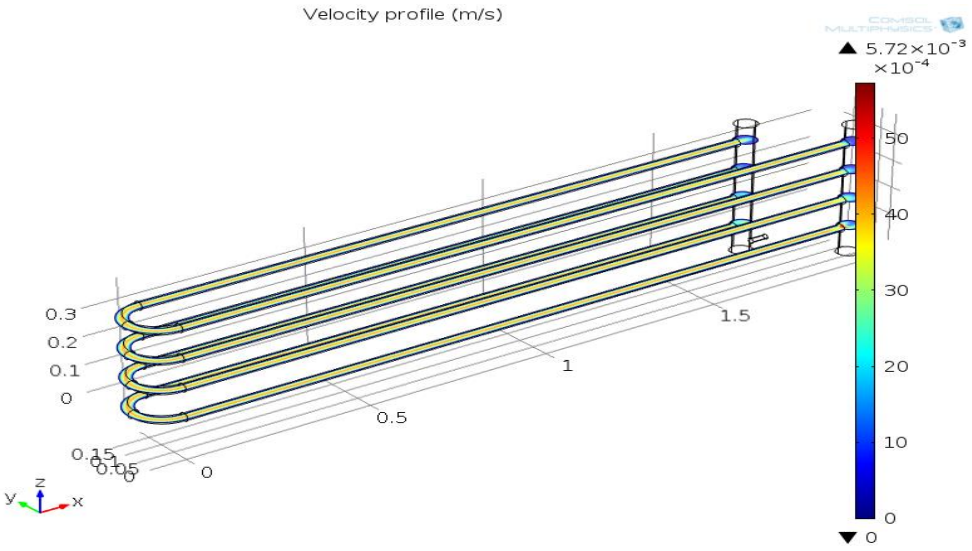

Figure I.1: Velocity profile for 3.8 m tube length, 10.5 cm tube spacing and 25 L/h volumetric flow rate.

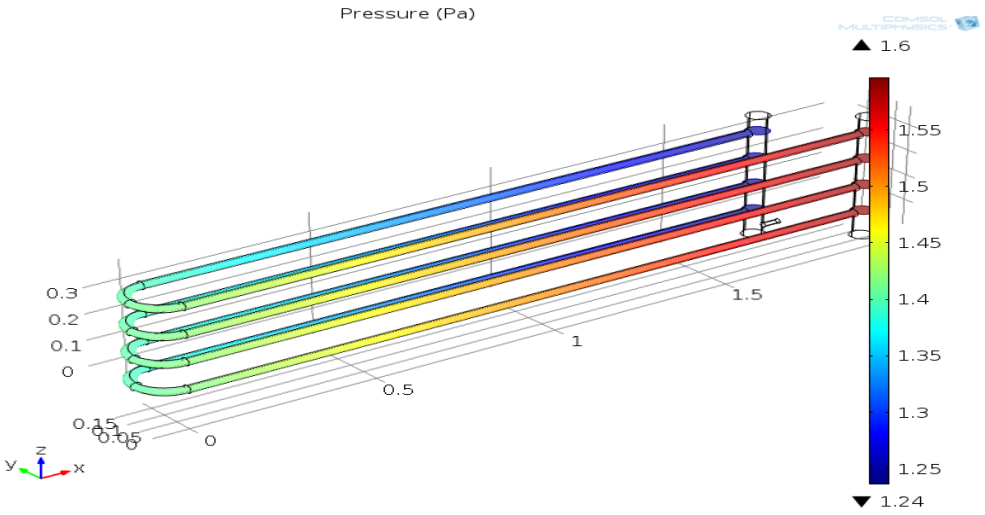

Figure I.2: Pressure profile for 3.8 m tube length, 10.5 cm tube spacing and 25 L/h volumetric flow rate.

APPENDIX J

OUTDOOR EXPERIMENTAL DATA

Table J.1: Daily variation in pH and cell concentration of RUN 092014. The experiment started on September 10, 2014.

Date	Day number	pH	Cell concentration (gdcw/Lc)	ODave
10.09.2014	1	7.14	0.153	0.329
11.09.2014	2	6.47	0.249	0.53525
12.09.2014	3	6.41	0.237	0.5085
13.09.2014	4	6.36	0.256	0.5505
14.09.2014	5	6.49	0.186	0.4
15.09.2014	6	6.46	0.168	0.361
16.09.2014	7	6.43	0.177	0.38
17.09.2014	8	6.34	0.158	0.34
18.09.2014	9	6.37	0.147	0.316
19.09.2014	10	6.40	0.119	0.255
20.09.2014	11	6.48	0.212	0.4545
21.09.2014	12	5.95	0.405	0.86975
22.09.2014	13	5.58	0.406	0.873
23.09.2014	14	5.10	0.463	0.995
24.09.2014	15	4.84	0.423	0.908
25.09.2014	16	4.67	0.391	0.83925
26.09.2014	17	4.61	0.313	0.67275
27.09.2014	18	4.55	0.260	0.55875
28.09.2014	19	4.85	0.259	0.55525
29.09.2014	20	5.14	0.291	0.62425

Table J.2: Daily variation in organic acid and sucrose concentration of RUN 092014. The experiment started on July 10, 2014.

Day	Concentration in mM					
	Lactic acid	**Formic acid**	**Acetic acid**	**Propionic acid**	**Butyric acid**	**Sucrose**
1	0.04	0.06	0.20	3.90	0.01	0.16
2	0.03	0.02	0.07	3.96	0.01	0.04
3	0.02	0.03	0.15	3.17	0.01	0.03
4	0.02	0.07	0.14	3.10	0.01	0.03
5	0.05	0.19	0.27	2.46	0.01	0.03
6	0.00	0.02	0.05	3.94	0.00	0.02
7	0.08	0.08	0.45	2.06	0.02	0.04
8	0.05	0.11	0.26	2.76	0.01	0.01
9	0.00	0.02	0.04	3.76	0.01	0.03
10	0.29	0.22	0.67	1.26	0.02	0.02
11	7.67	0.17	3.92	2.75	0.02	0.03
12	13.90	2.31	6.68	1.64	0.06	0.00
13	31.25	4.31	15.37	14.95	0.08	0.00
14	30.16	4.29	13.42	15.70	0.03	0.01
15	48.65	6.19	22.55	18.97	0.08	0.01
16	53.51	7.18	26.52	23.58	0.12	0.02
17	49.21	5.49	22.52	14.44	2.19	0.01
18	44.91	3.80	18.51	5.30	4.27	0.39
19	43.39	3.59	18.97	9.52	5.18	
20	35.77	3.05	18.82	7.45	5.15	

Table J.3: Daily variation in cell concentration of RUN 072015-R1. The experiment started on July 12, 2015.

Date	**Hour**	**Day**	**OD_1**	**OD_2**	**OD_3**	**OD_{ave}**	**Cell Conc. ($gdcw/L_c$)**
12.07.2015	18:30	0.5	0.632	0.632	0.632	0.632	0.294
13.07.2015	0.396	1.0	0.801	0.820	0.814	0.812	0.378
	19:30	1.5	1.173	1.195	1.204	1.191	0.554
14.07.2015	08:45	2.0	1.205	1.24	1.257	1.234	0.575
	18:00	2.5	1.563	1.577	1.582	1.574	0.733
15.07.2015	08:45	3.0	1.6	1.597	1.625	1.607	0.748
	18:30	3.5	1.567	1.555	1.565	1.562	0.727
16.07.2015	09:00	4.0	1.538	1.526	1.529	1.531	0.713
	19:00	4.5	1.276	1.28	1.276	1.277	0.595
17.07.2015	09:30	5.0	1.141	1.149	1.155	1.148	0.535
	19:00	5.5	1.133	1.134	1.129	1.132	0.527
18.07.2015	08:30	6.0	1.094	1.093	1.097	1.095	0.510
	18:30	6.5	1.096	1.108	1.106	1.103	0.514
19.07.2015	08:30	7.0	1.031	1.114	1.129	1.091	0.508
	18:30	7.5	1.125	1.131	1.135	1.130	0.526
20.07.2015	08:30	8.0	1.162	1.173	1.172	1.169	0.544
	19:00	8.5	1.102	1.102	1.111	1.105	0.514
21.07.2015	08:30	9.0	1.078	1.099	1.096	1.091	0.508
	19:00	9.5	1.140	1.150	1.140	1.143	0.532

Table J. 4: Daily variation in pH of RUN 072015-R1. The experiment started on July 12, 2015.

Date	**Hour**	**Day**	**pH_1**	**pH_2**	**pH_3**	**pH-ave**
12.07.2015	18:30	0	6.40	6.40	6.40	6.40
13.07.2015	08:30	0.5	6.54	6.53	6.54	6.54
	19:30	1.0	6.70	6.68	6.67	6.68
14.07.2015	08:45	1.5	6.70	6.68	6.67	6.68
	18:00	2.0	6.85	6.87	6.88	6.87
15.07.2015	08:45	2.5	6.86	6.92	6.95	6.91
	18:30	3.0	6.90	6.89	6.96	6.92
16.07.2015	09:00	3.5	6.93	6.91	6.90	6.91
	19:00	4.0	6.83	6.83	6.84	6.83
17.07.2015	09:30	4.5	6.77	6.78	6.84	6.80
	19:00	5.0	6.79	6.78	6.79	6.79
18.07.2015	08:30	5.5	6.68	6.73	6.74	6.72
	18:30	6.0	6.77	6.76	6.75	6.76
19.07.2015	08:30	6.5	6.74	6.74	6.75	6.74
	18:30	7.0	6.48	6.52	6.52	6.51
20.07.2015	08:30	7.5	6.53	6.53	6.54	6.53
	19:00	8.0	6.57	6.57	6.57	6.57
21.07.2015	08:30	8.5	6.57	6.59	6.58	6.58
	19:00	9.0	6.58	6.58	6.58	6.58

Table J.5: Daily variation in organic acid concentrations of RUN 072015-R1. The experiment started on July 12, 2015.

Day	Concentration (mM)				
	Lactic Acid	**Formic acid**	**Acetic acid**	**Propionic acid**	**Butyric acid**
0.5	0.00	0.00	40.00	0.00	0.00
1	0.00	0.01	29.22	0.04	0.66
1.5	0.03	0.04	26.63	0.04	0.62
2	0.06	0.15	26.59	0.10	0.77
2.5	0.07	0.22	22.20	0.08	0.75
3	0.13	0.26	20.67	0.10	0.76
3.5	0.13	0.26	20.67	0.10	0.76
4	0.10	0.07	18.99	0.03	0.65
4.5	0.18	0.49	19.16	0.15	0.54
5	0.00	0.51	36.54	0.47	0.12
5.5	0.00	0.50	38.48	0.33	0.17
6	0.02	0.59	38.85	0.55	0.45
6.5	0.03	0.55	38.23	0.60	0.40
7	0.09	0.21	38.16	1.01	1.18
7.5	0.09	0.21	38.16	1.01	1.18
8	0.13	0.25	37.75	2.05	0.42
8.5	0.02	0.45	36.29	0.00	0.40
9	0.00	0.02	37.64	0.00	0.00
9.5	0.00	0.00	36.81	0.00	0.00

Table J. 6: Biogas production of RUN 072015-R1. The experiment started on July 12, 2015.

Date	Day	H_2 %	CO_2 %	Total gas (mL)	Daily H_2 produced (mol)	H_2 productivity (mol/(m^3.h)	Daily solar radiation (W/m^2)
13.07.2015	1	96.8	3.2	171	0.006	0.038	248.63
14.07.2015	2	96.5	3.5	643	0.022	0.144	325.970
15.07.2015	3	97.6	2.4	372	0.013	0.084	297.760
16.07.2015	4	95.8	4.2	556	0.019	0.123	291.350
17.07.2015	5	93.0	7.0	165	0.005	0.036	322.201
18.07.2015	6	78.7	21.3	239	0.007	0.044	323.550
19.07.2015	7	87.2	12.8	429	0.013	0.087	327.940
20.07.2015	8	87.5	12.5	301	0.009	0.061	327.960
21.07.2015	9	6.5	93.5	2	0.000	0.000	328.530

Table J.7: Daily variation in cell concentration of RUN 072015-R2. The experiment started on July 12, 2015.

Date	Hour	Day	OD_1	OD_2	OD_3	OD_{ave}	Cell Conc. ($gdcw/L_c$)
12.07.2015	18:30	0	0.565	0.565	0.565	0.565	0.263
13.07.2015	0.396	0.5	0.578	0.600	0.614	0.597	0.278
	19:30	1.0	0.829	0.85	0.846	0.842	0.392
14.05.2015	08:45	1.5	0.83	0.897	0.905	0.877	0.408
	18:00	2.0	0.825	0.839	0.843	0.836	0.389
15.05.2015	08:45	2.5	0.767	0.851	0.892	0.837	0.390
	18:30	3	0.737	0.737	0.735	0.736	0.343
16.05.2015	09:00	3.5	0.718	0.725	0.732	0.725	0.338
	19:00	4.0	0.767	0.761	0.762	0.763	0.355
17.05.2015	09:30	4.5	0.771	0.77	0.774	0.772	0.359
	19:00	5.0	0.925	0.926	0.931	0.927	0.432
18.05.2015	08:30	5.5	0.922	0.931	0.925	0.926	0.431
	18:30	6	1.048	1.051	1.055	1.051	0.490
19.05.2015	08:30	6.5	1.069	1.072	1.072	1.071	0.499
	18:30	7.0	1.159	1.164	1.166	1.163	0.541
20.05.2015	08:30	7.5	1.109	1.133	1.135	1.126	0.524
	19:00	8.0	1.185	1.198	1.197	1.193	0.556
21.05.2015	08:30	8.5	1.156	1.16	1.161	1.159	0.540
	19:00	9.0	1.237	1.246	1.244	1.242	0.578
22.05.2015	08:45	10.0	1.138	1.146	1.149	1.144	0.533
23.05.2015	09:00	11.0	1.11	1.117	1.12	1.116	0.519
	19:00	11.5	1.281	1.1293	1.293	1.234	0.575
24.05.2015	08:30	12.0	1.105	1.025	1.025	1.052	0.490
	19:00	12.5	0.963	0.978	0.982	0.974	0.454

Table J.8: Daily variation in pH of RUN 072015-R2. The experiment started on July 12, 2015.

Date	Hour	Day	pH_1	pH_2	pH_3	pH-ave
12.07.2015	18:30	0	7.500	7.500	7.500	7.500
13.07.2015	0.396	0.5	7.310	7.300	7.300	7.303
	19:30	1.0	6.4	6.41	6.42	6.410
14.05.2015	08:45	1.5	6.4	6.39	6.4	6.397
	18:00	2.0	6.43	6.40	6.41	6.41
15.05.2015	08:45	2.5	6.38	6.42	6.45	6.42
	18:30	3	6.40	6.39	6.39	6.39
16.05.2015	09:00	3.5	6.43	6.40	6.39	6.41
	19:00	4.0	6.43	6.43	6.43	6.43
17.05.2015	09:30	4.5	6.41	6.40	6.42	6.41
	19:00	5.0	6.08	6.08	6.07	6.08
18.05.2015	08:30	5.5	6.05	6.06	6.05	6.05
	18:30	6	5.93	5.96	5.96	5.95
19.05.2015	08:30	6.5	5.95	5.95	5.97	5.96
	18:30	7.0	5.94	5.93	5.93	5.93
20.05.2015	08:30	7.5	6.00	6.00	5.99	6.00
	19:00	8.0	5.98	5.97	5.99	5.98
21.05.2015	08:30	8.5	5.99	6.01	6.02	6.01
	19:00	9	5.95	5.98	5.99	5.97
22.05.2015	08:45	9.5	6.01	6.00	6.02	6.01
23.05.2015	09:00	10.5	5.94	5.98	5.97	5.96
	19:00	11.0	5.94	5.92	5.93	5.93
24.05.2015	08:30	11.5	5.97	5.92	5.93	5.94
	19:00	12	5.77	5.76	5.76	5.76

Table J. 9: Daily variation in organic acid and sucrose concentrations of RUN 072015-R2. The experiment started on July 12, 2015.

	Concentration (mM)					
Day no	**Lactic acid**	**Formic acid**	**Acetic acid**	**Propionic acid**	**Butyric acid**	**Sucrose**
0.5	0.716	8.214	6.386	0.482	0.000	
1.0	0.616	8.217	7.640	0.547	0.000	0.045
1.5	0.683	8.221	6.934	0.543	0.000	0.048
2.0	0.699	7.926	7.267	0.529	0.000	0.047
2.5	0.785	8.036	7.150	0.503	0.000	0.046
3.0	0.797	7.692	7.150	0.429	0.019	0.047
3.5	0.668	7.505	7.060	0.669	0.000	0.051
4.0	0.262	7.371	7.037	1.179	0.000	0.048
4.5	0.057	7.277	6.943	1.532	0.000	0.042
5.0	0.083	10.927	8.600	1.703	0.073	0.035
5.5	0.173	10.521	8.915	1.897	0.000	0.035
6.0	0.254	10.614	9.646	2.353	0.363	0.035
6.5	0.173	10.521	8.915	1.897	0.000	0.032
7.0	0.254	10.614	9.646	2.353	0.363	0.030
7.5	0.347	9.264	9.316	2.246	0.450	0.028
8.0	0.690	7.848	8.429	2.228	0.752	0.017
8.5	0.608	7.464	8.315	2.201	0.918	0.032
9.0	0.783	7.425	7.488	1.571	9.043	0.032
10.0	0.402	8.461	9.005	3.214	13.471	0.060
10.5	0.061	2.484	11.299	10.564	6.637	0.040
11.0	0.156	5.132	12.522	9.354	13.607	0.021
11.5	0.236	5.633	13.562	4.889	16.331	0.025
12.0	0.156	5.132	12.522	3.452	13.607	0.020
12.5	0.212	6.159	14.454	0.752	18.322	

Table J.10: Biogas production of RUN 072015-R2. The experiment started on July 12, 2015.

Date	Gas content		Total gas (mL)	H_2 produced (mol)	H_2 productivity (mol $H_2/(m^3.h)$	Daily solar radiation (W/m^2)
	H_2%	CO_2 %				
13.07.2015	0.0	0.0	0.0	0.000	0.000	248.63
14.07.2015	0.0	0.0	0.0	0.000	0.000	325.970
15.07.2015	100.0	0.0	18	0.001	0.005	297.760
16.07.2015	0.0	0.0	0.0	0.000	0.000	291.350
17.07.2015	84.7	15.3	532	0.016	0.128	322.201
18.07.2015	53.5	46.5	506	0.010	0.077	323.550
19.07.2015	37.5	62.5	1484	0.020	0.158	327.940
20.07.2015	24.5	75.5	1865	0.016	0.129	327.960
21.07.2015	29.6	70.4	1298	0.014	0.109	328.530
22.07.2015	23.2	76.8	4732	0.039	0.311	326.900
23.07.2015	20.2	79.8	3851	0.028	0.220	320.450
24.07.2015	17.6	82.4	3090	0.019	0.155	319.270

Table J.11: Data taken from the weather station on July 21, 2015.

Time	Air Temperature (ºC)	Humidity	Dew Point (ºC)	Wind Speed (m/s)	Heat Index	Pressure	Solar Radiation (W/m^2)
12:00 AM	15.3	40	1.8	3.2	13.8	1006.5	0
12:05 AM	15.1	41	1.9	3.2	13.7	1006.5	0
12:10 AM	15.1	41	1.9	3.2	13.7	1006.5	0
12:15 AM	15	41	1.8	3.2	13.6	1006.6	0
12:20 AM	14.8	43	2.4	1.6	13.5	1006.5	0
12:25 AM	14.8	43	2.4	1.6	13.5	1006.6	0
12:30 AM	15.1	43	2.6	1.6	13.7	1006.5	0
12:35 AM	15.3	43	2.8	1.6	13.9	1006.6	0
12:40 AM	15.7	43	3.2	1.6	14.3	1006.5	0

Table J.11.continued

12:50 AM	16	44	3.7	1.6	14.7	1006.5	0
12:55 AM	15.9	45	4	1.6	14.6	1006.5	0
1:00 AM	15.6	44	3.4	1.6	14.3	1006.5	0
1:05 AM	15.8	44	3.6	3.2	14.5	1006.5	0
1:10 AM	15.9	45	4	3.2	14.6	1006.6	0
1:15 AM	15.5	47	4.2	1.6	14.3	1006.6	0
1:20 AM	14.9	48	4	1.6	13.8	1006.6	0
1:25 AM	14.4	50	4.1	1.6	13.3	1006.5	0
1:30 AM	14.1	51	4.1	1.6	13	1006.5	0
1:35 AM	13.8	52	4.1	3.2	12.8	1006.5	0
1:40 AM	13.8	51	3.8	3.2	12.8	1006.5	0
1:45 AM	13.6	52	3.9	3.2	12.6	1006.6	0
1:50 AM	13.6	53	4.1	3.2	12.6	1006.6	0
1:55 AM	13.4	53	4	3.2	12.4	1006.5	0
2:00 AM	13.2	54	4.1	1.6	12.3	1006.6	0
2:05 AM	13.2	54	4.1	3.2	12.3	1006.6	0
2:10 AM	13.2	54	4.1	3.2	12.3	1006.7	0
2:15 AM	13.3	54	4.2	3.2	12.4	1006.6	0
2:20 AM	13.3	54	4.2	3.2	12.4	1006.6	0
2:25 AM	13.2	54	4.1	3.2	12.3	1006.7	0
2:30 AM	13.1	55	4.3	3.2	12.2	1006.7	0
2:35 AM	13.2	55	4.3	3.2	12.3	1006.7	0
2:40 AM	13.1	55	4.3	3.2	12.2	1006.8	0
2:45 AM	13.1	55	4.3	3.2	12.2	1006.9	0
2:50 AM	13.4	54	4.3	1.6	12.4	1006.9	0
2:55 AM	13.8	54	4.6	4.8	12.8	1006.9	0
3:00 AM	14.3	53	4.8	3.2	13.3	1006.8	0
3:05 AM	14.4	53	5	0	13.4	1006.8	0
3:10 AM	14.1	54	4.9	1.6	13.2	1006.8	0

Table J.11.continued

3:15 AM	13.8	55	4.9	1.6	12.9	1006.8	0
3:20 AM	13.6	57	5.2	1.6	12.7	1006.7	0
3:25 AM	13.3	59	5.5	1.6	12.6	1006.7	0
3:30 AM	13.2	60	5.6	1.6	12.4	1006.7	0
3:35 AM	13.2	60	5.6	1.6	12.5	1006.6	0
3:40 AM	13.3	60	5.7	1.6	12.6	1006.6	0
3:45 AM	13.3	60	5.7	1.6	12.6	1006.6	0
3:50 AM	13.4	60	5.8	1.6	12.7	1006.6	0
3:55 AM	13.5	61	6.1	1.6	12.8	1006.6	0
4:00 AM	13.6	62	6.4	0	12.9	1006.6	0
4:05 AM	13.6	62	6.4	0	12.9	1006.6	0
4:10 AM	13.4	62	6.3	0	12.8	1006.6	0
4:15 AM	13.3	63	6.4	1.6	12.7	1006.7	0
4:20 AM	13.2	64	6.6	0	12.6	1006.6	0
4:25 AM	13.2	64	6.5	1.6	12.6	1006.6	0
4:30 AM	13.1	65	6.7	1.6	12.6	1006.7	0
4:35 AM	13.2	65	6.7	1.6	12.6	1006.7	0
4:40 AM	13.2	65	6.7	1.6	12.6	1006.7	0
4:45 AM	13.1	66	6.8	1.6	12.5	1006.6	0
4:50 AM	13	66	6.8	1.6	12.4	1006.6	0
4:55 AM	12.8	67	6.9	1.6	12.3	1006.7	0
5:00 AM	12.7	68	7	1.6	12.2	1006.7	0
5:05 AM	12.6	68	6.8	1.6	12.1	1006.8	0
5:10 AM	12.4	69	6.9	1.6	12	1006.8	0
5:15 AM	12.4	70	7.1	1.6	12.1	1006.8	0
5:20 AM	12.6	71	7.5	3.2	12.2	1006.8	0
5:25 AM	13	70	7.7	3.2	12.6	1006.8	0
5:30 AM	13.3	68	7.5	4.8	12.8	1007	0
5:35 AM	13.5	68	7.7	3.2	13	1007	0

Table J.11.continued

5:40 AM	13.4	68	7.6	3.2	12.9	1007.1	5
5:45 AM	13.2	68	7.4	1.6	12.7	1007	7
5:50 AM	13.1	69	7.5	1.6	12.7	1007.1	10
5:55 AM	13.1	69	7.5	1.6	12.6	1007.1	13
6:00 AM	13.1	70	7.7	1.6	12.6	1007.2	15
6:05 AM	13.2	70	7.9	1.6	12.8	1007.1	19
6:10 AM	13.4	71	8.3	0	13	1007.2	25
6:15 AM	13.7	70	8.3	1.6	13.2	1007.1	31
6:20 AM	14.2	69	8.6	1.6	13.7	1007.2	40
6:25 AM	14.7	68	8.9	3.2	14.3	1007.2	50
6:30 AM	15.3	68	9.5	1.6	14.9	1007.2	61
6:35 AM	15.9	67	9.8	1.6	15.6	1007.2	75
6:40 AM	16.5	65	9.9	1.6	16.1	1007.3	89
6:45 AM	17.2	64	10.3	0	16.8	1007.3	105
6:50 AM	17.9	60	10	0	17.4	1007.3	116
6:55 AM	18.5	59	10.3	1.6	18	1007.2	123
7:00 AM	19.2	60	11.3	0	18.9	1007.3	132
7:05 AM	19.9	51	9.4	0	19.2	1007.3	151
7:10 AM	20.6	47	8.8	1.6	19.6	1007.3	182
7:15 AM	20.9	49	9.8	1.6	20	1007.2	214
7:20 AM	21.2	47	9.4	1.6	20.1	1007.1	231
7:25 AM	21.6	47	9.8	0	20.7	1007.2	247
7:30 AM	22	46	9.8	1.6	21.2	1007.3	264
7:35 AM	22.3	45	9.8	1.6	21.6	1007.1	281
7:40 AM	22.3	45	9.8	1.6	21.6	1007.1	299
7:45 AM	22.7	44	9.8	1.6	22.1	1007.1	316
7:50 AM	22.8	43	9.6	1.6	22.3	1007.1	326
7:55 AM	22.8	43	9.6	3.2	22.3	1007	324
8:00 AM	22.7	45	10.1	3.2	22.1	1007.2	338

Table J.11.continued

8:05 AM	22.7	45	10.1	1.6	22.1	1007.1	378
8:10 AM	22.6	43	9.4	3.2	21.9	1007	399
8:15 AM	22.6	43	9.4	1.6	21.9	1007	415
8:20 AM	22.9	44	10	1.6	22.4	1007	432
8:25 AM	23.3	42	9.7	1.6	22.9	1007	448
8:30 AM	23.8	41	9.7	1.6	23.4	1007	459
8:35 AM	23.9	40	9.5	3.2	23.5	1007	462
8:40 AM	24.2	40	9.7	1.6	23.7	1007	460
8:45 AM	24.4	40	10	1.6	23.9	1007	454
8:50 AM	24.7	39	9.8	1.6	24.2	1006.9	446
8:55 AM	24.9	37	9.2	3.2	24.3	1007	439
9:00 AM	24.9	38	9.6	3.2	24.4	1007	441
9:05 AM	25.2	37	9.4	1.6	24.6	1006.9	451
9:10 AM	25.3	36	9.2	3.2	24.7	1006.9	469
9:15 AM	25.4	36	9.3	1.6	24.8	1006.8	504
9:20 AM	25.8	36	9.6	1.6	25.2	1006.8	546
9:25 AM	25.8	34	8.8	4.8	25.1	1006.9	594
9:30 AM	25.6	36	9.4	3.2	24.9	1006.9	632
9:35 AM	25.7	35	9.1	3.2	24.9	1006.9	658
9:40 AM	25.7	34	8.7	4.8	25	1007	674
9:45 AM	25.9	32	8	4.8	25.1	1007	691
9:50 AM	26.2	32	8.2	3.2	25.3	1006.9	706
9:55 AM	26.6	31	8.1	3.2	25.6	1007	721
10:00 AM	26.9	30	7.9	3.2	25.8	1007	733
10:05 AM	27.1	31	8.5	3.2	26	1006.9	745
10:10 AM	27.3	30	8.2	3.2	26.2	1007	763
10:15 AM	27.3	28	7.2	4.8	26.1	1007	775
10:20 AM	27.3	28	7.2	3.2	26.1	1006.9	792
10:25 AM	27.5	26	6.3	8	26.2	1006.9	801

Table J.11.continued

10:30 AM	27.2	26	6	8	25.8	1006.9	812
10:35 AM	27.1	28	7	4.8	25.9	1006.9	825
10:40 AM	27.6	27	6.9	4.8	26.3	1007	836
10:45 AM	27.8	28	7.6	3.2	26.6	1006.9	844
10:50 AM	27.9	27	7.2	4.8	26.7	1006.9	857
10:55 AM	28.2	26	6.9	4.8	26.8	1006.9	868
11:00 AM	27.9	26	6.6	6.4	26.6	1006.9	875
11:05 AM	28	27	7.3	4.8	26.7	1006.8	883
11:10 AM	28.1	27	7.3	4.8	26.8	1006.8	890
11:15 AM	28.2	27	7.4	4.8	26.9	1006.8	892
11:20 AM	28.8	27	7.9	3.2	27.6	1006.7	901
11:25 AM	29.3	24	6.7	3.2	27.8	1006.7	909
11:30 AM	29.4	23	6.1	4.8	27.9	1006.7	919
11:35 AM	29.1	23	5.8	4.8	27.6	1006.7	925
11:40 AM	28.8	22	5	3.2	27.3	1006.6	928
11:45 AM	29	20	3.8	4.8	27.3	1006.6	935
11:50 AM	29.2	19	3.2	3.2	27.4	1006.6	950
11:55 AM	29.3	20	4	4.8	27.6	1006.6	950
12:00 PM	29.4	18	2.6	3.2	27.7	1006.6	954
12:05 PM	29.8	20	4.4	4.8	28.1	1006.6	956
12:10 PM	30.1	18	3.1	3.2	28.2	1006.6	962
12:15 PM	30.1	19	3.9	4.8	28.2	1006.6	965
12:20 PM	30.1	20	4.6	4.8	28.3	1006.5	967
12:25 PM	30	22	6	4.8	28.3	1006.6	969
12:30 PM	29.9	21	5.2	6.4	28.2	1006.5	970
12:35 PM	30.2	21	5.5	3.2	28.5	1006.5	974
12:40 PM	30.3	21	5.6	6.4	28.6	1006.3	975
12:45 PM	30.4	21	5.7	4.8	28.7	1006.4	971
12:50 PM	30.8	21	6	3.2	29	1006.4	973

Table J.11.continued

12:55 PM	31	18	3.9	4.8	28.9	1006.4	975
1:00 PM	31	18	3.9	4.8	28.9	1006.3	976
1:05 PM	31.1	20	5.5	4.8	29.1	1006.3	969
1:10 PM	31.4	18	4.3	4.8	29.2	1006.3	972
1:15 PM	31.7	16	2.8	6.4	29.3	1006.3	977
1:20 PM	31.3	16	2.5	8	29	1006.3	976
1:25 PM	31.4	15	1.7	3.2	29	1006.2	975
1:30 PM	31.8	16	2.9	3.2	29.4	1006.2	972
1:35 PM	31.7	16	2.8	6.4	29.2	1006.2	970
1:40 PM	31.8	18	4.5	4.8	29.6	1006.2	963
1:45 PM	31.8	17	3.7	4.8	29.4	1006.1	960
1:50 PM	31.9	16	2.9	4.8	29.6	1006.1	958
1:55 PM	31.8	15	1.9	8	29.3	1006.3	956
2:00 PM	31.9	17	3.8	4.8	29.7	1006.2	949
2:05 PM	32.6	16	3.5	3.2	30.6	1006.1	946
2:10 PM	32.6	15	2.6	6.4	30.4	1006.1	945
2:15 PM	32.7	15	2.7	4.8	30.6	1006.1	940
2:20 PM	32.4	15	2.5	4.8	30.3	1006.2	937
2:25 PM	32.4	13	0.5	4.8	30.2	1006.1	931
2:30 PM	32.3	12	-0.7	4.8	30	1006.2	919
2:35 PM	32.3	12	-0.7	4.8	30	1006.2	918
2:40 PM	32.3	12	-0.7	4.8	30	1006	903
2:45 PM	32.1	11	-2.1	8	29.6	1006.1	902
2:50 PM	32.1	11	-2.1	6.4	29.6	1006.2	890
2:55 PM	32.1	11	-2.1	6.4	29.5	1006.2	885
3:00 PM	32.1	12	-0.9	6.4	29.7	1006.2	872
3:05 PM	31.9	14	1.1	8	29.6	1006.2	859
3:10 PM	32.3	14	1.4	3.2	30.1	1006.1	849
3:15 PM	32.3	14	1.4	4.8	30.2	1006	836

Table J.11.continued

3:20 PM	32.4	14	1.5	3.2	30.2	1006	823
3:25 PM	32.3	15	2.4	8	30.2	1005.9	810
3:30 PM	32.4	15	2.5	4.8	30.3	1005.9	798
3:35 PM	32.6	15	2.6	3.2	30.5	1005.9	416
3:40 PM	32.9	14	1.9	3.2	30.7	1005.9	147
3:45 PM	32.8	16	3.7	4.8	30.8	1005.9	65
3:50 PM	32.3	16	3.3	4.8	30.3	1005.7	96
3:55 PM	32.2	16	3.2	6.4	30.2	1005.8	203
4:00 PM	32.1	17	3.9	9.7	29.9	1005.6	496
4:05 PM	32	18	4.7	9.7	29.9	1005.7	691
4:10 PM	32.1	17	4	6.4	30	1005.6	683
4:15 PM	32.3	16	3.3	4.8	30.2	1005.6	675
4:20 PM	32.3	16	3.3	6.4	30.2	1005.6	659
4:25 PM	32.4	16	3.3	4.8	30.3	1005.5	642
4:30 PM	32.4	16	3.4	6.4	30.4	1005.4	628
4:35 PM	32.7	14	1.7	6.4	30.4	1005.5	619
4:40 PM	32.6	13	0.6	6.4	30.3	1005.5	606
4:45 PM	32.4	13	0.4	8	30.1	1005.5	592
4:50 PM	32.3	13	0.4	8	30.1	1005.5	577
4:55 PM	32.4	14	1.5	6.4	30.3	1005.5	559
5:00 PM	32.6	13	0.6	6.4	30.3	1005.5	544
5:05 PM	32.7	13	0.7	4.8	30.4	1005.6	531
5:10 PM	32.6	12	-0.5	8	30.2	1005.6	517
5:15 PM	32.2	13	0.3	9.7	29.9	1005.6	498
5:20 PM	32.1	13	0.2	6.4	29.7	1005.6	483
5:25 PM	32	13	0.1	6.4	29.6	1005.6	465
5:30 PM	32	13	0.1	6.4	29.6	1005.6	449
5:35 PM	31.9	13	0.1	8	29.4	1005.7	432
5:40 PM	31.9	13	0	6.4	29.3	1005.6	416

Table J.11.continued

5:45 PM	31.9	14	1.1	4.8	29.6	1005.6	401
5:50 PM	31.9	14	1.1	4.8	29.6	1005.6	382
5:55 PM	31.8	14	1	6.4	29.2	1005.6	366
6:00 PM	31.6	14	0.8	6.4	29	1005.7	348
6:05 PM	31.3	14	0.6	8	28.9	1005.8	332
6:10 PM	31.4	16	2.5	4.8	29.1	1005.8	313
6:15 PM	31.5	15	1.7	3.2	29.1	1005.9	300
6:20 PM	31.3	15	1.6	4.8	29	1005.9	282
6:25 PM	31.2	14	0.5	4.8	28.9	1006	263
6:30 PM	31	15	1.3	6.4	28.8	1005.9	245
6:35 PM	30.9	16	2.2	3.2	28.8	1005.9	226
6:40 PM	30.9	17	3	4.8	28.8	1006	205
6:45 PM	30.7	18	3.6	4.8	28.7	1006	189
6:50 PM	30.6	18	3.5	4.8	28.7	1006	171
6:55 PM	30.3	18	3.4	4.8	28.5	1006	150
7:00 PM	30.1	18	3.2	3.2	28.3	1006.1	132
7:05 PM	29.8	19	3.7	3.2	28.1	1006.1	91
7:10 PM	29.6	19	3.5	3.2	27.8	1006.2	34
7:15 PM	29.2	19	3.2	4.8	27.5	1006.3	28
7:20 PM	29.1	19	3.1	4.8	27.3	1006.4	26
7:25 PM	28.9	20	3.7	3.2	27.3	1006.4	25
7:30 PM	28.7	20	3.5	3.2	27.1	1006.5	24
7:35 PM	28.6	20	3.4	4.8	26.9	1006.5	22
7:40 PM	28.5	21	4	4.8	26.9	1006.6	20
7:45 PM	28.3	21	3.9	4.8	26.7	1006.6	18
7:50 PM	28.2	22	4.5	4.8	26.7	1006.7	16
7:55 PM	28.1	22	4.4	3.2	26.6	1006.8	14
8:00 PM	27.9	23	4.8	4.8	26.4	1007	12
8:05 PM	27.8	23	4.7	3.2	26.3	1007	10

Table J.11.continued

8:10 PM	27.6	24	5.2	1.6	26.1	1007	6
8:15 PM	27.3	25	5.5	1.6	25.8	1007.1	3
8:20 PM	27	25	5.3	1.6	25.6	1007.1	0
8:25 PM	26.8	26	5.7	1.6	25.4	1007.3	0
8:30 PM	26.6	27	6	0	25.3	1007.3	0
8:35 PM	26	28	6.1	1.6	24.9	1007.4	0
8:40 PM	25.5	29	6.2	1.6	24.6	1007.4	0
8:45 PM	25.2	29	5.9	0	24.4	1007.5	0
8:50 PM	25.1	30	6.3	0	24.4	1007.6	0
8:55 PM	24.7	31	6.4	1.6	23.9	1007.7	0
9:00 PM	23.9	33	6.6	1.6	23.1	1007.8	0
9:05 PM	23.1	35	6.8	1.6	22.3	1007.9	0
9:10 PM	22.6	36	6.8	1.6	21.6	1007.9	0
9:15 PM	22.9	37	7.4	3.2	22.1	1008.1	0
9:20 PM	23.6	36	7.6	1.6	22.9	1008.1	0
9:25 PM	23.9	35	7.5	1.6	23.3	1008.2	0
9:30 PM	24.1	36	8.1	1.6	23.5	1008.4	0
9:35 PM	24	36	8	1.6	23.4	1008.4	0
9:40 PM	23.8	37	8.2	0	23.2	1008.5	0
9:45 PM	23.3	38	8.2	1.6	22.7	1008.6	0
9:50 PM	22.7	40	8.4	1.6	21.9	1008.6	0
9:55 PM	22.6	42	9	1.6	21.9	1008.7	0
10:00 PM	23.2	41	9.2	3.2	22.6	1008.7	0
10:05 PM	23.6	41	9.5	1.6	23.1	1008.7	0
10:10 PM	23.7	41	9.6	1.6	23.2	1008.7	0
10:15 PM	23.6	41	9.6	1.6	23.2	1008.8	0
10:20 PM	23.1	42	9.5	1.6	22.6	1008.8	0
10:25 PM	22.5	44	9.6	1.6	21.8	1008.9	0
10:30 PM	22.5	45	10	1.6	21.8	1008.9	0

TableJ.11.continued

10:35 PM	22.6	46	10.3	0	22	1008.9	0
10:40 PM	22.6	46	10.3	1.6	22	1009	0
10:45 PM	22.7	46	10.5	1.6	22.2	1009	0
10:50 PM	22.6	47	10.7	1.6	22.1	1009	0
10:55 PM	22.8	46	10.6	3.2	22.3	1009.1	0
11:00 PM	22.8	46	10.6	1.6	22.4	1009.2	0
11:05 PM	22.9	46	10.7	3.2	22.4	1009.2	0
11:10 PM	22.9	46	10.7	1.6	22.6	1009.2	0
11:15 PM	22.9	46	10.7	3.2	22.6	1009.2	0
11:20 PM	22.9	46	10.7	3.2	22.4	1009.4	0
11:25 PM	22.9	45	10.4	6.4	22.5	1009.4	0
11:30 PM	23.1	45	10.5	4.8	22.7	1009.4	0
11:35 PM	23.1	44	10.1	4.8	22.6	1009.4	0
11:40 PM	23.1	44	10.1	3.2	22.6	1009.4	0
11:45 PM	22.9	44	10	1.6	22.4	1009.5	0
11:50 PM	22.8	45	10.2	4.8	22.3	1009.5	0
11:55 PM	22.7	44	9.8	4.8	22.2	1009.5	0
12:00 AM	22.8	44	9.9	3.2	22.2	1009.5	0

Table J.12: Temperature data taken on July 21, 2015.

Hour (min)	Reactor 2		Reactor 1															
	T4	T12	T1	T2	T3	T4	T5	T6	T7	T8	T1	T2	T3	T4	T9	T10	T11	T12
0	17.7	18.9	17.1	17.3	18.2	19.4	19.0	18.9	18.3	19.4	17.1	17.3	18.2	19.4	17.2	17.3	16.6	17.0
10	16.1	18.0	16.5	16.1	16.7	18.7	18.2	18.1	17.5	18.5	16.5	16.1	16.7	18.7	16.1	16.1	15.5	15.7
20	15.5	17.2	16.1	15.4	16.2	17.8	17.4	17.2	16.7	17.6	16.1	15.4	16.2	17.8	15.2	15.4	14.7	15.0
30	15.3	16.8	15.9	14.7	15.8	17.0	16.7	16.5	16.0	16.9	15.9	14.7	15.8	17.0	14.7	14.7	14.1	14.4
40	14.6	16.2	15.6	14.5	15.2	16.3	16.1	15.9	15.3	16.3	15.6	14.5	15.2	16.3	14.3	14.5	13.9	14.1
50	14.5	15.7	15.6	14.3	15.0	15.7	15.6	15.4	14.9	15.8	15.6	14.3	15.0	15.7	14.2	14.3	13.7	13.9
60	15.0	16.3	15.6	14.2	15.3	15.4	15.2	15.1	14.5	15.5	15.6	14.2	15.3	15.4	14.1	14.2	13.6	13.9
70	14.0	15.4	16.1	13.5	14.7	15.2	14.9	14.8	14.2	15.2	16.1	13.5	14.7	15.2	13.4	13.5	13.0	13.2
80	13.6	15.2	16.9	13.1	14.3	14.7	14.4	14.3	13.8	14.8	16.9	13.1	14.3	14.7	13.0	13.1	12.5	12.8
90	13.6	15.1	17.3	12.9	14.2	14.2	14.1	13.9	13.4	14.4	17.3	12.9	14.2	14.2	12.8	12.9	12.3	12.6
100	13.3	14.3	17.2	12.7	13.9	13.9	13.6	13.4	13.0	13.9	17.2	12.7	13.9	13.9	12.5	12.7	12.1	12.3
110	12.5	13.8	16.7	11.9	13.2	13.6	13.2	13.0	12.5	13.5	16.7	11.9	13.2	13.6	11.9	11.9	11.4	11.6
120	12.4	13.3	16.3	11.6	12.8	13.2	12.8	12.7	12.2	13.1	16.3	11.6	12.8	13.2	11.6	11.6	11.1	11.4
130	13.2	14.2	15.9	12.2	13.6	12.8	12.5	12.4	11.9	12.8	15.9	12.2	13.6	12.8	12.2	12.2	11.7	12.0
140	12.9	13.7	15.4	11.7	13.1	12.7	12.5	12.3	11.8	12.7	15.4	11.7	13.1	12.7	11.7	11.7	11.2	11.5
150	12.6	13.3	15.0	11.4	12.9	12.7	12.2	12.0	11.6	12.5	15.0	11.4	12.9	12.7	11.4	11.4	10.9	11.2
160	11.7	12.8	14.7	11.2	12.1	12.4	11.9	11.7	11.3	12.2	14.7	11.2	12.1	12.4	11.0	11.2	10.6	10.8
170	11.8	12.8	14.1	10.9	12.3	12.1	11.7	11.6	11.2	12.1	14.1	10.9	12.3	12.1	10.8	10.9	10.4	10.6

Table J.12.continued

180	11.4	12.5	13.9	10.7	11.9	11.9	11.4	11.3	10.8	11.7	13.9	10.7	11.9	11.9	10.6	10.7	10.2	10.4
190	12.2	13.0	13.5	10.7	12.5	11.6	11.1	11.0	10.6	11.5	13.5	10.7	12.5	11.6	10.7	10.7	10.2	10.5
200	10.8	12.0	13.0	10.2	11.4	11.5	11.0	10.9	10.4	11.3	13.0	10.2	11.4	11.5	10.2	10.2	9.7	10.0
210	11.0	12.1	12.7	10.2	11.4	11.3	10.8	10.6	10.2	11.1	12.7	10.2	11.4	11.3	10.1	10.2	9.7	9.9
220	11.1	11.8	12.6	10.1	11.3	11.0	10.5	10.4	10.0	10.9	12.6	10.1	11.3	11.0	10.1	10.1	9.6	9.8
230	10.5	11.6	12.5	9.8	11.2	10.8	10.3	10.2	9.8	10.6	12.5	9.8	11.2	10.8	9.7	9.8	9.4	9.5
240	11.0	11.6	12.5	9.5	11.2	10.6	10.1	10.0	9.5	10.4	12.5	9.5	11.2	10.6	9.5	9.5	9.0	9.2
250	10.0	11.3	12.5	9.3	10.4	10.4	10.0	9.9	9.4	10.3	12.5	9.3	10.4	10.4	9.3	9.3	8.9	9.0
260	10.0	11.0	12.8	9.3	10.5	10.3	10.0	9.8	9.3	10.1	12.8	9.3	10.5	10.3	9.3	9.3	8.9	9.1
270	9.6	10.9	13.2	9.1	10.2	10.1	9.7	9.6	9.2	10.0	13.2	9.1	10.2	10.1	9.0	9.1	8.6	8.9
280	10.2	10.8	13.3	9.1	10.5	10.0	9.5	9.4	9.0	9.9	13.3	9.1	10.5	10.0	9.1	9.1	8.7	8.9
290	10.3	11.0	13.8	8.9	10.5	9.8	9.4	9.3	8.8	9.7	13.8	8.9	10.5	9.8	8.9	8.9	8.4	8.6
300	9.3	10.5	13.9	8.6	9.9	9.7	9.2	9.1	8.6	9.4	13.9	8.6	9.9	9.7	8.6	8.6	8.2	8.4
310	9.4	10.6	13.6	8.6	10.0	9.6	9.1	9.0	8.5	9.4	13.6	8.6	10.0	9.6	8.6	8.6	8.1	8.4
320	9.5	10.5	13.3	8.5	9.9	9.4	8.9	8.8	8.4	9.2	13.3	8.5	9.9	9.4	8.5	8.5	8.1	8.3
330	9.8	10.8	12.9	8.6	10.2	9.4	8.9	8.8	8.4	9.2	12.9	8.6	10.2	9.4	8.6	8.6	8.2	8.5
340	9.9	10.6	12.5	8.6	10.3	9.5	8.7	8.7	8.3	9.2	12.5	8.6	10.3	9.5	8.6	8.6	8.2	8.4
350	9.7	10.7	12.7	8.5	10.2	9.5	8.8	8.8	8.3	9.2	12.7	8.5	10.2	9.5	8.6	8.5	8.1	8.4
360	11.0	11.9	12.9	9.4	11.2	9.8	9.2	9.1	8.9	9.7	12.9	9.4	11.2	9.8	9.5	9.4	9.0	9.2
370	11.7	12.7	13.9	10.3	12.1	11.0	9.7	9.9	9.5	10.4	13.9	10.3	12.1	11.0	10.6	10.3	9.9	10.3

Table J.12.continued

380	12.9	13.6	15.0	11.6	13.3	12.5	11.2	10.8	10.8	11.6	15.0	11.6	13.3	12.5	11.8	11.6	11.1	11.5
390	13.9	14.1	16.3	12.6	14.4	14.1	12.4	12.4	11.9	12.8	16.3	12.6	14.4	14.1	12.8	12.6	12.1	12.3
400	14.9	15.1	18.0	13.9	15.2	15.7	13.9	14.0	13.6	14.6	18.0	13.9	15.2	15.7	13.9	13.9	13.3	13.6
410	16.1	16.4	19.4	15.5	16.2	17.5	15.7	15.8	15.5	16.3	19.4	15.5	16.2	17.5	15.4	15.5	14.9	15.1
420	17.8	17.6	20.9	17.1	17.5	19.2	17.6	17.8	17.4	18.5	20.9	17.1	17.5	19.2	16.9	17.1	16.4	16.8
430	18.6	18.6	22.3	18.7	18.5	20.7	19.6	19.8	19.5	20.6	22.3	18.7	18.5	20.7	18.5	18.7	18.0	18.4
440	18.4	19.1	23.3	19.8	19.3	22.1	21.6	21.6	21.3	22.3	23.3	19.8	19.3	22.1	19.6	19.8	19.1	19.6
450	19.6	19.8	24.0	21.1	20.2	23.3	23.3	23.3	22.8	23.8	24.0	21.1	20.2	23.3	20.8	21.1	20.3	20.7
460	19.0	20.3	24.3	21.3	20.7	24.2	24.5	24.5	24.1	25.2	24.3	21.3	20.7	24.2	21.0	21.3	20.5	21.0
470	19.3	20.5	24.7	22.0	23.0	25.3	25.8	25.8	25.3	26.5	24.7	22.0	23.0	25.3	21.6	22.0	21.2	21.6
480	21.3	21.3	25.6	23.1	22.3	25.8	27.1	27.0	26.5	27.5	25.6	23.1	22.3	25.8	22.7	23.1	22.2	22.8
490	22.0	21.7	26.3	24.0	22.5	26.0	27.8	27.7	27.2	28.2	26.3	24.0	22.5	26.0	23.6	24.0	23.1	23.6
500	22.3	22.5	26.7	24.2	22.8	26.6	28.4	28.3	27.8	28.9	26.7	24.2	22.8	26.6	23.8	24.2	23.2	23.7
510	22.2	22.7	27.2	25.2	22.9	27.6	29.2	29.0	28.5	29.6	27.2	25.2	22.9	27.6	24.8	25.2	24.0	24.5
520	22.9	23.3	27.8	25.4	23.5	28.3	29.8	29.4	28.8	29.8	27.8	25.4	23.5	28.3	25.2	25.4	24.2	24.8
530	23.6	30.0	28.2	25.9	23.5	28.6	29.6	29.4	28.9	29.9	28.2	25.9	23.5	28.6	25.7	25.9	24.7	25.2
540	23.9	30.1	28.6	26.0	23.9	28.3	30.0	29.7	29.2	30.1	28.6	26.0	23.9	28.3	25.8	26.0	24.8	25.3
550	24.6	30.8	29.0	27.2	24.4	28.8	30.3	30.1	29.6	30.6	29.0	27.2	24.4	28.8	27.0	27.2	26.1	26.5
560	24.4	31.5	29.2	28.0	24.7	29.1	30.9	30.8	30.2	31.3	29.2	28.0	24.7	29.1	27.8	28.0	26.9	27.4
570	25.3	32.2	29.7	28.3	24.8	29.6	31.7	31.5	30.9	32.1	29.7	28.3	24.8	29.6	28.2	28.3	27.4	27.9

Table J.12.continued

580	25.5	32.8	30.1	29.3	25.3	30.1	32.4	32.2	31.5	32.7	30.1	29.3	25.3	30.1	29.2	29.3	28.3	28.7
590	24.9	33.1	30.8	29.8	24.7	30.7	31.9	32.1	31.7	32.9	30.8	29.8	24.7	30.7	30.0	29.8	28.8	29.3
600	24.1	32.7	31.1	28.8	33.1	31.2	32.5	32.4	32.0	33.1	31.1	28.8	33.1	31.2	28.7	28.8	27.7	27.9
610	25.1	32.0	32.0	30.1	32.5	31.0	32.8	32.6	31.8	32.8	32.0	30.1	32.5	31.0	30.1	30.1	29.0	29.6
620	25.7	32.4	31.9	32.0	32.8	31.2	32.8	32.7	32.2	33.1	31.9	32.0	32.8	31.2	31.1	31.2	30.2	30.8
630	27.5	33.0	32.3	33.0	33.2	31.1	33.7	33.3	32.8	33.7	32.3	33.0	33.2	31.1	31.4	31.3	30.3	31.0
640	29.0	25.0	33.2	35.0	35.0	33.0	35.0	35.0	36.0	35.0	33.2	35.0	35.0	33.0	33.0	32.0	31.0	32.0
650	30.5	37.9	37.5	36.0	38.0	35.4	37.4	37.7	37.7	38.3	37.5	36.0	38.0	35.4	33.7	33.3	32.5	33.0
660	30.9	38.6	36.7	35.8	38.5	35.2	37.9	38.3	38.1	38.6	36.7	35.8	38.5	35.2	34.1	33.5	32.5	32.9
670	31.2	39.0	37.3	35.9	39.0	35.6	38.2	38.2	38.3	38.7	37.3	35.9	39.0	35.6	35.0	34.1	33.3	33.6
680	31.9	39.0	36.9	36.5	38.8	36.1	38.8	38.6	38.3	38.8	36.9	36.5	38.8	36.1	36.2	35.2	34.5	34.9
690	32.7	38.9	37.4	36.3	38.8	36.2	38.8	38.5	38.3	38.8	37.4	36.3	38.8	36.2	35.0	34.5	33.7	34.1
700	33.1	38.7	37.2	36.6	38.4	36.2	38.4	37.8	37.6	38.2	37.2	36.6	38.4	36.2	35.5	34.5	33.5	33.7
710	33.8	38.5	37.3	36.2	38.2	35.8	38.0	37.3	37.3	38.1	37.3	36.2	38.2	35.8	36.0	34.7	33.8	33.7
720	34.2	38.3	37.0	35.4	37.9	35.3	38.0	37.4	37.3	38.0	37.0	35.4	37.9	35.3	35.6	34.2	33.2	33.1
730	33.7	38.8	37.5	36.7	38.5	36.1	38.7	37.6	37.4	38.0	37.5	36.7	38.5	36.1	37.1	35.8	34.8	34.8
740	33.6	39.3	38.2	37.1	38.9	36.6	38.0	37.9	37.8	38.5	38.2	37.1	38.9	36.6	36.5	35.4	34.6	34.7
750	35.5	36.7	35.8	36.7	35.3	34.4	37.9	37.9	37.7	38.2	35.8	36.7	35.3	34.4	36.5	35.7	34.7	34.8
760	34.7	31.7	31.0	32.8	30.2	29.7	34.9	31.9	31.6	32.8	31.0	32.8	30.2	29.7	37.1	35.2	32.9	33.3
770	37.0	29.0	27.6	29.2	27.7	27.0	32.3	28.1	28.0	29.5	27.6	29.2	27.7	27.0	36.7	34.2	32.3	33.0

Table J.12.continued

780	37.5	29.4	27.3	30.5	27.3	27.5	34.4	30.5	29.8	30.2	27.3	30.5	27.3	27.5	35.5	34.1	33.2	33.7
790	38.7	30.7	31.5	32.2	30.3	29.3	31.8	31.2	32.0	32.5	31.5	32.2	30.3	29.3	35.8	33.3	32.7	33.8
800	36.7	29.2	30.6	30.8	28.4	27.9	31.2	28.5	28.9	29.7	30.6	30.8	28.4	27.9	35.3	33.3	31.5	32.3
810	35.9	27.6	28.5	32.2	26.7	28.0	33.2	29.8	29.7	29.8	28.5	32.2	26.7	28.0	36.3	35.3	34.0	34.5
820	35.6	29.3	30.1	32.0	28.9	29.0	31.4	30.2	30.6	31.5	30.1	32.0	28.9	29.0	36.2	34.0	32.5	33.6
830	36.9	30.9	29.2	29.9	30.0	29.0	31.2	28.3	27.9	29.9	29.2	29.9	30.0	29.0	36.5	34.6	32.5	33.7
840	37.1	28.4	27.9	31.5	27.1	27.8	33.1	29.5	28.2	30.1	27.9	31.5	27.1	27.8	36.1	35.3	33.0	34.1
850	35.9	31.2	29.8	31.0	30.8	30.0	30.9	28.5	28.1	29.8	29.8	31.0	30.8	30.0	36.5	34.3	32.5	33.7
860	36.3	29.0	28.1	31.8	27.8	28.3	33.2	29.4	29.0	30.1	28.1	31.8	27.8	28.3	35.2	34.5	32.3	33.1
870	37.3	28.9	28.1	29.9	27.5	27.6	31.5	28.5	29.0	29.8	28.1	29.9	27.5	27.6	35.6	33.4	31.9	32.9
880	36.7	28.3	26.8	29.2	27.1	26.8	31.4	27.8	28.4	29.6	26.8	29.2	27.1	26.8	35.3	33.5	31.9	32.9
890	36.8	29.2	28.8	30.4	28.0	28.0	31.8	28.8	29.4	30.6	28.8	30.4	28.0	28.0	35.2	33.4	32.4	33.3
900	42.0	28.5	27.2	29.5	27.5	27.3	30.3	26.8	27.5	29.0	27.2	29.5	27.5	27.3	35.8	33.9	32.5	33.5
910	44.1	29.3	28.9	32.2	27.9	28.8	32.0	29.8	29.6	30.4	28.9	32.2	27.9	28.8	36.2	35.1	34.8	35.5
920	42.2	28.7	27.2	27.9	27.8	27.0	31.4	26.9	26.1	28.0	27.2	27.9	27.8	27.0	35.8	33.5	31.9	33.2
930	40.6	29.7	26.7	31.2	28.0	28.9	34.7	30.6	29.2	29.3	26.7	31.2	28.0	28.9	35.3	34.5	33.8	34.4
940	41.1	28.8	25.9	29.9	28.0	27.9	31.6	28.5	28.0	29.2	25.9	29.9	28.0	27.9	34.6	32.9	31.6	32.8
950	41.0	29.6	30.2	31.6	28.2	29.0	33.8	30.4	30.0	30.9	30.2	31.6	28.2	29.0	33.5	34.7	34.7	35.3
960	38.6	28.2	29.0	29.7	27.3	27.2	30.9	28.0	28.2	29.5	29.0	29.7	27.3	27.2	34.8	33.7	34.0	37.0
970	37.0	28.5	28.8	31.0	27.3	27.8	31.6	30.3	30.3	30.8	28.8	31.0	27.3	27.8	35.3	33.9	33.7	35.5

Table J.12.continued

980	37.8	29.3	29.0	29.8	28.8	28.0	30.0	28.9	29.3	30.3	29.0	29.8	28.8	28.0	35.8	33.7	32.6	33.9
990	35.1	26.0	27.5	30.8	27.2	28.0	30.7	28.6	28.8	29.9	27.5	30.8	27.2	28.0	35.6	34.0	32.2	32.8
1000	36.2	25.2	26.4	29.8	24.4	25.4	29.2	27.4	27.7	28.7	26.4	29.8	24.4	25.4	35.9	33.8	32.3	33.3
1010	38.1	27.9	28.0	29.5	26.0	26.2	31.0	30.5	30.6	30.8	28.0	29.5	26.0	26.2	35.6	34.6	34.1	34.6
1020	37.8	30.7	29.4	28.1	29.5	27.8	28.6	28.2	29.0	30.4	29.4	28.1	29.5	27.8	35.6	33.4	32.2	33.1
1030	38.2	28.1	26.7	29.7	25.9	26.4	28.7	27.7	28.7	30.0	26.7	29.7	25.9	26.4	35.1	34.3	32.4	33.2
1040	35.7	31.8	30.3	31.3	31.2	30.3	26.6	29.2	31.1	32.3	30.3	31.3	31.2	30.3	34.5	32.7	32.3	33.3
1050	35.8	31.2	28.8	30.9	30.2	29.6	28.3	26.7	27.6	29.5	28.8	30.9	30.2	29.6	35.8	34.2	32.5	33.5
1060	36.0	28.1	26.8	31.1	27.1	27.9	29.8	27.8	27.8	28.9	26.8	31.1	27.1	27.9	33.7	33.4	32.2	32.8
1070	35.1	29.1	28.5	29.7	28.7	28.2	28.1	29.2	29.7	30.7	28.5	29.7	28.7	28.2	32.4	31.5	31.5	32.2
1080	35.0	30.5	29.3	28.7	30.0	28.5	27.3	27.3	28.9	30.5	29.3	28.7	30.0	28.5	32.9	31.3	30.2	31.2
1090	36.0	27.8	26.2	28.8	26.2	26.3	28.5	26.5	26.8	28.7	26.2	28.8	26.2	26.3	33.8	32.9	31.3	32.0
1100	34.7	32.2	31.0	30.0	31.7	29.7	30.2	30.8	31.0	32.1	31.0	30.0	31.7	29.7	32.8	32.1	31.7	32.3
1110	34.3	34.3	33.3	31.4	33.8	31.2	32.4	33.1	33.2	34.2	33.3	31.4	33.8	31.2	33.0	32.3	31.8	32.1
1120	34.8	35.7	34.9	32.2	35.2	32.0	33.7	34.3	34.4	35.2	34.9	32.2	35.2	32.0	33.5	32.9	32.4	32.6
1130	33.0	35.4	34.9	32.5	34.9	32.3	34.2	34.6	34.7	35.5	34.9	32.5	34.9	32.3	33.0	32.7	32.2	32.1
1140	32.7	34.9	35.9	33.0	34.6	32.7	34.0	34.2	34.2	34.8	35.9	33.0	34.6	32.7	32.5	32.4	32.0	31.9
1150	31.4	33.3	33.5	32.2	33.3	31.8	32.7	32.8	32.8	33.2	33.5	32.2	33.3	31.8	31.4	31.3	31.0	31.0
1160	31.0	32.2	33.7	31.4	32.1	31.1	31.5	31.7	31.6	32.0	33.7	31.4	32.1	31.1	30.6	30.5	30.3	30.2
1170	30.5	31.3	32.0	30.8	31.3	30.5	30.6	30.8	30.7	31.0	32.0	30.8	31.3	30.5	30.0	30.0	29.8	29.7

Table J.12.continued

1180	29.8	30.6	30.0	30.2	30.5	30.0	29.9	30.1	30.0	30.3	30.0	30.2	30.5	30.0	29.4	29.3	29.2	29.1
1190	29.8	29.9	29.8	29.8	29.9	29.5	29.2	29.5	29.4	29.7	29.8	29.8	29.9	29.5	29.2	29.0	28.8	28.8
1200	29.5	29.4	29.2	29.3	29.3	29.0	28.6	28.8	28.8	29.1	29.2	29.3	29.3	29.0	28.5	28.5	28.3	28.2
1210	28.8	28.9	28.7	28.9	28.9	28.7	28.2	28.5	28.4	28.7	28.7	28.9	28.9	28.7	28.0	28.0	27.8	27.8
1220	28.2	28.5	28.2	28.4	28.4	28.2	27.8	28.0	27.9	28.2	28.2	28.4	28.4	28.2	27.6	27.5	27.3	27.3
1230	26.0	27.9	27.3	27.9	27.8	27.6	26.9	27.4	27.3	27.6	27.3	27.9	27.8	27.6	25.6	26.0	25.9	25.8
1240	26.6	30.6	24.9	27.0	25.3	26.7	23.0	24.6	24.0	28.3	24.9	27.0	25.3	26.7	24.5	24.3	24.4	24.4
1250	25.6	28.5	28.3	26.3	28.4	26.1	27.5	28.1	28.0	28.2	28.3	26.3	28.4	26.1	25.8	25.8	25.8	25.1
1260	22.2	26.9	28.6	25.4	26.8	25.2	26.1	26.5	26.3	26.5	28.6	25.4	26.8	25.2	23.5	23.6	23.4	22.9
1270	23.5	25.3	29.3	24.3	25.3	24.0	24.6	24.9	24.8	25.1	29.3	24.3	25.3	24.0	23.3	23.4	23.2	22.8
1280	25.5	24.8	29.3	24.1	24.8	23.9	23.9	24.4	24.3	24.7	29.3	24.1	24.8	23.9	24.5	24.5	24.3	24.2
1290	24.4	24.6	27.0	24.2	24.6	23.9	23.7	24.1	24.0	24.2	27.0	24.2	24.6	23.9	23.2	23.1	23.0	22.8
1300	24.1	24.2	26.0	24.0	24.2	23.7	23.4	23.7	23.6	23.8	26.0	24.0	24.2	23.7	22.7	22.7	22.6	22.5
1310	23.0	23.5	25.0	23.3	23.4	23.1	22.7	22.9	22.9	23.1	25.0	23.3	23.4	23.1	21.8	21.8	21.6	21.5
1320	25.2	23.4	23.7	23.3	23.4	23.2	22.6	22.9	22.9	23.3	23.7	23.3	23.4	23.2	23.9	23.8	23.6	23.6
1330	24.8	23.5	23.8	23.5	23.5	23.4	22.8	23.1	23.1	23.4	23.8	23.5	23.5	23.4	23.7	23.5	23.5	23.4
1340	22.8	23.3	23.7	23.3	23.2	23.1	22.7	22.8	22.7	23.0	23.7	23.3	23.2	23.1	21.7	21.7	21.6	21.5
1350	24.3	22.7	23.2	22.8	22.8	22.7	22.1	22.3	22.2	22.6	23.2	22.8	22.8	22.7	22.6	22.6	22.4	22.4
1360	23.8	22.6	23.0	22.8	22.6	22.5	21.9	22.1	22.0	22.3	23.0	22.8	22.6	22.5	22.5	22.4	22.3	22.3
1370	24.0	22.6	22.9	22.6	22.5	22.5	21.8	22.1	22.0	22.4	22.9	22.6	22.5	22.5	22.7	22.7	22.5	22.5

Table J.12.continued

1380	23.2	22.5	22.8	22.7	22.5	22.4	21.8	22.0	22.0	22.3	22.8	22.7	22.5	22.4	21.7	21.7	21.5	21.5
1390	23.8	22.5	22.8	22.6	22.5	22.5	21.7	22.0	22.0	22.3	22.8	22.6	22.5	22.5	22.4	22.3	22.2	22.2
1400	24.0	22.5	22.9	22.7	22.5	22.5	21.8	22.1	22.0	22.4	22.9	22.7	22.5	22.5	22.5	22.4	22.3	22.3
1410	23.8	22.6	23.0	22.8	22.6	22.6	21.9	22.2	22.2	22.5	23.0	22.8	22.6	22.6	22.5	22.4	22.2	22.3
1420	23.8	22.7	23.1	22.9	22.7	22.7	21.9	22.2	22.2	22.5	23.1	22.9	22.7	22.7	22.5	22.4	22.3	22.3
1430	23.9	22.6	23.0	22.8	22.5	22.6	21.9	22.1	22.1	22.5	23.0	22.8	22.5	22.6	22.6	22.6	22.4	22.4
1440	24.0	22.6	22.9	22.8	22.6	22.6	21.9	22.1	22.1	22.4	22.9	22.8	22.6	22.6	22.5	22.5	22.3	22.3

APPENDIX K

SAMPLE CALCULATION

K.1 Sample Calculation for Productivity

A sample calculation for the productivity for RUN 072015-R1 on July 16, 2015 was shown below. The total gas produced was 556 mL, and the hydrogen percentage was 95.8%. Day time was 14 hours. The volume of Reactor 1 (R1) was 11 L.

$$V_{H2} = (556\ mL) \cdot (0.958) = 532\ mL \qquad (K.1)$$

$$n_{H2} = \frac{PV_{H2}}{RT} \qquad (K.2)$$

$$n_{H2} = \frac{(0.9\ bar)(532\ mL)}{\left(85.14\ \frac{bar.mL}{mol.K}\right)(303K)} = 0.019\ mol \qquad (K.3)$$

Recall

$$Productivity = \frac{Hydrogen\ produced}{Reactor\ Volume \cdot Time} \qquad (2.7)$$

$$Productivity = \frac{0.019\ mol}{(0.011\ m^3) \cdot (14\ h)} \qquad (K.4)$$

$$Productivity = 0.123 \frac{mol}{(m^3.h)} \qquad (K.5)$$

K.2 Sample Calculation for Substrate Conversion Efficiency

A sample calculation for the substrate conversion efficiency (Y_{H2}) for RUN 072015-R1 on July 16, 2015 was performed below. On July 16, 2015 in the morning, acetic acid concentration in the reactor was adjusted to 40 mM (0.440 mol). Acetic acid measured in the morning on July 17, 2015 before feeding was 36.54 mM (0.402 mol). Hydrogen produced on July 16, 2015 was 0.019 mol as calculated previously.

Recall:

$$Y_{H2} = \frac{Hydorgen\ produced}{\begin{array}{c}Theoretical\ hydrogen\ that\ could\ be\ produced \\ if\ all\ the\ substrate\ was\ used\ for\ H2\ production\end{array}} x100 \qquad (2.6)$$

Theoretically, 4 mol of hydrogen can be produced from 1 mol of acetic acid (see Reaction 2.16).

$$Y_{H2} = \frac{0.019\ mol}{(0.440\ mol - 0.402\ mol) \cdot 4} \cdot 100 = 12.5\ \% \qquad (K.6)$$

Substrate conversion efficiency for RUN 072015-R2 was calculated in the same way. Since sucrose is the substrate, theoretically, 24 mol of hydrogen can be produced from 1 mol of sucrose (Reaction 2.17). Therefore, while calculating the theoretical hydrogen production, sucrose consumption was multiplied with 24 instead of 4.

K.3 Sample Calculation for Light Conversion Efficiency

A sample calculation for the light conversion efficiency for RUN 072015-R1 on July 16, 2015 was shown below. The daily solar radiation was 322.20 W/m^2. Hydrogen density was 0.0899 kg/m^3 (8.99x10^{-5} g/mL). The irradiated area was calculated as 1.685 m^2.

Recall:

$$\eta = \frac{V_{H2} \cdot \rho_{H2} \cdot 33.61}{I \cdot A \cdot t_{H2}} \cdot 100 \tag{2.8}$$

$$\eta = \frac{(532\ mL) \cdot (8.99 \cdot 10^{-5}\ g/mL) \cdot \left(33.61 \frac{W.h}{g}\right)}{\left(526.46 \frac{W}{m^2}\right) \cdot (1.685\ m^2) \cdot (14\ h)} \cdot 100 = 0.01295\ \% \tag{K.7}$$